

Friedrich-Alexander-Universität Erlangen-Nürnberg



Master Thesis

Impact of Diffuse and Disturbed Reflections on Room Geometry Inference Algorithms

submitted by
Stefan A. Wirler

submitted
April 1, 2019

Supervisor / Advisor
Youssef El Baba M.Sc.

Reviewers
Prof. Dr. ir. Emanuël Habets



International Audio Laboratories Erlangen
A joint institution of the
Friedrich-Alexander-Universität Erlangen-Nürnberg (FAU) and
the Fraunhofer-Institut für Integrierte Schaltungen IIS.



Erklärung

Hiermit versichere ich an Eides statt, dass ich die vorliegende Arbeit selbstständig und ohne Benutzung anderer als der angegebenen Hilfsmittel angefertigt habe. Die aus anderen Quellen oder indirekt übernommenen Daten und Konzepte sind unter Angabe der Quelle gekennzeichnet. Die Arbeit wurde bisher weder im In- noch im Ausland in gleicher oder ähnlicher Form in einem Verfahren zur Erlangung eines akademischen Grades vorgelegt.

Erlangen, April 1, 2019

Stefan A. Wirler

Acknowledgements

Before we start with the examination of the impact of diffuse and disturbed reflections, I want to express my gratitude in everybody involved in this project.

First, I want to thank Prof. Dr. ir. Emanuël Habets, for making it possible to work in an outstanding group at the International Audio Laboratories in Erlangen. He also provided the basis of the implemented room-impulse generator, which was extended to generate first-order diffuse reflections and was the basis of the investigation of the impact.

My biggest thank goes out to my advisor Youssef El Baba. I am thankful for his support throughout the thesis. The fruitful discussions, which sometimes lasted for hours, were inspiring and provided me with the needed information. With the discussions and the provided ideas, it was possible to implement a first-order room impulse response generator for the examination of the diffuse reflections. Throughout my studies, I never conducted image based signal processing, and he provided me with the needed knowledge to use it in the thesis. Additionally, he provided the core of the thesis. He let me use his algorithm, investigate it, and try to break it with diffuse reflections. Thank you very much, Youssef, for providing outstandingly support, ideas ,and information throughout this thesis.

I want to thank everybody else involved in this thesis and the process. I am thankful for everybody who supported me throughout this time and to my friends providing time to relax, with the right beverage, in stressful situations.

Last, I want to thank my family, especially my parents Albert and Anneliese, who played a huge role in making it possible to conduct my studies. Also, I want to thank my brothers, Michael and Maximilian, who always provided support when needed.

Abstract

Room geometry inference algorithms are used to provide information about the reflector locations. These algorithms are applied in the context of e.g. sound-source localization, speaker tracking and dereverberation. For the estimation of the reflector locations, the sound reflections of the walls are used. As we don't live in a perfect world, reflections occur which are not reflected specular, but into random directions. These reflections can impair the performance of such algorithms. In this context, it is needed to study the impact of these diffuse reflections.

In this thesis, we address the problem of simulating first-order diffuse reflections. An approach is proposed to simulate these reflections with three different models and directly obtain the pressure room impulse response. With the three models, it is possible to simulate different conditions. Further, we examine the behavior of the simulation and the different methods.

With the simulation of the diffuse reflections, the impact on a state-of-the-art room geometry inference algorithm is carried out. We show the performance under different diffuse conditions with a microscopic and a macroscopic view. The microscopic view is concerned with the impact on the time-of-arrival detection of the wall reflections. On the other hand, the macroscopic view provides an overview of average performance metrics. By the gained knowledge, we then propose filtering techniques to cope with diffuse reflections for robustness in diffuse conditions. Specifically, we use image-based filtering techniques, the bilateral filter, and an extended gradient filter to equalize the impact of diffuse reflections. With the application of the filtering techniques, we are able to improve the overall performance of the algorithm in diffuse conditions.

Contents

Erklärung	i
Acknowledgements	iii
Abstract	v
1 Introduction	3
1.1 Thesis Organization	4
1.2 Main Contributions	5
2 Geometric Room Acoustics	7
2.1 Reflections in Room Acoustics	7
2.2 Characterization of Diffuse Reflections	11
2.3 Ray-Based Modeling Techniques	13
2.4 Surface-Based Modeling Techniques	16
2.5 Hybrid Method	17
2.6 Modeling Diffuse Reflections	18
2.7 Summary	23
3 Simulation of First-Order Diffuse Reflections	25
3.1 Overview	25
3.2 Specular Direction and Diffuse Direction	28
3.3 Air Absorption and Delay	28
3.4 Reflection Factor	29
3.5 Diffusion Strength Factor	29
3.6 Normalization Factor	34
3.7 Scattering Coefficient	36
3.8 Specular and Diffuse Transfer Function	37
3.9 High-Pass Filter	38
3.10 Computational Complexity	38
3.11 Comparison of the Different Distributions	40
3.12 Simulated Diffuse Reflections	43

CONTENTS

3.13	Summary	47
4	Impact of Diffuse Reflections	49
4.1	Overview	49
4.2	Evaluation Setup	52
4.3	A Microscopic View on the Impact of Diffuse Reflections	53
4.4	A Macroscopic View on the Impact of Diffuse Reflections	57
4.5	Countermeasures for Diffuse Reflections	63
4.6	Evaluation of the Countermeasures	68
4.7	Summary	75
<hr/>		
5	Conclusions	77
A	TOA Detection and Disambiguation Metrics	79
B	Reflector Localization Performance Metrics	93
	Bibliography	105

Chapter 1

Introduction

The use of room geometry inference (RGI) algorithms is concerned with the localization of reflecting boundaries of a room. They correspond, for simple shaped rooms, to the four walls, the ceiling, and the floor. These algorithms can be applied in several applications e.g., speaker tracking [VB01] or sound-source localization [RF03]. The locations of the reflectors can be determined by the time-of-arrival (TOA) of the corresponding first-order reflections of a reflective boundary. For the evaluation of such algorithms, room impulse response (RIR) generators are used. With these simulators, it is possible to simulate a RIR, which contains the acoustic reflections of a room. A widely used geometric method is the ray-based image source method as described in [AB79]. This method is able to find all possible specular reflections in a deterministic way. A specular reflection is based on the assumption of a perfectly reflecting surface. In this context, the sound is reflected by the same angle as the angle of the incoming sound (w.r.t to the surface/wall normal).

However, the fact that simulators are used which are only capable of simulating specular reflections is a limitation in the evaluation of, e.g. RGI algorithms. In research, strong evidence was found that diffuse reflections at a surface reflection occur [Hod91]. Different types of materials and other properties, such as rough surfaces, can lead to diffuse reflections. Therefore, in a real environment, the reflections are not only of specular nature. In this case, the sound is not only reflected in the specular direction, but also into non-specular directions.

The modeling of these effects is included in commercially available simulators such as ODEON and CATT-Acoustics, which are using ray-tracing to obtain the energy impulse response. Although these simulators are capable of modeling these effects, their aim is the modeling of complex geometries and auralization. In [SMD09], Schimmel presented a simulator, which is capable of simulating specular and diffuse reflections. This simulator relies on the statistical ray-tracing approach to obtain an energy-time histogram and the pressure impulse response from the energy-time histogram. One drawback of such simulator is the use of reflection distributions, which are

1. INTRODUCTION

only valid for certain cases, especially for the crucial reflections in terms of an RGI- Algorithms. These reflections are the first-order reflections, as they can be used to gain information, e.g. about the locations of reflecting walls. Hence, a simulator is needed, which is capable of simulating the first-order diffuse reflections.

In the context of the evaluation of RGI algorithms, the use of only specular reflection simulators leads to the neglection of the effects of diffuse reflections. As these algorithms should provide robustness in real-environment, the impact of such diffuse reflections should be investigated.

This thesis is therefore concerned with the modeling and simulation of diffuse reflections and their impact on a state-of-the-art RGI algorithm. An approach is presented, for the modeling of the first-order diffuse reflections with different scattering distributions. In this approach, the distributions are not used in terms of probability of a reflection, but they are applied directly to obtain the strength and the directions of diffuse reflections. From this simulation, the impact of the diffuse reflections is investigated and evaluated. Further, with the knowledge of the impact of diffuse reflections, countermeasures are presented to cope with the effects.

1.1 Thesis Organization

The main structure of this thesis is split into two parts. The first part of this thesis is concerned with the modeling, the simulation, and implementation of diffuse reflections. In the second part, the implemented RIR Generator is used to investigate the impact of the diffuse reflection on a state-of-the-art RGI-Algorithm.

In Chapter 2, an overview of geometric room acoustics is given. This includes the description of reflections in room acoustics. Also, the characteristics of diffuse reflections are described. Furthermore, a general overview of room acoustic modeling techniques is given. Then, existing modeling techniques for diffuse reflections are described more in detail.

In Chapter 3, the implementation of a RIR generator, which is capable of modeling first-order diffuse reflections is described. This includes the concept of the simulation as well as the incorporation of three different models. Afterward, a brief comparison of the used models and the resulting simulated diffuse reflections is given.

In Chapter 4, the impact of the diffuse reflections on a state-of-the-art algorithm is investigated. The algorithm is tested for different conditions of diffuse reflections. A microscopic and a macroscopic view examines the impact. Further, countermeasures for the diffuse reflections are proposed and evaluated.

In Chapter 5, a final conclusion of the thesis is given and future work is indicated.

1.2 Main Contributions

The main contributions of this thesis are as follows.

First, we introduce an RIR Generator capable of simulating first-order diffuse reflections. The simulator is able to directly calculate the diffuse pressure impulse response on the basis of three different methods.

Second, we provide a better understanding of the impact of diffuse reflection through extensively testing a state-of-the-art algorithm for different diffuse conditions. The impact is evaluated in a microscopic and macroscopic view, on the algorithm.

Third, we propose filtering approaches, to cope with the impact of diffuse reflections. With these filtering approaches, it is possible to equalize the effects of diffuse reflections.

Chapter 2

Geometric Room Acoustics

In this chapter, an overview about geometric room acoustics is given. First, an overview is provided of reflections in room acoustics and ways to describe them in geometrical room acoustics. In the beginning, specular and diffuse reflections are introduced as well as a way to describe diffuse reflections in room acoustics. Next, a characterization of the diffuse reflections is given. The second part describes the different modeling techniques in computerized calculation of geometrical room acoustics. These are the ray-based, the surface and the hybrid-methods. Afterwards, the modeling of diffuse reflection is described specifically. Several methods that have been introduced in the past are presented.

2.1 Reflections in Room Acoustics

In the following, an overview of the types of reflections and ways to describe them in room acoustics is given. First, an introduction about specular and diffuse reflections is presented. Further, the coefficients used for modeling diffuse reflections and ways to describe their behavior is carried out.

2.1.1 Specular Reflections

In geometrical room acoustics, the description of the sound is not wave-based but replaced with the concept of sound rays. Therefore, the wave properties are neglected. The assumption of rays is valid, in case of a short wavelength of the sound compared to dimension of the room. Sound reflections occur at boundaries, such as walls, furniture etc. In case of a large and smooth surface, a simple relationship between the incident angle (angle of the incoming sound ray w.r.t to surface normal) and the reflection angle (angle of the reflected sound ray w.r.t to surface normal) can be

2. GEOMETRIC ROOM ACOUSTICS

found. As known from optics, the relation between the incident and the reflection angle can be written in vector notation after Kuttruff [Kut17] as

$$\mathbf{r} = \mathbf{i} - 2\langle \mathbf{i}, \mathbf{n} \rangle \mathbf{n}, \quad (2.1)$$

where \mathbf{r} is the vector pointing in the direction of the reflected angle, \mathbf{i} is the vector pointing in the direction of the incident angle and \mathbf{n} represents the normal vector of the reflecting surface.

2.1.2 Diffuse Reflections

Rough Surfaces

In a realistic environment, the assumption of a smooth surface is mostly not given. Therefore, the assumption of only specular reflections is not applicable. Given a rough surface, the reflection depends on the wavelength as well as on the dimension of the surface texture. In case of a significant bigger wavelength compared to the surface texture, the reflection will not be disturbed and reflected specularly. In the opposite case, given a significant smaller wavelength compared to the texture of the reflecting surface, the sound will be reflected also specular but with a different direction due to the obstacles. Therefore, the direction of the reflection changes and Snell's law is not applicable anymore. In the intermediate case of a wavelength with half of the surface texture size, the sound will be scattered and lead to diffuse reflections. The behaviour of sound at irregular surfaces was studied early by Twersky [Twe57] and Biot [Bio68]. The most important result of this studies was published by Biot in 1968. He introduced a generalized model to describe different types of surface irregularities. Using this model, the reflections can be described as radiating dipoles. But, the incorporation of his model in geometrical room acoustics is not common, instead an easier approximation is used. This approximation is the decomposition of the reflection into a diffuse and specular reflected portion. The portion of the diffuse and reflected energy of the reflected sound is described by the scattering coefficient (see 2.1.5). In most cases, the distribution of the diffuse reflections in geometric room acoustics, due to scattering, is described by Lambert's law (see Section 2.1.3).

An evidence of diffuse reflections was found by Hodgson in [Hod91]. The author found consistent deviations of real measurements and predictions, which do not took diffusion into account. Therefore, the author hypothesized that diffuse surface reflections occur. For this reason he implemented a simulation technique, which takes into account diffuse surface reflections. The results lead him to the conclusion that the differences in the measurements and the experiments are due to surface diffusion. He carried out his experiments in empty halls and therefore the differences have to be introduced by diffusely reflecting surfaces. He provided strong evidence, that nonrigid walls of untreated rooms are highly diffusely reflecting.

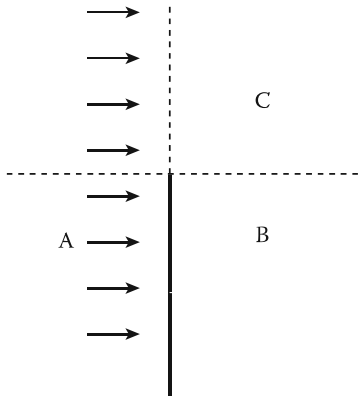


Figure 2.1: Schematic illustration of a semi-finite wall after [Kut17].

Diffraction

Another phenomenon, which can cause non specular reflection is diffraction. Diffraction can occur at obstacles with finite length or free edges. If the sound wave hits such an obstacle with a finite length or a free edge, it will not be purely specularly reflected. The simplest case of diffraction shall be explained by the example of a semi-finite wall, depicted in Figure 2.1.

The first intuitive thought is that the wave is reflected back into zone A, while the “shadow-zone” B remains free of sound. This is true for small wavelength, compared to the finite obstacle. However, given the case of a higher wavelength, the shadow-zone B is experiencing sound due to diffraction. Furthermore, the sound in zone C is disturbed by diffraction. Hence, diffraction can be considered as the spreading of sound in all directions. The modeling of diffraction in geometric room acoustics is often neglected, however it is possible to incorporate this effect. The models used are e.g. the secondary source approach (corresponding to Huygens Principle) [TSK01], models which include the Geometrical Theory of Diffraction (GTD) [Kel62] or the Uniform Theory of Diffraction (UTD) [KP74] and the “uncertainty principle” [Ste10].

2.1.3 Lambert’s Law

As described above, not only specular reflections, but also diffuse reflections due to rugged surfaces occur. A way to describe diffuse reflections, is the use of Lambert’s law from optics. It is used to describe perfectly diffuse reflections. Lambert’s law is often applied in geometrical room acoustic modeling. It states, that the intensity of a diffuse reflection only depends on the angle of the reflected sound and is independent of the incident angle. The intensity of the diffuse reflected sound is distributed proportional to the cosine of the reflection angle. This reads as

$$I_d(\theta_{diff}) \propto I_i \cos(\theta_{diff}), \quad (2.2)$$

2. GEOMETRIC ROOM ACOUSTICS

where $I_d(\theta_d)$ is the intensity of the diffuse sound w.r.t. to the reflection angle θ_{diff} of the diffuse reflections and I_i the intensity of the incident sound. One reason for the wide usage of Lambert's law is the ability to incorporate the model as a point reflecting source, which is a good fit for most geometrical models in acoustics. Cox and D'Antonio stated that scattering will approximately follow the assumption of Lambert's law, but only for very high frequencies and for a random rough surface. For other real surfaces Lambert's model doesn't fit well. They also remarked that this assumption is only sufficient for the late reverberant part and some believe that a uniform distribution provides a better fit for early diffuse reflections [CD09]. Another possibility considered by Siltanen is using the directional properties of diffuse reflections [SLKS07].

2.1.4 Absorption

The assumption of total reflection of the energy is only true for an ideal case of reflection. In a real environment the reflecting boundaries are not ideally reflecting. A portion of the energy of the incident sound is absorbed. The amount of the absorbed energy depends on the material, the frequency and on the angle of incidence of the sound [Kut17]. The angle dependent absorption factor is defined as

$$\alpha(\theta) = 1 - |R(\theta)|^2, \quad (2.3)$$

where $|R(\theta)|^2$ describes the amount of reflected energy, obtained from the normal wall impedance. In acoustic room models the frequency dependency is often neglected. In geometrical room acoustics the random incident absorption coefficient α is used. Hence, only the frequency dependency is taken into account for a specific boundary material. The reflected energy can then be written as

$$E_r = E_i(1 - \alpha), \quad (2.4)$$

with E_r as the reflected sound energy and E_i as the energy of the incident sound.

2.1.5 Scattering Coefficient

The scattering coefficient describes the portion of the specular and diffuse reflected energy at a wall reflection, due to the roughness of the surface. It is defined as the ratio between the specular and non-specular reflected energy and therefore

$$E_s = (1 - s)E_r \quad E_d = sE_r. \quad (2.5)$$

Where s is the scattering coefficient and E_r the total reflected energy. E_s and E_d are the energy of the specular and diffuse reflected energy, respectively. The value of the scattering coefficient can vary between 0 and 1. Similiar to the absorption coefficient, the scattering coefficient is

also dependent on the frequency as well as the incident angle [VM00]. The scattering coefficient is mostly used in room geometric models as a frequency dependent coefficient, but the angle dependency is neglected in common models. With consideration of the absorption factor the specular and reflected energy can be denoted as

$$E_s = (1 - \alpha)(1 - s)E_r \quad E_d = (1 - \alpha)sE_r. \quad (2.6)$$

It should be noted, that the scattering coefficient should not be confused with the diffusion coefficient. In some descriptions of computer models, the term diffusion coefficient is used with the same definition as the scattering coefficient [Cox06]. Another term used in literature for the scattering coefficient is diffuse-reflecting coefficient.

2.1.6 Diffusion coefficient

The diffusion coefficient indicates the quality of a diffuser. It is used to describe the uniformity of the reflected sound. If the diffusion coefficient is $d = 1$, the reflected sound is distributed uniformly and if $d = 0$ the sound is reflected in a specific direction. This is in a stark contrast to the assumption of Lambert's law for diffuse reflections. For this reason, the diffusion coefficient should not be used in geometric room models, as it is not compatible with the models used in room geometry algorithms [Cox06].

2.1.7 Bidirectional Reflectance Distribution Function

The Bidirectional Reflectance Distribution Function (BRDF) was originally used in optics and is applied in computer graphics. Instead of describing the diffuse reflection by one factor, the BRDF describes the reflection as a function of the incident and the reflection angle, at a given frequency [SAWG91]. Another consideration in terms of the use in acoustics is the temporal dependency of the BRDF, compared to optics. However, the temporal dependency is often neglected in practical use. Using the BRDF in room acoustic modeling is described in [SLKS07]. In this approach the BRDF is constructed with the absorption and scattering coefficient for given materials. Usage of measured BRDF's was not possible as there is no data available. The authors' idea was to blend the ideal specular and the ideal diffuse BRDF weighted by the scattering coefficient.

2.2 Characterization of Diffuse Reflections

In the following, an overview about the influence and the characteristics of diffuse reflections is given. The main source is the paper of Dalenbäck [DKS94], who did research about the characteristics and properties of diffuse reflections. The research he did was in terms of auralization,

2. GEOMETRIC ROOM ACOUSTICS

but the found effects of diffuse reflections can help understanding the impact of diffuse reflection on room geometry inference algorithms.

2.2.1 The Reflection Combinations

Dalenbäck had a view on the different types of reflection combinations. In an environment with existing diffusely and specularly reflecting surfaces, four different types of reflection combinations can occur. These four different combinations are the specular – specular (S-S), the specular – diffuse (S-D), the diffuse – specular (D-S) and the diffuse-diffuse (D-D) combination. He also had a look into the capability of handling the combinations, for different types of modeling techniques. The S-S combinations can be solved by the Image-Source method, the hybrid method, cone or beam tracing and ray-tracing. The author also stated that every one of these methods can be extended to include all four different types of combinations. For the modeling of D-D combinations the radiosity-method is the most suitable, as it models only complete diffuse reflections.

2.2.2 Impact of Diffuse Reflections

The investigation of diffuse reflections from Dalenbäck lead him to conclusions about the effects of diffuse reflections [DKS94]. He stated that the most fundamental property of diffuse reflections is the occurrence of reflections in non-specular regions. In addition, a diffuse reflecting surface, will decrease the energy of specular reflections and transport them into regions, which are not covered by specular reflections.

2.2.3 Temporal Smearing and Amplitude Smoothing

A consequence of the occurrence of reflections in non-specular regions is the temporal smearing of the specular reflections. This effect is of high interest, as the specular reflections are used in room geometry inference algorithms. Causing the temporal smearing and amplitude smoothing is the nature of a diffuse reflecting surface. The sound of a source, can cover a diffuse reflecting surface completely, therefore the sound will be reflected in all directions from this surface. In this case, the receiver is also covered by diffuse reflections, as the specular path is always the shortest path and the diffuse reflections will arrive later. Hence, the diffuse reflecting surface will lead to temporal smearing of the specular reflection. The other effect of a diffuse reflecting surface is the amplitude smoothing due to the transport of energy in non-specular regions.

2.3 Ray-Based Modeling Techniques

Several different approaches have been introduced over time. A common approach is the ray-based modeling of reflections in a room. The ray-based approach can be divided into two mainly used methods. One of them is the image-source (IS) method. The IS method is mostly used to model the specular reflections in a room. The other ray-based method is the ray-tracing (RT) method.

2.3.1 Image-Source Model

The IS model is widely used for the simulation of specular reflections. With the assumption of only specular reflections, the image source method is able to exactly model the early specular reflections. In [AB79], Allen and Berkeley used the image-source method to determine the RIR with a computerized simulation. The main advantage of this method is the ability to exactly model the early specular reflections [AB79], under the assumption that only perfectly specular reflections occur in a room. Another reason why this method is often used is the simplicity for rectangular shaped rooms (shoe-box room). This method has been widely used by many authors, some examples are [KKF93] [GJ72] and [LL88]. The basic principle of the IS method is the mirroring of source at reflective surfaces of a room. The path between these image-sources and the receiver then corresponds to the path of the first-order reflections. Then, these image-sources again are mirrored at the surfaces of their respective boundaries.

Theoretically, this can be done up to an infinite high reflection order. But due to the computational load induced by the higher order reflections, only a certain reflection order is feasible. Therefore, for the simulation of the reverberant tail, other methods are used. One method, proposed by [LJ10], is to model the reverberant tail as an random process, by predicting the energy decay of the tail. An extension of the IS method was introduced by Borish et al., they extended the method to arbitrary polyhedra [Bor84b]. In a recent study by Aretz et al., it was shown that the use of an angle-dependent and complex reflection factor (see 2.1.4 can lead to more accurate predictions especially for low frequencies [ADV14]). It was also stated that the diffraction effects should be taken into account for rooms with arbitrary geometry at low frequencies.

2.3.2 Ray-Tracing

The other ray-based modeling approach is the ray-tracing technique. The first description of ray-tracing in order to obtain a time-energy response was given by Krokstad et al. [KSS68]. Instead of a deterministic calculation of the reflections, the RT method is a stochastic method and relies on e.g. Monte Carlo simulation, for finding the possible paths. The basic principle of ray-tracing is the shooting of a finite number of rays from the source, which are traveling on rays throughout the room and register their energy (or intensity, power) if they arrive at

2. GEOMETRIC ROOM ACOUSTICS

the receiver. The distribution of the emitted rays can be predefined according to the source, or emitted randomly per Monte Carlo simulation. The path of the emitted rays is then traced throughout the room. If the ray intersects with a wall, it will be attenuated according to the walls reflection coefficient and redirected into a new direction. The direction depends on the type of reflection, either specular (reflected according to Snell's law) or diffuse (random direction). The handling of the diffuse reflections is described more detailed in 2.6. Also, the attenuation due to the propagation path length has to be taken into account. In case of a valid path from source to receiver (ray hits receiver), the energy carried by the ray is registered. To capture the rays, the receiver is modeled as a volumetric detector. The modeling as volumetric detector is needed, as with a point like receiver, the hit probability would tend to zero. The shape of the volumetric detector is not restricted to one particular shape. It is common to use spherical, cylindrical or surface detectors. For the detection of the arriving angle, the volumetric, or e.g. the spherical detector is separated into spherical bins. Then the energy of the arriving rays is accumulated at time m and at frequency k for every spherical bin i . This results in the time-frequency histogram $E_i(m, k)$.

The termination of the rays is usually done by two different methods [KJM05]. The first method is to terminate the rays, after the energy that is carried by a ray has reached a certain threshold or to terminate the ray after a certain amount of reflections. The other method is the “Russian Roulette” method. At each reflection a ray has a certain probability of getting destroyed.

A drawback of the ray-tracing method, compared to the IS method, is the possibility to not capture every reflection [SV99]. This is due to the discretization of the radiation pattern. The discretization can lead to non-covered angles in the pattern and therefore to non-covered possible paths. Another source of the problem is the use of volumetric detectors. It can lead to the detection of paths, which are not valid for the exact receiver position [Leh93]

As a result, the ray-tracing method, yields the energy impulse response. This is mostly sufficient to obtain room acoustical parameters, but for simulation purposes the pressure impulse response has to be regained. A way to regain the pressure impulse response is by shaping a noise signal, with the estimated energy impulse response [Sch]. After Schimmel et al. [SMD09], first a noise process is created for each spherical bin,

$$p_i(t) = \sum_r \delta(t - \tau_r), \quad (2.7)$$

with the number of arrivals $A_i(n) = \int_0^{\Delta t} p_i(t - n\Delta t) dt$. The number of arrivals is distributed after Poisson as

$$Pr[A_i(n) = m] = \frac{(\gamma_i(n))^m e^{-\gamma_i(n)}}{m!}, \quad (2.8)$$

with $\gamma_i(n) \propto \sum_k E_i(n, k)$. The next step is to shape the created noise signal $p_i(t)$ according to the time-energy histogram $E_i(n, k)$. This has to be done for every spherical bin. To obtain the final impulse response, all obtained responses, for each spherical bin, are superimposed.

The modeling of diffraction in ray-tracing is modeled by the uncertainty principle. With the uncertainty principle, rays that pass near an edge are diverted. The closer the rays pass the diffracting edge, the stronger is the diversion. This principle was introduced by Stephenson in [SS07] and given further insight in [Ste10]. An extension of this principle was done by Schröder and Pohl, aiming to include diffraction in 3D models [SP09].

2.3.3 Beam-Tracing

In the section before, ray-tracing was described as well as the problems that arise by use of discretized rays and volumetric detectors. An approach to encounter these problems, is beam tracing. Instead of modeling the receiver as a volumetric object, the rays are expanded to a volumetric object that covers a solid angle. Hence, the receiver can be modeled as a point-like receiver. First-order reflections of a beam are simply treated by specularly reflecting the beam. In cases where the beam is reflected by two boundaries the beam has to be split up, however, this isn't done every time due to high computational load. A publication which first introduced the idea of beam tracing was done by Haviland and Thaneder [HT73]. The authors modeled the beams as a pyramidal beam, which can be represented by three rays. An implementation of this proposed method was done by Walsh et al. [WD81]. A problem in beam-tracing was the false splitting of the beam at multiple reflective boundaries. This problem was encountered by adaptive beam-tracing [DL00] as well as by adaptive pyramid-tracing [CRT00]. Here, they suggested to split the beams into smaller beams at plane edges as well as edges from occluding planes. An advantage of beam-tracing is the ability to compute the pressure impulse response instead of the energy. Jeong et al. achieved higher accuracy by including the phase information, for the early response at mid-frequencies [JIR08]. They also included an angle-dependent reflection coefficient, but only achieved small improvements in accuracy. All these approaches are only used to model specular reflections. Dalenbäck achieved the modeling of diffuse reflection by storing the diffuse energy at surface patches at each pass. These surface patches then propagate the stored diffuse energy in successive passes [Dal96].

Another variation of beam-tracing is the frustum tracing, which was introduced by Lauterbach et al. [LCM07]. With frustum tracing it is possible to add diffraction effects to the simulation, by utilizing the uniform theory of diffraction [KP74]. This computation of diffraction effects with frustum tracing was described by Chandak et al. in [CLT⁺08].

2.4 Surface-Based Modeling Techniques

A different approach, in contrast to ray-based approaches, are the surface based approaches, such as the radiosity method, which originates from thermodynamics or a more recent surface based approach is the acoustic radiance transfer (ART) method, proposed in [SLKS07].

2.4.1 Acoustical-Radiosity Method

The radiosity method originated from an optics paper, which first proposed the main equations [Yam26]. This method is energy based and has been widely used in illumination for computer graphics. The first description using the acoustical-radiosity (AR) method in acoustics, was proposed by Kuttruff [Kut17]. In the AR method the boundaries are meshed, i.e. the walls are subdivided into smaller surface elements. After the meshing, the contribution between all wall elements and the source are determined with the form-factors. These created smaller surface elements, then act as an secondary source. In [Sve02], Svensson described, the normal intensity at each wall as

$$I_{n,i}(t) = I_{n,0 \rightarrow i}(t) + \sum_{j \neq i} F_{ji} \rho_j I_{n,j} \left(t - \frac{r_{j \rightarrow i}}{c} \right) \Delta S_j, \quad (2.9)$$

where $I_{n,0 \rightarrow i}(t)$ is the intensity contributed from the source to the i -th wall element, ρ_j is the energy reflection coefficient of element j , ΔS is the wall element size of element j . The form factor F_{ij} describes the contribution from element i to element j , following Lambert's law of ideal diffusion. Mathematically this can be written as

$$F_{j,i} = \frac{\cos\theta_i \cos\theta_j}{\pi r_{ji}^2}. \quad (2.10)$$

This description of the AR method only handles diffuse reflections, as the form factor follows Lambert's law of ideally diffuse reflections (Equation 2.10). The AR method was implemented e.g. in [LBB00] [TG97]. For handling all reflection combinations, Korany stated that the AR method needs to be extended [KBA01]. In [HN06], Hodgson compared specular ray-tracing, diffuse ray-tracing and the radiosity method in terms of predicting room acoustical parameters. The AR method performed as well as the diffuse ray-tracing and better than specular ray-tracing. The author concluded, that the assumption of purely diffuse reflections is less limiting than the assumption of purely specular reflections. But this assumption is only valid for predicting of room acoustic parameters.

2.4.2 Room Acoustic Rendering Equation

In 2007, Siltanen introduced the room acoustic rendering equation [SLKS07]. In his paper he constructed an integral equation that generalizes known methods in room acoustic modeling. His proposed equation is based on the “rendering equation” for light propagation, known from computer graphics. He extended this equation in terms of time dependency. Additionally, he extended the radiosity method, as the radiosity method suffers from the assumption of only perfect diffuse reflections. Hence, he proposed a method to take into account the BRDF and called it the Acoustic Radiance Transfer Function (ART). With this extension, arbitrary reflection properties can be modelled. The principles of the ART Function and the AR method stay the same, however, with the use of BRDF’s the emitted energy is dependent on the incident angle. Antani et al. further improved this approach, in terms of complexity reduction [ACTM12]. The drawback of the reduction in complexity is the loss of accuracy of their method. As well as the AR method, the ART method is mainly suited for the modeling of diffuse and late reflection [SLKS07]. In [BRD13], Bai et al. proposed a method to model the early reflections more accurate compared to the traditional ART method.

2.5 Hybrid Method

In recent years, the main focus on modeling the room acoustic was on methods, that use different approaches and combine them. The main idea behind the hybrid method is to separately simulate the specular and the diffuse reflection. The specular reflections are mainly simulated by the IS method or by beam-tracing. On the other hand, the diffuse reflections can be modeled by RT methods, as well as, surface based methods. Vorländer introduced a method, which combines the IS method with an RT method [Vor89]. An implementation of a hybrid method which uses the AR method to model the diffuse reflections and the beam-tracing approach for the specular reflections, was proposed by Lewers in [Lew93]. Tenenbaum et al. developed a model that combines ray-tracing with a surfaced-based algorithm [Ten07]. More recently, Koutsouris proposed the CARISM model [KBJJ13]. It combines the IS method and the AR method in such way, as the early part of the impulse response is modeled by a combination of the IS method and the AR method (specular and diffuse reflections) and the late part of the response only by the AR method (diffuse reflections). In [MBJN15], Marbjerg introduced PARISM, based on the CARISM model. The main difference of PARISM, is the ability to model specular and diffuse reflections with complex-valued and angle-dependent boundary conditions. He also introduced a way, to regain the pressure impulse response from the energy impulse response.

2.6 Modeling Diffuse Reflections

In the section before, the main modeling techniques of geometrical room acoustics were described. The direct modeling of diffuse reflections with the introduced methods is only possible for the radiosity method and the acoustic radiance transfer method. With no further refinement of ray-tracing or image source methods, the modeling of diffuse reflections is not possible. In this section, different approaches for modeling diffuse reflection with ray-tracing as well as techniques with image sources are introduced. At first, a description of the modeling of scattered sound is given. The next part are different modeling approaches in ray-tracing techniques for diffuse reflections. Also a short overview for image source approaches is given.

2.6.1 Scattering Models

The modelation of scattering due to wall irregularities relies on the assumption of ideal diffuseness described by Lambert's cosine law. The main difference between the modeling techniques is the handling of the directionality of the diffuse reflections [DKS94]. The two most common ways are the Hybrid Reflectence Model (HRM) and models based on Vector Mixing (VM). In [SP13], Schröder had a further look into the directional distributions of these two methods. In the following, this will be used as reference if not stated otherwise. The HRM models the specular and diffuse reflections separately. The energy of the reflection is split up between the specular and the diffuse part, according to the scattering coefficient s . The energy portions for the specular and diffuse part are donated as E_s and E_d , respectively. The portions of the energy can be described as in Equation 2.6 by

$$E_s = (1 - \alpha)(1 - s)E_r \quad E_d = (1 - \alpha)sE_r. \quad (2.11)$$

Then the specular energy portion E_s is further distributed in the direction corresponding to 2.1. The diffuse reflected energy portion E_d is distributed after the used diffusion model e.g. Lambert's law.

The VM method, in contrast to the HRM, combines the specular and diffuse reflections. The direction is calculated as a combination of the directions of the specular and the diffuse component, weighted by the scattering coefficient. Mathematically this can be written as

$$\mathbf{v}_{out} = (1 - s)\mathbf{e}_{spec} + s\mathbf{e}_{scat}. \quad (2.12)$$

The direction of \mathbf{e}_{spec} is given by the incidence direction and the direction of \mathbf{e}_{scat} is given by the distribution of the diffuse reflections (Lambert's law). Schröder stated, that the vector mixing

model should be used for surfaces which scatter in a specific direction. A brief description about the VM method is given in [Chr05]. This method is implemented in commercial simulation software such as ODEON or CATT.

2.6.2 Ray-Tracing with Randomized Directions

Kuttruff proposed a technique to model diffuse reflections with randomized ray directions. Hodgson did the first implementation of this method [Hod96]. The splitting of the specular and diffuse part is handled by the scattering coefficient and the absorption coefficient (see Equation 2.11). The decision whether a diffuse or a specular reflection occurs is made by generating a random number between 0 and 1. If the scattering coefficient is bigger than the generated number, the reflection is treated as diffuse reflection. In case of a smaller s , the reflection is modeled specular. Two random numbers (X_1, X_2) , in case of a diffuse reflection, determine the direction of the ray. The first random number X_1 determines the azimuthal angle and is chosen in the interval of $[-\pi, \pi]$. The polar angle is found by $\arccos(\sqrt{X_2})$, with a random number $X_2 = [0, 1]$.

Dalenbäck considered this method as convenient for the late reverberant part, but not suitable for the early specular reflections [DKS94]. A drawback is the need of a high number of rays, as it gives fewer, but stronger reflections with the use of a small number of rays, instead of many weak reflections. Another disadvantage of this method is the frequency dependency of the scattering coefficient. The computation has to be done for every frequency band separately, if the scattering coefficient is changing over frequency. This particular problem of frequency-dependent scattering coefficient was encountered by Embrech et al. [Emb00]. With his proposed method the computation of the diffuse reflections can be done simultaneously for all frequencies. He applied the method on a randomized directions algorithm, which he proposed in [Emb82]. The method is not restricted to this particular algorithm but can be applied on every other randomized directions algorithm. The novelty of his approach is the introduction of the splitting coefficient θ and a correction term. The splitting coefficient, defined for a surface, is not dependent on the frequency and independent from the scattering coefficient. At each wall hit of a ray, a random number X is generated. In the case of $X \leq \theta$, the reflection is diffuse and specular for the opposite case. To correct the frequency-dependency of the scattering factor, he scaled the energy at a certain frequency. In case of a diffuse reflection, the correction is done by $\frac{s(f)}{\theta}$ and for specular reflection by $\frac{1-s(f)}{1-\theta}$. With the use of the splitting factor, the ray-tracing is started for all frequency band simultaneously, instead of each frequency band separately.

2.6.3 Diffuse Rain

The diffuse rain algorithm is a stochastic ray-tracing process described in [Hei93]. Schröder et al., modified this algorithm to take effects, such as (flutter) echos, into account [SDV07][LSVA07]. One main advantage of this method is the reduction of rays without losses in accuracy [PSV11]. The diffuse rain algorithm treats wall hits similarly to the radiosity method. At each wall hit, a secondary source is casted, which is radiating into the receiver's direction.

In the beginning, the sound source is emitting the sound energy rays into the room. These rays are then traced throughout the room. If a ray intersects with a wall, a portion is absorbed according to the wall's absorption factor. In addition, the type of reflection is determined. This is determined in the same way as in Kuttruff's approach, as well as the random direction in case of a diffuse reflection (see Section 2.6.2). The difference to Kuttruff's approach is the additional casting of a secondary source at the point of impact. The secondary source then contributes to every receiver visible from the point of impact. The energy observed by the visible receiver, due to the secondary source is described as

$$E_s = E_t(1 - \alpha) \iint_{\Omega} w(\theta) d\Omega \quad (2.13)$$

where $w(\theta)d\Omega$ determines the probability that the sound is scattered in the direction of the angle Ω and E_t is the ray energy before the impact. With the assumption of Lambert's law, the probability is written as

$$w(\theta)d\Omega = \frac{1}{\pi} \cos(\theta) d\Omega \quad (2.14)$$

The ray containing the energy E_s is shot in the direction of the receiver. Then, the energy at the receiver is registered and the ray is terminated. This process is repeated for every frequency band, due to the frequency dependent scattering and absorption coefficient.

The proposed method is used to model the late reverberations, by Schröder et al. [SDV07]. However, Schimmel et al. implemented a simulator that utilizes the diffuse rain algorithm to model diffuse reflections occurring at low reflection orders for "shoebox" rooms [SMD09]. The early specular reflections are modeled by the IS method. Wabnitz et al. used this implementation and extended it to a multi-channel RIR generator [WEJvS10]

2.6.4 Split Up of Early Part and Late Part

The approach described in [Nay92] utilizes a transition order (TO). Here, the early and the late part of the reflections are split at a specified order by a user-defined TO. In the approach by

Naylor the early reflections were assumed to be purely specular up to the transition order. The main issue with this approach, is the assumption of ideally specular reflection up to a TO, as diffuse reflections also occur at the first reflections [Lam96]. For this reason, the approach was further extended [RC03]. The early part is handled by an IS method and secondary sources combinations. At detection of an IS, a secondary source is casted. This secondary source emits a number of rays according to the scattering coefficient. These rays are then traced up to the transition order. Additionally, the emitted rays, again cast a new secondary source at each wall impact.

After the transition order is reached, the reflections are handled by a randomization process, similar as described in Section 2.6.2. The main difference is the treatment of the wall hits. If a ray hits a wall, the hit creates a secondary source, which is radiating into the hemisphere according to Lambert's law. Each of the created secondary sources contribute to all visible receivers. The direction of the ray, which hits the wall, is then determined by the method described in 2.6.2.

2.6.5 Diffused Energy Decay with Reverberation Time of the Room

The main assumption in this method is the decay of the diffused reflected energy with the reverberation time of the room. The prediction of the energy decay is done by Sabine's or Eyring's Formula. With the estimated decay, the temporal smearing of the diffused reflections is simulated. If a ray hits a wall, a fraction of the energy is accounted as diffuse reflected energy. This fraction of energy is then decaying with the beforehand estimated energy decay. The result of the calculated decay is then processed with the ray-tracing model and will simulate the time-smearing effect of the diffuse reflections. The energy decay approach was used by several authors [MM76][HSP80][NMT93]. However, the spatial distribution is not taken into account in their publications. Therefore, Lam introduced a modified approach called the modified scattered diffuse energy model (SU model) [Lam96].

2.6.6 Filters on Specular Paths

This method was described first by Borish in [Bor84a]. In this method, the specular paths are calculated. Also, for every specular reflection a filter is estimated and applied. This filter accounts for the temporal smearing of the specular reflection. One disadvantage of this method is the production of the diffuse reflection with only one specular path. Due to this, no spatial distribution is produced. An similar approach was proposed by D'Antonio, with the difference of incorporating measured or theoretically calculated scattering coefficients.

2. GEOMETRIC ROOM ACOUSTICS

2.6.7 Approximate Cone-Tracing

The only beam-tracing technique that is able to handle diffuse reflections is the approach based on approximate beam tracing, introduced by Dalenbäck [Dal96]. The term approximate cone-tracing is used, as only the center ray is traced and not the cone itself. The basis of modeling diffuse reflection is the division of the diffuse reflecting surface into patches. The properties of these patches are defined by the absorption and the scattering coefficient. These patches then will act as a secondary source for diffuse reflections. The algorithm uses the concept of “passes” along the reflecting surfaces of the room. Initially, the primary-rays (specular rays) are traced and at impact with a patch, the energy carried by these primary rays is captured for the corresponding patch and attenuated according to the scattering coefficient. The captured energy is stored in the “primary list” of all patches. This “primary list” can be seen as an impulse response of the stored energy in the patches. The center of the patches then acts as a secondary source, which sends out secondary rays in the next pass. The rays emitted by the source are weighted by the reflection model e.g. Lambert’s law. If a ray encounters a receiver, not only the particular reflection is added to the echogram (energy-time response) but the whole “primary list” that is associated with the patch. The same principle applies for the secondary rays. If a secondary ray hits a diffuse reflecting patch, the energy is stored in the “secondary list”. Additionally, the primary list is adjusted by the scattering coefficient and the absorption. At the end of the second pass, the secondary list is used as the primary list for the second pass. This procedure is then repeated, until the necessary detail is reached.

2.6.8 Image Sources

In contrast to most other methods, this method utilizes image sources to model the diffuse reflections. The use of image source clouds was briefly considered by Lehnert and Blauert in [LB92], but not further discussed. For the simulation, the assumption is stated, that the diffuse reflections can be modelled as spatially spread specular reflections. In [DKS94], Dalenbäck described this method more in detail. The possible locations of the image sources are determined by the location of the source, the receiver and the diffuser as well as the size of the diffusor. In Figure 2.2 the creation of a valid image source space in the 2-dimensional case is shown. The half-spheres are created by the distance from the source to the diffuser edges P and Q, respectively. The edges determine the center of the half-spheres with a radius of p and q. The valid positions are then determined by the non-overlapping areas of the half-spheres. These non-overlapping areas correspond to positions with a higher distance to the receiver, compared to the specular source. Additional to the non-overlapping areas, the diffuse image sources are only allowed to be placed in a narrow cone.

Another approach to model diffuse reflections with image sources was done by Siltanen et al. in

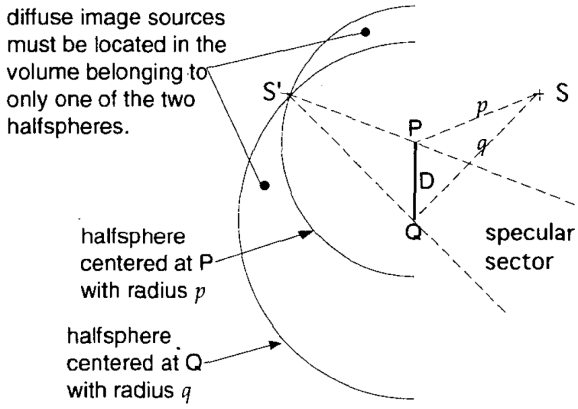


Figure 2.2: Handling of diffuse reflections with image sources after [DKS94].

[SLTS12]. Instead of modeling the diffuse reflections with Lambert's Law, they incorporated the more generalized model by Biot [Bio68]. The drawback of their method is the validity for mid- or high-frequencies. In their proposed approach the model is valid for frequencies lower than 500Hz, which depends on the roughness of the surface.

2.7 Summary

The modeling of diffuse reflections is a hard task, especially in geometric room acoustics. Most of the approaches were developed and validated in terms of auralization and estimation of room acoustic parameters. One reason for the issues with these models is the use of Lambert's Law, to model the diffuse reflections. It is a good approximation in terms of modeling the diffuse reflections in the later part of the RIR. For the modeling of the diffuse reflections, occurring at early reflections from the boundaries in an enclosed space, it is mostly not sufficient. Another reason is the specific properties of the reflecting surface. The shape of a surface determines the amount of scattered energy as well as the frequency dependency and the direction of the diffusely reflected sound.

In geometric room acoustics, there are a lot of different factors, which can lead to a false simulation of the room properties. Geometric room acoustics only can model the properties for higher frequencies. The assumptions that are made in geometrical room acoustics do not hold for low frequencies, as the wave-based effects are neglected. Therefore, the existing methods used in geometric room acoustics, are able to simulate the properties or the RIR only to a certain degree of accuracy. In terms of modeling specular reflections, the image source method and the beam-tracing method can yield exact results. For the modeling of diffuse reflections, the existing methods are also limited in accuracy. The method that utilizes randomization of the directions is sufficient for the later diffuse reflections. Similarly, the acoustic radiosity method is limited

2. GEOMETRIC ROOM ACOUSTICS

due to the assumption of only ideal diffuse reflections with Lambert's law. For the modeling of diffuse reflections for the early part and therefore for the important reflections, other ways to model them have to be introduced.

Chapter 3

Simulation of First-Order Diffuse Reflections

In this chapter, a description of the implemented RIR generator for the first-order diffuse reflections is given. It deals with the handling of diffusely reflecting walls and the issue of how model a diffuse reflecting environment for the first-order diffused reflections. First, an overview and the concept of the implemented RIR generator is presented. Afterwards, the calculation of the pressure impulse response and the determination of the strength of the diffuse reflection for three different methods is described. Also, a brief comparison of the three different implemented methods is carried out.

3.1 Overview

The basis of the algorithm for calculating the first-order diffuse reflections is an already implemented RIR generator, based on the Image Source Method. Therefore, the specular part was not implemented and will not be described in this chapter. In [Hab06], a detailed explanation of the used method can be found¹. This implementation was kindly provided by Prof. Dr. ir. Emanuël Habets². The calculation of the RIR is done in the frequency domain, due to the frequency dependency of the scattering coefficient. As described in Chapter 2, the scattering coefficient describes the amount of diffusely reflected energy and is taken into account to calculate the energy of the diffuse reflections. Also, contrasting to existing RIR generators, which can handle diffuse reflections, the RIR is not obtained by the time-energy histogram as in ray-based approaches. The pressure impulse response is directly calculated in a similar manner as in the

¹The implementation referred here, is done in the time domain but is equivalent to the frequency domain implementation.

²<https://www.audiolabs-erlangen.de/fau/professor/habets>

3. SIMULATION OF FIRST-ORDER DIFFUSE REFLECTIONS

image source method. For the determination of the whole impulse response, the room transfer functions of the specular and the first-order diffused parts are calculated and combined as

$$H_{ov}(\omega) = H_{sp}(\omega) + H_{diff}(\omega), \quad (3.1)$$

where $H_{ov}(\omega)$ is the overall room transfer function³, $H_{sp}(\omega)$ the specular transfer function and $H_{diff}(\omega)$ the transfer function of the first-order diffuse reflections.

The specular part of the impulse response is calculated by the image source method. In the time domain, the reflections are modeled as delayed Dirac impulses with a certain attenuation. The impulse response h_{diff} is then described by

$$h_{diff}(t) = \sum_{i=1}^R a_i \delta(t - \tau_i), \quad (3.2)$$

where $\delta(t)$ is the dirac impulse, R is the number of diffuse reflections, a_i is the attenuation of the i -th reflection and τ_i is the delay of the i -th reflection.

In the frequency domain this reads as

$$H_{diff}(\omega) = \sum_{i=1}^R a_i(\omega) e^{-j\omega\tau_i}. \quad (3.3)$$

For the modeling of the diffuse reflections, it has to be obtained which attenuation should be assigned to the diffuse reflections. Further, the delay of the diffuse reflections has to be obtained. In the following, the concept of how these diffuse reflections are modeled is described.

3.1.1 Concept

The modeling of the diffuse reflections is done similarly to the radiosity method. In the radiosity method, the reflecting boundaries of a room (walls, floor, and ceiling) are divided into diffuse reflecting patches. The difference to the radiosity method is the determination of the strength and the direction of the diffuse reflections. In Figure 3.1, the split up into squared diffusely reflecting patches is shown. For the modeling of the diffuse reflections, one patch is represented by a sound source which will contribute to the final obtained impulse response. These sources are placed on each reflecting boundary, with a selectable spacing d_{ph} between each adjacent sound source. Hence, the geometry of the patches is squared, and the area of one patch is described by $A_p = d_{ph}^2$. In the following, the diffuse reflecting sources will be referred to as

³The room transfer function is the fourier transform of the room impulse response $H(\omega) = \mathcal{F}\{h(t)\}$.

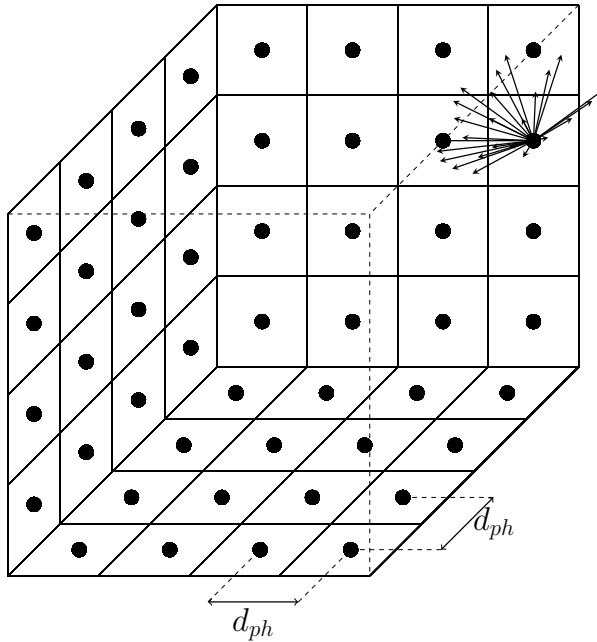


Figure 3.1: Schematic depiction of the divided surfaces into patches with the phantom sources indicated by the black spots

“phantom image sources” or only “phantom sources”. This implementation is only able to handle shoe-box (rectangular) rooms. The scattering coefficient can be chosen individually for each of the reflecting boundaries.

The basic concept of this model is the assumption that at every point at a wall a reflection occurs. If a sound source is emitting a spherical wave, the wave will be reflected at each point of a wall. These points of reflections then are described by the phantom image sources. The phantom image sources are used to model the point of reflection as a new sound source, which will contribute as a diffuse reflection. Also, a part of the sound is reflected specularly, which will not contribute as a reflection in the final impulse response. Therefore, the phantom image sources are only able to contribute to the impulse response with the diffuse portion of the reflection. The diffuse amount of the energy is then scattered into non-specular directions. The possible directions of the non-specular reflection depend on the scattering distribution that is used and therefore if the phantom source will contribute to the diffuse part of the impulse response. Instead of deciding, whether the reflection is contributing as a diffuse reflection by comparing a random number with the scattering coefficient, the phantom image sources will always contribute if the receiver lies within the possible directions. When the phantom source is contributing to the diffuse impulse response, the question is, at which strength these phantom sources should contribute to the diffuse impulse response. The strength of the diffuse reflection depends on a variety of different factors: air absorption, reflection coefficient, scattering coefficient, and the scattering distribution. In the following, the modeling of the diffuse reflection and the determination of the

3. SIMULATION OF FIRST-ORDER DIFFUSE REFLECTIONS

diffuse reflections is described in detail.

3.2 Specular Direction and Diffuse Direction

For the determination of the strength of the diffuse reflection, two directions have to be known - the direction of the incident specular reflection and the direction of the diffuse reflection. The direction of the incident specular reflection can be determined by the position of the source and the receiver. The incident direction of the specular reflection is then described by

$$\mathbf{v}_{sp,inc} = \mathbf{p}_{ph,i} - \mathbf{p}_{src}, \quad (3.4)$$

where $\mathbf{v}_{sp,inc}$ is the direction of the specular incident reflection, $\mathbf{p}_{ph,i} = [x_{ph,i} \ y_{ph,i} \ z_{ph,i}]$ is the position of the i -th phantom source and $\mathbf{p}_{src} = [x_{src} \ y_{src} \ z_{src}]$ the position of the sound source. The outgoing direction of the specular reflection $\mathbf{v}_{sp,out}$ is then determined by Equation 2.1. The diffuse direction is obtained in the same manner by the position of the phantom image source and the receiver position $\mathbf{p}_{rec} = [x_{rec} \ y_{rec} \ z_{rec}]$ as

$$\mathbf{v}_{diff} = \mathbf{p}_{rec} - \mathbf{p}_{ph,i} \quad (3.5)$$

3.3 Air Absorption and Delay

The attenuation due to the air absorption is calculated by the $\frac{1}{r^2}$ law. It states that the energy of the sound is proportional to the inverse of the squared length of the traveled distance r . As we are obtaining the pressure impulse response, this law can be taken into account by taking the square root of the energy based law.

The factor that describes the attenuation due to the air is defined by

$$\frac{1}{4\pi r}. \quad (3.6)$$

The important part of this relation is the determination of the traveled distance for a diffuse reflection. As mentioned above, the diffuse reflections are generated by the phantom image sources. Thus, the overall path length is described by the length of the specular path and the diffuse path. The specular path is defined as the path length from source to the phantom image source $\|\mathbf{v}_{sp,inc}\|$. The diffuse path length is defined as the path from the phantom image source to the receiver $\|\mathbf{v}_{diff}\|$. Then, both paths combined will correspond to the path length of the whole reflection. The overall path length for one diffuse reflection is then obtained by

$$r = \|\mathbf{v}_{sp,inc}\| + \|\mathbf{v}_{diff}\|. \quad (3.7)$$

With the knowledge of the path length, the delay time (or travel time) τ of the diffuse reflection is simply obtained by

$$\tau = \frac{r}{c}, \quad (3.8)$$

where c is the speed of sound in air ($c = 343 \frac{\text{m}}{\text{s}}$).

3.4 Reflection Factor

The reflection factor describes the amount of the overall reflected portion of a wall reflection. The reflection factor is directly related to the absorption coefficient described in Section 2.1.4. The reflection factor, has to be included in the model, as the absorption due to the walls has to be taken into account. The reflection factor β is defined as

$$\beta(\omega) = \sqrt{1 - \alpha(\omega)}, \quad (3.9)$$

where α is the energy-based reflection coefficient.

3.5 Diffusion Strength Factor

The diffusion strength factor is used to describe the strength or attenuation of the diffuse reflection. The diffusion strength factor should not be confused with the diffusion coefficient (see Section 2.1.6). This factor is dependent on the used scattering distribution. In the algorithm, three different types of scattering distributions are implemented. These are the Lambertian distribution, a tilted version of the Lambertian distribution and vector mixing (VM). VM also uses the Lambertian distribution but takes the scattering coefficient for the possible directions into account. In the following, the computation of the diffusion strength factor for the three different distribution is carried out. Here, the factor is obtained in terms of their intensity. How these factors are incorporated for obtaining the pressure response is defined in Section 3.8.

3.5.1 Lambertian Distribution

The calculation of the diffusion strength coefficient for the Lambertian distribution is straightforward and can be directly calculated with the knowledge about the position of the phantom source and the receiver. As described in Equation 2.2, the intensity is proportional to the cosine of the diffuse reflection. The angle of the diffuse reflection is obtained by the diffuse vector \mathbf{v}_{diff} and the wall normal \mathbf{n} (normal vector of the reflecting surface) of the phantom source, as seen in

3. SIMULATION OF FIRST-ORDER DIFFUSE REFLECTIONS

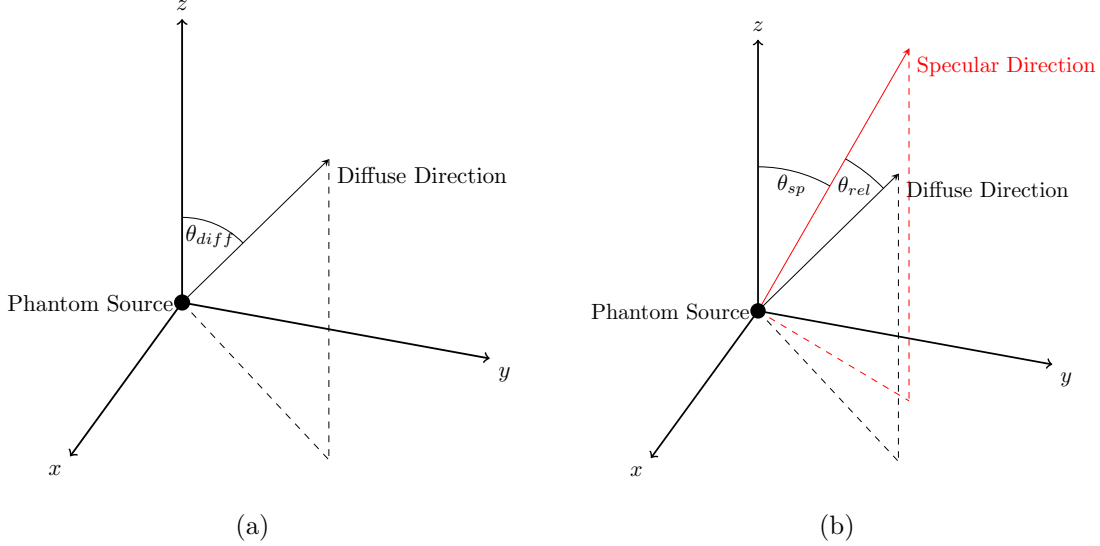


Figure 3.2: Schematic depiction of the used reflection angles for Lambertian distribution θ_{diff} in (a) and for the tilted Lambertian distribution θ_{rel} in (b). The z-axis corresponds to the wall normal of the reflecting surface.

Figure 3.2a. The angle θ_{diff} is then calculated by

$$\theta_{diff} = \text{atan} \left(\frac{\|\mathbf{v}_{diff} \times \mathbf{n}\|}{\mathbf{v}_{diff} \cdot \mathbf{n}} \right). \quad (3.10)$$

The diffusion strength factor d is directly obtained by the Lambertian cosine law, as

$$d = \cos(\theta_{diff}). \quad (3.11)$$

3.5.2 Tilted Lambertian Distribution

A way to achieve a directionality is to take the specular direction into account and tilt the Lambertian distribution according to the outgoing specular vector. The angle θ_{rel} used to calculate the diffuse coefficient, is the angle between the diffuse direction and the specular direction (see Figure 3.2a). The diffusion strength factor can then be determined by

$$d = \cos(\theta_{sp} - \theta_{diff}) = \cos(\theta_{rel}), \quad (3.12)$$

where θ_{sp} is the angle between the specular direction and the corresponding wall normal and is

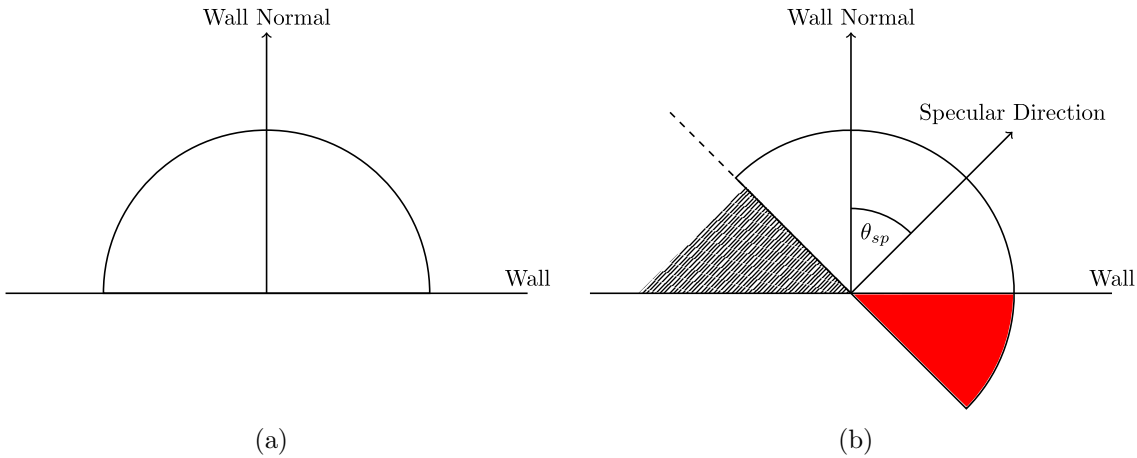


Figure 3.3: Scattering directions of the Lambertian distribution in (a) and the tilted Lambertian distribution in (b) indicated by semicircle in 2D.

calculated by

$$\theta_{sp} = \text{atan} \left(\frac{\|\mathbf{v}_{sp,inc} \times \mathbf{n}\|}{\mathbf{v}_{sp,inc} \cdot \mathbf{n}} \right). \quad (3.13)$$

The main difference between the normal Lambertian distribution and the tilted Lambertian distribution is the directionality now gained through the dependency on the specular direction. Also, as in [Chr05] described, the tilt of the distribution leads to a “shadow zone”, where no diffuse reflection occurs. In Figure 3.3, the directions of the scattering of the Lambertian and the tilted Lambertian distributions are shown. In Figure 3.3b, the “shadow zone”, created by the tilt is indicated by the shaded area.

3.5.3 Vector Mixing

In VM, the determination of the diffusion strength factor is not as straightforward as with the Lambertian or tilted Lambertian distribution. As described in Section 2.6, the possible directions are determined by the mixing of the specular reflection direction and the diffuse reflection direction scaled by the scattering coefficient. Hence, the possible directions of the diffuse reflection depend on the specular direction as well as on the scattering coefficient $s(\omega)$. In the following the frequency dependency of $s(\omega)$ is omitted for the sake of simplicity.

For taking every possible diffuse direction into account, the scattered directions can be described by a hemisphere with a radius of s . The potential directions of the diffuse reflections then are

3. SIMULATION OF FIRST-ORDER DIFFUSE REFLECTIONS

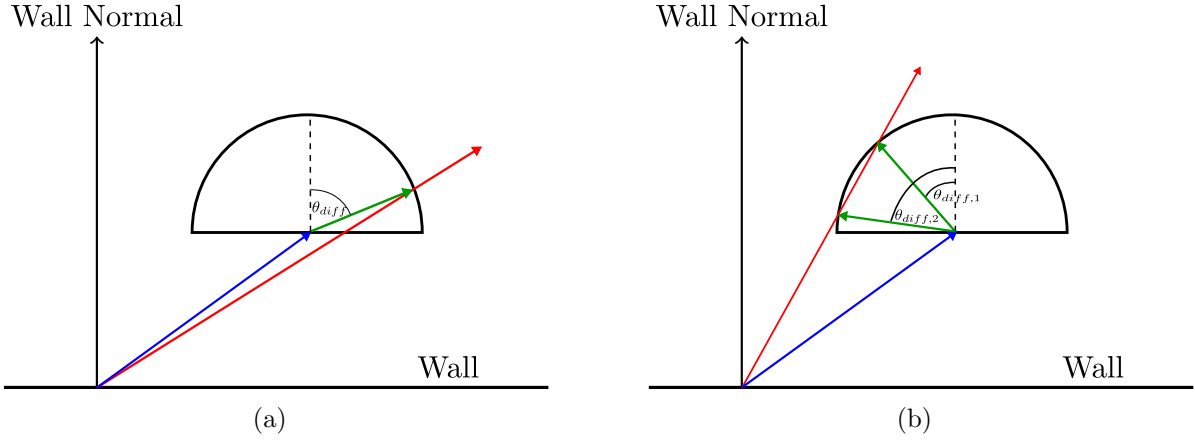


Figure 3.4: Schematic depiction of vector mixing for the case of one diffuse help vector in (a) and for the case of two diffuse help vectors in (b).

defined by

$$\mathbf{v}_{hem}(\theta, \phi) = \begin{pmatrix} x_{hem}(\theta, \phi) \\ y_{hem}(\theta, \phi) \\ z_{hem}(\theta, \phi) \end{pmatrix} = s \begin{pmatrix} \sin(\theta) \cos(\phi) \\ \sin(\theta) \sin(\phi) \\ \cos(\theta) \end{pmatrix} \quad \text{with} \quad 0 \leq \theta \leq \frac{\pi}{2}, \quad 0 \leq \phi \leq 2\pi \quad (3.14)$$

where $\mathbf{v}_{hem}(\theta, \phi)$ describes all possible diffuse reflections in dependency of the elevation θ and the azimuth ϕ . Note, that Equation 3.14 only holds, if the wall normal is described by $\mathbf{n} = [0 \ 0 \ 1]$. For other cases the direction of the hemisphere has to be changed according to the direction of the wall normal.

The hemisphere is then added with the normalized specular direction scaled by $(1 - s)$. Then all possible diffuse directions, with respect to the reflection point, can be written as

$$\mathbf{v}_{dir}(\theta, \phi) = (1 - s) \frac{\mathbf{v}_{sp,out}}{\|\mathbf{v}_{sp,out}\|} + \mathbf{v}_{hem}(\theta, \phi) \quad (3.15)$$

with $\mathbf{v}_{dir}(\theta, \phi)$ as all possible diffuse directions.

The reflection contribute as a diffuse reflection, if the diffuse direction vector \mathbf{v}_{diff} lies within the directions described by \mathbf{v}_{dir} . For a small scattering coefficient, the reflection tends to a specular direction, and for a high scattering coefficient, the diffuse reflection will be reflected in more directions. These properties are discussed more in detail in Section 3.11.

The diffusion strength factor for VM is not found by the diffuse direction, but is found by the diffuse help vector as seen in Figure 3.4a. Hereby, the blue vector indicates the scaled specular direction, the red vector indicates the diffuse direction, and the green vector corresponds to the diffuse help vector. The diffuse help vector is calculated with the help of the specular direction,

the diffuse direction, and the scattering coefficient. The diffusion strength factor is obtained in the same way as in the Lambertian distribution, by the angle of the diffuse help vector to the wall normal (see Equation 3.11). One property and difference to Lambertian and the tilted Lambertian distribution is the probability of the existence of two diffuse help vectors. Due to the convexity of the hemisphere, there are cases where \mathbf{v}_{diff} can be defined by two different diffuse help vectors. This case is depicted in Figure 3.4b, where the direction of the diffuse vector is equal to two different possible diffuse help directions. In this case, the diffusion strength factor is found by adding up the diffusion strength factors found by the two diffuse help vectors. For the determination of the diffuse help vector Equation 2.12 can be written as

$$\mathbf{v}_{diff,help} = \mathbf{v}_{diff} - (1-s) \frac{\mathbf{v}_{sp,out}}{\|\mathbf{v}_{sp,out}\|} \quad (3.16)$$

To obtain, if the reflection lies within the possible direction and to find the diffuse help vector, the line-sphere intersection relation from analytic geometry is used. The circumstance that a sphere is used in a relationship described by a hemisphere will be accounted for later. This relation can be expressed as

$$t_{1/2} = -(\mathbf{l} \cdot (\mathbf{o} - \mathbf{c})) \pm \sqrt{(\mathbf{l} \cdot (\mathbf{o} - \mathbf{c}))^2 - (\|\mathbf{o} - \mathbf{c}\|^2 - r^2)} \quad (3.17)$$

where t describes the distance along the line, \mathbf{l} describes the direction of the line intersecting with the sphere, \mathbf{o} is the origin of the line and r the radius of the sphere. The need for this calculation is due the fact, that the direction of the resulting vector \mathbf{v}_{diff} is known, but not its length. With the knowledge about the direction of the diffuse reflection and the direction of the specular reflection, the distance to the intersection points and therefore the length of the reflection vectors can be found. Substituting Equation 3.17 to match VM, it can be written as

$$t_{1/2} = -(\mathbf{v}_{diff} \cdot (-\mathbf{v}_{center})) \pm \sqrt{(\mathbf{v}_{diff} \cdot (-\mathbf{v}_{center}))^2 - (\|\mathbf{-v}_{center}\|^2 - s^2)} \quad (3.18)$$

where $\mathbf{v}_{center} = (1-s) \frac{\mathbf{v}_{sp,out}}{\|\mathbf{v}_{sp,out}\|}$ is determined by the scaled normalized specular vector, \mathbf{o} is omitted as the origin of the line is used as the origin of the coordinate system, the direction of the line is described by the diffuse vector \mathbf{v}_{diff} and the radius of the sphere corresponds to the scattering coefficient s .

The intersection points and therefore the scaled diffuse vectors are calculated by

$$\mathbf{v}_{diff,scaled,1/2} = \frac{\mathbf{v}_{diff}}{\|\mathbf{v}_{diff}\|} t_{1/2} \quad (3.19)$$

Now it has to be accounted for, that the calculation of the intersection points is carried out with

3. SIMULATION OF FIRST-ORDER DIFFUSE REFLECTIONS

respect to a sphere. Hence, every intersection point that lies in the lower half of the sphere has to be omitted, as these intersection points do not correspond to valid diffuse reflection vectors. A valid diffuse reflection vector is found if the intersection point lies in the upper half of the sphere with respect to the wall. This relation can be described as

$$|\mathbf{v}_{diff,scaled,1/2} \cdot \mathbf{n}| > |\mathbf{v}_{center} \cdot \mathbf{n}| \quad (3.20)$$

where \mathbf{n} is the normal to the corresponding reflecting wall.

The diffuse help vectors are then found by Equation 3.16. The corresponding angles between the wall normal \mathbf{n} and $\mathbf{v}_{diff,help}$ is calculated in the same manner as in Equation 3.10 and Equation 3.13 as

$$\theta_{diff,1/2} = \text{atan} \left(\frac{\|\mathbf{v}_{diff,scaled,1/2} \times \mathbf{n}\|}{\mathbf{v}_{diff,scaled,1/2} \cdot \mathbf{n}} \right) \quad (3.21)$$

For no valid intersection point, no diffuse reflection occurs and therefore $d = 0$. In the case of one valid intersection point, the calculation of d is determined as in Equation 3.11. In the case of two valid reflection points, the diffusion strength factor is calculated by

$$d = \cos(\theta_{diff,1}) + \cos(\theta_{diff,2}) \quad (3.22)$$

3.6 Normalization Factor

One important point to consider for the modeling of diffuse reflections is the scattering into more than one direction at a reflection point. Therefore, the scattered energy is not only contained in one diffuse reflection but is split up into all diffuse reflections at a reflection point. To account for this, a normalization taking this effect into account has to be made. The normalization is done by finding all diffusion strength factors for the corresponding distribution. Without the normalization, the assumption of energy conservation would not hold anymore, as the diffuse reflections would lead to a creation of energy.

The total amount of diffusion strength factors is found by the integration of the distribution over all directions, which can again be described by a hemisphere.

3.6.1 Lambertian Distribution

The Lambertian distribution scatters into all directions, described by a hemisphere, therefore the normalization factor can be found in spherical coordinates by

$$1 \stackrel{!}{=} n_{Lam} \iint_{\Omega} \cos(\theta) d\Omega = n_{Lam} \int_0^{2\pi} \int_0^{\pi} \cos(\theta) d\phi d\theta \quad (3.23)$$

$$1 \stackrel{!}{=} n_{Lam} 2\pi \rightarrow n_{Lam} = \frac{1}{2\pi}. \quad (3.24)$$

3.6.2 Tilted Lambertian Distribution

To determine the normalization factor for the tilted Lambertian distribution, the tilt of the distribution has to be taken into account. As described in [Chr05], the tilt of the Lambertian distribution leads to some reflections, which would be reflected into the wall. This effect is depicted in Figure 3.3b. The part which is reflected into the wall is shown as the red area. As reflections into the wall can not occur in a real environment, this loss has to be accounted for. To compensate for this loss of reflections, the normalization factor is corrected according to the specular reflection angle. The normalization factor of the tilted Lambertian distribution n_{Tilt} is then obtained by

$$1 \stackrel{!}{=} n_{Tilt} \int_0^{\pi} \int_0^{pi/2} \cos(\theta) d\theta d\phi + \int_0^{\pi} \int_0^{pi/2 - \theta_{sp}} \cos(\theta) d\theta d\phi \quad (3.25)$$

$$1 \stackrel{!}{=} n_{Tilt} \pi (1 + \cos(\theta_{sp})) \rightarrow n_{Tilt} = \frac{1}{\pi} \frac{1}{1 + \cos(\theta_{sp})}. \quad (3.26)$$

3.6.3 Vector Mixing

The normalization of VM is not a constant factor as in the Lambertian distribution or only dependent on the specular direction as in the tilted Lambertian distribution. In VM, the scattering coefficient determines the possible directions of the diffuse reflections. Hence, the normalization is also dependent on the scattering coefficient. In contrast to the Lambertian (Equation 3.23) and the tilted Lambertian distribution (Equation 3.25), no closed form solution for the normalization factor was found.

The integration is carried out for every possible diffuse direction, hence for directions described by a hemisphere. It means, for every possible diffuse direction the calculation of the diffusion

3. SIMULATION OF FIRST-ORDER DIFFUSE REFLECTIONS

strength factor for VM is applied. The determination of the normalization factor for VM can be written as

$$1 \stackrel{!}{=} n_{VM} \iint_{\Omega} VM(\mathbf{v}(\theta, \phi), s) d\Omega \quad (3.27)$$

$$1 \stackrel{!}{=} n_{VM} \int_0^{2\pi} \int_0^{\pi} VM(\mathbf{v}(\theta, \phi), s) d\phi d\theta \rightarrow n_{VM} = \frac{1}{\int_0^{2\pi} \int_0^{\pi} VM(\mathbf{v}(\theta, \phi), s) d\phi d\theta} \quad (3.28)$$

where $\mathbf{v}(\theta, \phi)$ are the possible diffuse directions and $VM(\mathbf{v}(\theta, \phi), s)$ is used as a placeholder for the calculation process. The calculation process is not further explained. It is the same calculation process as for the determination of the diffusion strength factor explained in 3.5.3. In the implementation this calculation is carried out by numerical integration, to determine the normalization factor.

3.7 Scattering Coefficient

The scattering coefficient describes the amount of specular and diffuse reflected energy (see Section 2.1.5). Hence, the scattering coefficient cannot be taken directly into account when calculating the pressure impulse response. In the model, the scattering coefficient is used to split the amount of diffuse and specular energy. It determines, how much of the energy is diffusely reflected by the phantom sources. Also, the scattering coefficient is used for the specular reflections⁴. The specular reflections also have a diffusely reflected portion and are therefore attenuated according to the scattering coefficient. For this reason, the scattering coefficient has to be used in such a way that it can be directly incorporated for the pressure impulse response. In [MDW⁰¹], Martin used the constant power panning curve, to mix the specular and the diffuse reflections. The specular g_s and the diffuse mixing factor g_d , are obtained after the following relation as

$$g_s^2 + g_d^2 = 1. \quad (3.29)$$

This relation is used to directly obtain the specular and the diffuse mixing factor from the scattering coefficient. The specular and the diffuse mixing component then read as

⁴Here: The specular reflections, which are contributing to the pressure room impulse response, obtained by the image source method.

$$g_s = \cos(s \frac{\pi}{2}) \quad (3.30)$$

$$g_d = \sin(s \frac{\pi}{2}). \quad (3.31)$$

These factors can then be directly incorporated in the obtaining of the strength of the specular and the diffuse reflections.

3.8 Specular and Diffuse Transfer Function

With the described factors above, the room transfer function for the specular and the diffuse reflections can be defined. The transfer function of the specular part is only extended by one factor compared to the original function. In the model, at a reflection point, a portion is always reflected diffusely and specularly. This also holds for the specular reflection obtained by the receiver. Hence, the scattering coefficient is incorporated in the specular transfer function by the specular mixing factor $g_s(\omega)$. The specular transfer function is then described by

$$H_{spec}(\omega) = \sum_{i=1}^S \frac{1}{4\pi r_i} \beta_{ov}(\omega) g_s(\omega) e^{-j\omega\tau_i}, \quad (3.32)$$

where r_i is the path length of the specular reflection, $\beta_{ov}(\omega)$ is the overall reflection factor of all walls involved and τ_i is the delay of the specular reflection.

With the incorporation of the diffuse mixing factor, the specular reflection is attenuated according to the scattering coefficient.

For the diffuse part, all the described factors are now incorporated into the diffuse transfer function. One has to note, that the diffusion strength factor and the normalization factor are factors obtained in terms of intensity. Therefore, the corresponding area of the phantom source A_{ph} is taken into account. This incorporation of the area is justified by the assumption, that for every phantom source, the whole wall patch, represented by a phantom source, is contributing to the reflection and $E \propto IA$. Due to the intensity based determination of d and n , the square root is taken in order to use it in the pressure based room transfer function. Finally, the room transfer function for the diffuse part reads as

$$H_{diff}(\omega) = \sum_{i=1}^M \frac{1}{4\pi r_i} \beta_i(\omega) g_d(\omega) \sqrt{A_{ph,i} d_i(\omega) n_i(\omega)} e^{-j\omega\tau_i}. \quad (3.33)$$

3. SIMULATION OF FIRST-ORDER DIFFUSE REFLECTIONS

With this equation found, the first-order diffuse reflection can be calculated. In the implementation, the scattering coefficient and the reflection factor can be chosen individually for each of the six reflecting boundaries. As these two factors are frequency dependent factors, they can be selected individually for specific frequency bands. The frequency dependent calculation is then proceeded for every frequency bin. To obtain the scattering coefficients and the absorption factor, a linear interpolation between the chosen factors in the frequency bins is proceeded.

3.9 High-Pass Filter

The modeling of the diffuse reflections is based on a geometric model. Therefore, the simulation is only valid for high frequencies. For this reason, a high-pass filter is included to filter the diffuse impulse response for non-valid frequencies. The high-pass filter is implemented in the same way as described in [AB79].

3.10 Computational Complexity

When using VM, one issue that has to be considered for the implementation is the high complexity of calculation of the diffuse impulse response. For the calculation of the first-order diffuse reflections with the Lambertian or the tilted Lambertian distribution, the complexity of the algorithm is on an acceptable level, as the frequency dependent factors are taken into account only by the calculation of the overall transfer function. Here, the diffusion strength factor and the normalization factor just have to be calculated for each phantom source individually. In contrast to that, VM is of high complexity due to the frequency dependency of the directions and therefore, of the normalization. Hence, the diffusion strength factor and the normalization factor have to be calculated individually for every frequency bin, and then this calculation has to be done for every phantom source.

To deal with the complexity problem, especially in VM, the easiest way to speed up the calculation is the parallelization of the calculation process of diffusion strength factor and the normalization factor. However, the speeding up due to parallelization is limited to the available parallel calculation processes. For a more efficient way, the costliest calculation step should be simplified. Therefore, the normalization factors were pre-calculated for every combination of the scattering coefficient and the specular reflection directions. These values were then stored in a lookup table.

The possible specular reflection directions are described by

$$\mathbf{v}_{sp,pre}(\theta, \phi) = \begin{pmatrix} x_{sp,pre}(\theta, \phi) \\ y_{sp,pre}(\theta, \phi) \\ z_{sp,pre}(\theta, \phi) \end{pmatrix} = \begin{pmatrix} \sin(\theta) \cos(\phi) \\ \sin(\theta) \sin(\phi) \\ \cos(\theta) \end{pmatrix} \quad \text{with} \quad \begin{aligned} 0 \leq \theta &\leq \frac{\pi}{2} \\ 0 \leq \phi &\leq 2\pi \end{aligned} \quad (3.34)$$

As this is a discretized calculation, the angular resolution, as well as the resolution of the scattering coefficients, are limited. The chosen angular resolution for θ and ϕ was determined to 0.5° and the resolution of s to 0.05. To obtain the calculated normalization factors, the scattering coefficient and the specular direction vector have to be the same as the ones used in the pre-calculation. Due to the limited angular resolution, the used pre-calculated vector must satisfy the following condition written as

$$\operatorname{argmin}_{\mathbf{v} \in \mathbf{V}} \left(\left\| \mathbf{v} - \frac{\mathbf{v}_{sp,out}}{\|\mathbf{v}_{sp,out}\|} \right\| \right), \quad (3.35)$$

where \mathbf{V} is the set of vectors pre-calculated by Equation 3.34 and $\mathbf{v}_{sp,out}$ is the outgoing specular reflection vector. Here, the Euclidean distance is used to find the most similar vector compared to the outgoing specular reflection vector. The Euclidean distance can be used, as the vectors are normalized and share the same origin.

For the examination of the effect of the lookup table the simulation time, a comparison with and without the use of the described look-up table was made. The chosen number of phantom sources is $N_{ph} = 11500$ and the number of frequency bins $N_f = 4097$. Here, the sampling frequency is not important, as it defines the maximum simulatable frequency and the frequency resolution. Therefore, the simulation time is not affected by the sampling frequency. The simulation was done 15 times and the mean calculation time is shown in Table 3.1. With the use of a lookup

	With Look-Up Table	Without Look-Up Table
Simulation Time in s	74.91	875.46

Table 3.1: Simulation time of the diffuse reflections with and without lookup table.

table, the calculation was sped up by a factor of over 10. This speedup is essential, as the simulation will be used to calculate a high amount of RIRs (see Section 4.2). Here, it has to be noted, that the calculation time can differ from the ones obtained due to the different processing power of the computer used for the calculation.

3. SIMULATION OF FIRST-ORDER DIFFUSE REFLECTIONS

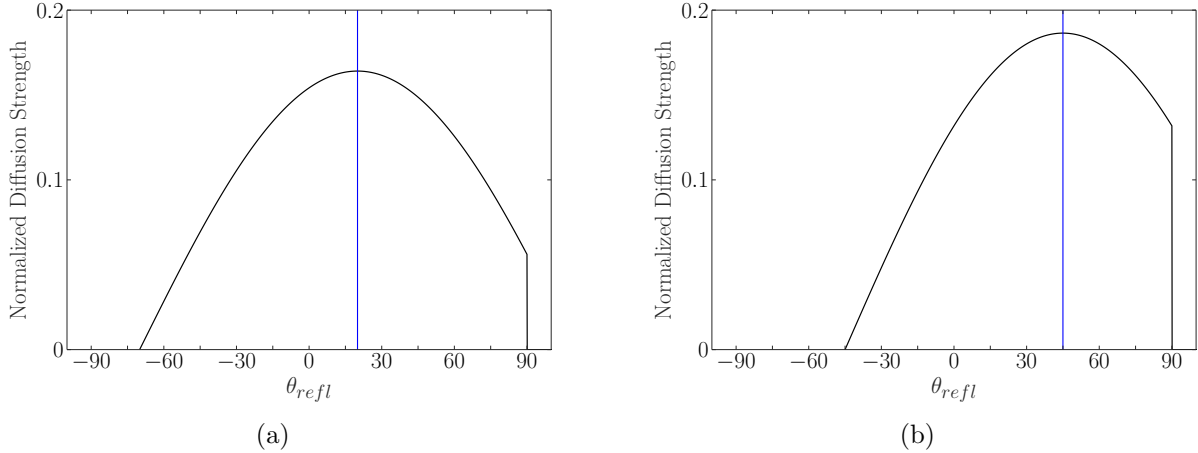


Figure 3.5: Directional distribution of the diffusion strength factor of the tilted Lambertian distribution for $\theta_{sp} = 20^\circ$ in (a) and $\theta_{sp} = 45^\circ$ in (b).

3.11 Comparison of the Different Distributions

In the following, a comparison between the three different methods (the Lambertian distribution, the tilted Lambertian distribution as well as the VM) and their expected behavior is carried out.

The main difference between the three implemented methods or distributions is their behavior in terms of the directionality. Here, the term specular direction describes the direction of the specular direction as defined in 3.2.

3.11.1 Lambertian Distribution

As the Lambertian distribution has no directionality at all, the diffusion strength factor only depends on the direction of the diffuse reflection. This means the direction of the specular reflection is not influencing the behavior of the distribution. In the case of the implemented method, every phantom source will contribute to the final obtained diffuse first-order reflections, no matter how the parameters are chosen.

3.11.2 Tilted Lambertian Distribution

The tilted Lambertian distribution has in contrast to the Lambertian distribution a higher directionality due to the tilt with the specular direction. It will lead to different behavior regarding the directionality compared to the Lambertian distribution. In Figure 3.5, the reflection distributions - or more specific the normalized diffusion strength factor for two different specular reflection angles 20° and 45° , can be seen. In the Figures, the blue line indicates the direction of the specular reflection. The angles of -90° and 90° correspond to the walls and

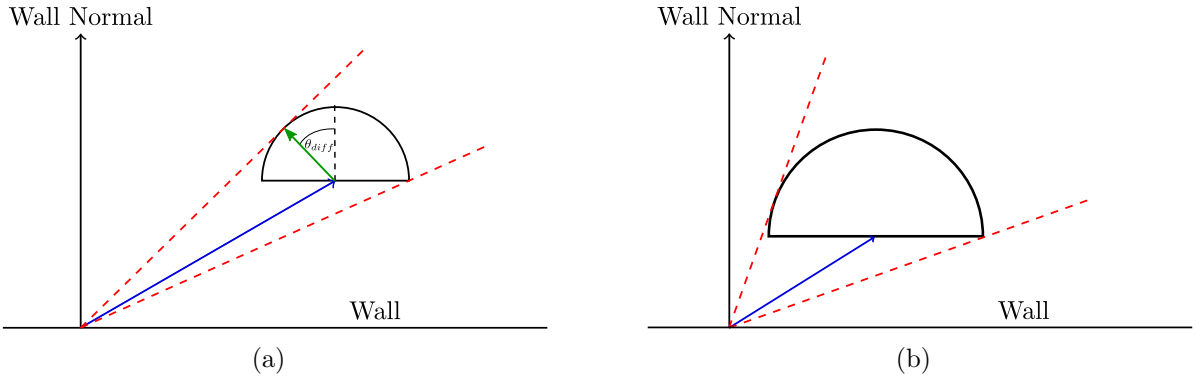


Figure 3.6: Possible directions of the vector mixing method for a small scattering coefficient (a) and a higher scattering coefficient (b).

therefore, to the maximum possible reflection angle. Note, that this depiction is in 2D, but the distribution is implemented in 3D. This depiction is valid for the 3D case, as it can be applied to every reflection angle due to symmetry. It can be seen, that the maximum of the distribution is always at the direction of the specular outgoing reflection. Furthermore, there is no contribution to the "shadow-zone". Hence, the tilted Lambertian distribution leads to regions where no diffuse reflection can occur.

Due to this directionality, the tilted Lambertian distribution will lead to stronger diffuse reflection at the real specular reflection⁵. The diffuse direction of phantom sources, which are positioned near the real specular reflection point of the original sound source, will have similar directions compared to their corresponding specular reflection direction. Therefore, the reflections around the real specular reflection should have a higher amplitude compared to the Lambertian distribution. Reflection points, which do not lie in the region of the specular reflection, will have a higher attenuation due to the higher difference to the specular reflection. Also, there will be phantom sources which will not contribute to the diffuse impulse response due to the "shadow-zone" introduced by the tilt of the Lambertian distribution. For this reason, the Lambertian distribution and the tilted Lambertian distribution should lead to a different first-order diffused reflection for the same set-up.

3.11.3 Vector Mixing

A direct comparison of VM in terms of directionality is hardly possible, as the directionality is dependent on the scattering coefficient as well as on the specular direction. With the combination of the scattering coefficient and the specular direction, the highest directionality can be achieved. In terms of directionality, the VM method can behave as a specular reflection or as completely diffuse as the Lambertian distribution. These edge cases occur for the scattering coefficient of

⁵Here, the real specular reflection is the specular reflection obtained by the IS method

3. SIMULATION OF FIRST-ORDER DIFFUSE REFLECTIONS

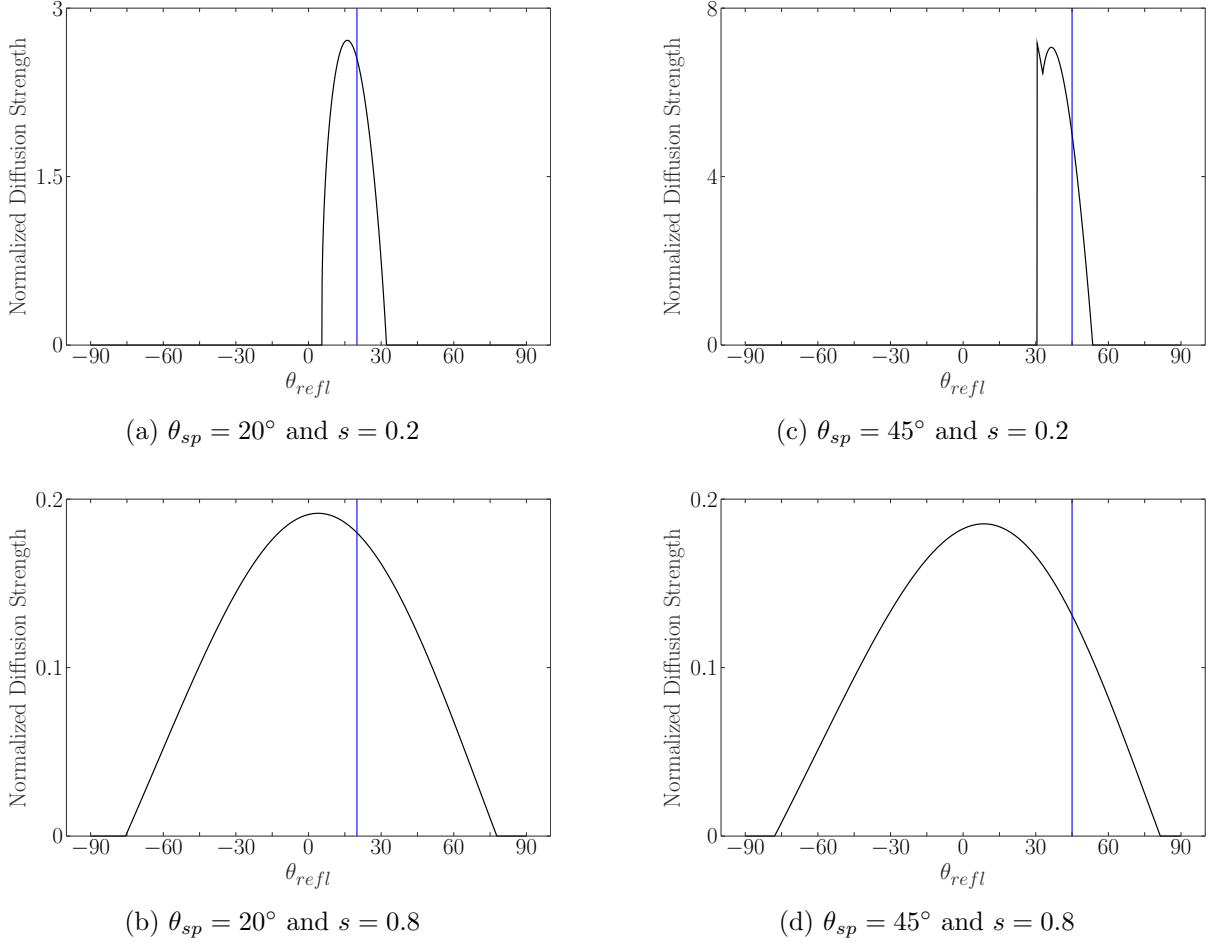


Figure 3.7: Directional distribution of the diffusion strength factor for different specular reflection angles and scattering coefficients.

$s=0$ (specular) or for $s=1$ (completely diffuse). In these cases, the diffuse component or the specular component in VM are completely vanished (see Equation 3.14 and Equation 3.15). In-between these edge cases, the directionality is higher for lower scattering coefficient.

In Figure 3.6, the directions for the same incident specular reflection angle and different scattering coefficient are depicted schematically. In Figure 3.6a, the higher directionality due to the smaller scattering coefficient is seen. The red dashed lines indicate the maximum possible directions. The opening of this cone highly depends on the radius of the hemisphere and therefore on the scattering coefficient. In Figure 3.6a, another effect caused by the convexity of the hemisphere is depicted. In the case of a small scattering coefficient or a high specular reflection angle, the limit of the direction does not correspond to a diffuse angle of 90° . In Figure 3.6a, this case is indicated by the green diffuse help vector, where the direction limit is not defined by $\theta_{diff} = 90^\circ$ but by an angle other than 90° . Therefore, at low scattering coefficients or a high specular reflection angle (w.r.t. the wall normal), the VM method can lead to an abrupt drop of the

diffusion strength factor at the edge of the possible directions.

In Figure 3.7c, the distribution of such a case is shown. It illustrates the VM distribution for a specular reflection angle of $\theta_{sp} = 45^\circ$. At the reflection angle of about 30° , the above-described case occurs. Also, a second peak after the abrupt drop occurs in the distribution of the normalized diffusion strength factor due to two valid diffuse help vectors in this region. Hence, a slight change of the diffuse direction can lead from a strong diffuse reflection to no diffuse reflection. Another difference compared to the tilted Lambertian distribution is the different location of the maximum of the diffuse reflections.

In VM, the maximum of the diffuse reflection is only located in the direction of the specular reflection if $s=0$. This effect is caused by the use of the scattering hemisphere perpendicular to the reflecting boundary. Only for a specular incident angle of $\theta_{diff} = 0^\circ$, the maximum of the diffuse reflection would correspond to the specular direction. For the other cases, the maximum of the diffusion strength factor is always shifted w.r.t to the specular direction. In addition, this shift of the maximum is more pronounced for a higher specular reflection direction (compare Figure 3.7a and Figure 3.7c). Also, the loss of directionality of the VM method is shown in Figure 3.7b and Figure 3.7d. Only a slight change of the directionality can be observed for both cases of $\theta_{sp} = 20^\circ$ and $\theta_{sp} = 45^\circ$.

In overall, the Lambertian distribution is the easiest way to model diffuse reflections. Due to the non-directionality, the Lambertian distribution only holds for edge cases where the scattering is totally diffuse. Further, the tilted Lambertian distribution is a simple change of the Lambertian distribution to take into account a directionality for diffuse reflections. The most flexible way to model diffuse reflections is the obtaining of the diffuse reflections by using the VM method. Due to the dependence of the directionality w.r.t to the scattering coefficient, higher or lower directionality can be simulated. Additionally, with the use of different scattering coefficients for different frequency bands, the VM should lead to more realistic simulations. With VM, the diffuse reflections can behave like a totally diffuse reflection or more specular like for low scattering coefficients.

3.12 Simulated Diffuse Reflections

In the section before, the behavior of the different methods was described. In this section, the impact of the input parameters, of the first-order diffuse reflections is shown. For this reason, a first-order diffused reflection is simulated for different input parameters, such as the spacing of the sources, different scattering coefficients, and the different methods.

3. SIMULATION OF FIRST-ORDER DIFFUSE REFLECTIONS

3.12.1 Number of Phantom Sources - Spacing

First, the impact of the spacing d_{ph} on the generated first-order diffuse reflection is examined. Here, the reflection of a boundary with an area of $A = 30m^2$ was used. The spacing of the phantom sources, as well as the room size, defines the number of phantom sources. Therefore, it will impact the number of received diffuse reflections.

Also, the used method or distribution will impact the number of received diffuse reflections, due to their directionality. A smaller spacing between the sources should lead to more realistic results. This applies, in hindsight of the used assumption, that every point of a wall is diffusely reflecting. For the choice of the spacing, also the sampling frequency is important. It defines the time distance between two occurring diffuse reflections. The following impulse response of one first-order diffuse reflection was obtained for different spacings with $d_{ph} = \{0.2, 0.3, 0.4, 0.5, 0.6, 0.7\}m$. For this simulation, VM was used. The sampling frequency was chosen to $f_s = 96kHz$. For the frequencies from $500Hz - 48kHz$, the scattering coefficient was chosen to $s = 0.5$ and the reflection coefficient to $\beta = 1$.

In Figure 3.8, the modeled first-order diffuse reflection of one diffuse reflecting wall is shown. The first peak in the simulated reflections corresponds to the specular reflection of the wall. The peaks following the specular reflection correspond to the diffuse reflections. In Figure 3.8f and 3.8c, the diffuse reflections are arriving more sparsely and just at certain times, due to the smaller amount of phantom sources.

Another property of the used model is seen, when comparing the amplitude of the diffuse reflections for a choice of a small spacing and a large spacing. For large spacing, the diffuse reflections have a higher amplitude compared to the diffuse reflections for a smaller spacing. It can already be explained by the used model for the diffuse transfer function (see Equation 3.33). Due to the incorporation of the reflecting area, one diffuse reflection represents a bigger diffusely reflecting area and therefore leads to a higher amplitude of a single diffuse reflection.

Also, for a big spacing between the phantom sources, late diffuse reflections are not detected anymore. In Figure 3.8c and 3.8f, no diffuse reflections are arriving at the receiver after $\approx 22ms$. Whereas for a small spacing, these diffuse reflections are detected as seen in Figure 3.8a and 3.8d. Therefore, a spacing which is chosen too small can lead to unsatisfactory results, especially in VM.

Here, one should keep in mind, that these diffuse impulse responses were obtained by the use of VM. Due to the higher directionality of VM, the described differences due to the choice of spacing are more pronounced compared to the Lambertian and the tilted Lambertian distribution. Hence, the spacing should be chosen carefully. With a large spacing or a low number of phantom sources, the obtained diffuse reflections can yield an unsatisfactory result.

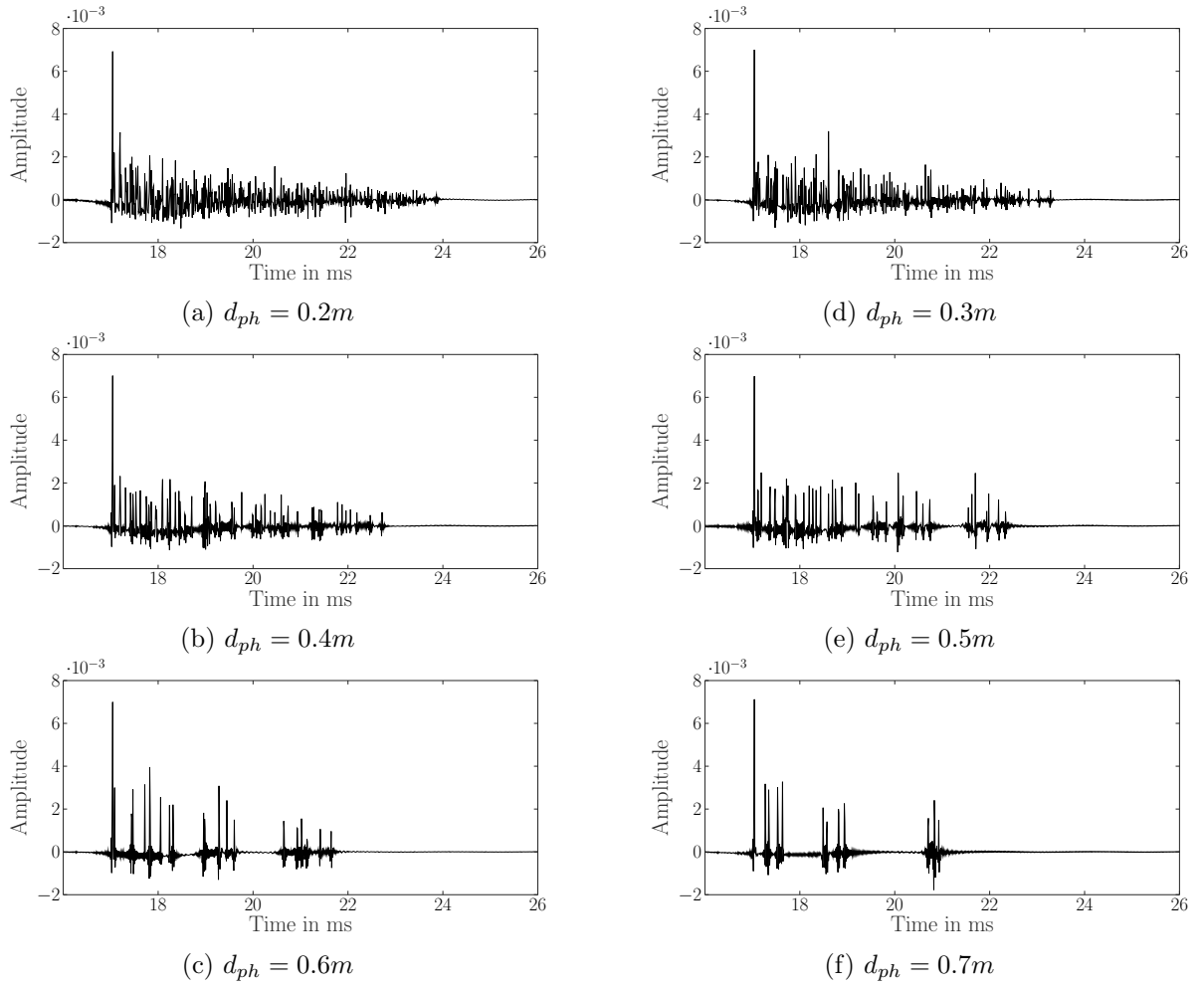


Figure 3.8: Simulated first-order diffuse reflections for different spacing of the phantom sources.

3.12.2 Different Scattering Coefficients

In the following, the differences between the Lambertian, the tilted Lambertian, and VM for different scattering coefficients are examined. For the evaluation of different scattering parameters, the influence is investigated, as above, by one first-order diffuse reflection. The chosen sampling frequency is at $f_s = 96kHz$, the distance between the phantom sources $d_{ph} = 0.2m$ and five different sets of scattering coefficient are used, shown in Table 3.2.

In Figure 3.9, the obtained diffuse first-order reflection for the Lambertian distribution (3.9k-3.9o), for the tilted Lambertian distribution (Figures 3.9f - 3.9j) and for the VM method are shown (3.9a-3.9e). As described in Section 3.11, only in the VM method the directionality is influenced by the scattering coefficient. This dependency is seen at the set of impulse responses for different scattering coefficients. For a small scattering coefficient (Set 1), VM yields the highest directionality. Therefore, as depicted in Figure 3.9a, for small scattering coefficients it

3. SIMULATION OF FIRST-ORDER DIFFUSE REFLECTIONS

f	250 Hz	400Hz	500Hz	1kHz	2kHz	4kHz	8kHz	16kHz	32kHz	48kHz
Set 1	0.05	0.05	0.05	0.10	0.15	0.15	0.15	0.20	0.20	0.25
Set 2	0.10	0.10	0.10	0.20	0.30	0.30	0.30	0.40	0.40	0.40
Set 3	0.15	0.15	0.15	0.30	0.45	0.45	0.45	0.60	0.60	0.60
Set 4	0.20	0.20	0.20	0.40	0.60	0.60	0.60	0.80	0.80	0.80
Set 5	1	1	1	1	1	1	1	1	1	1

Table 3.2: Frequency dependent scattering coefficients for five different sets.

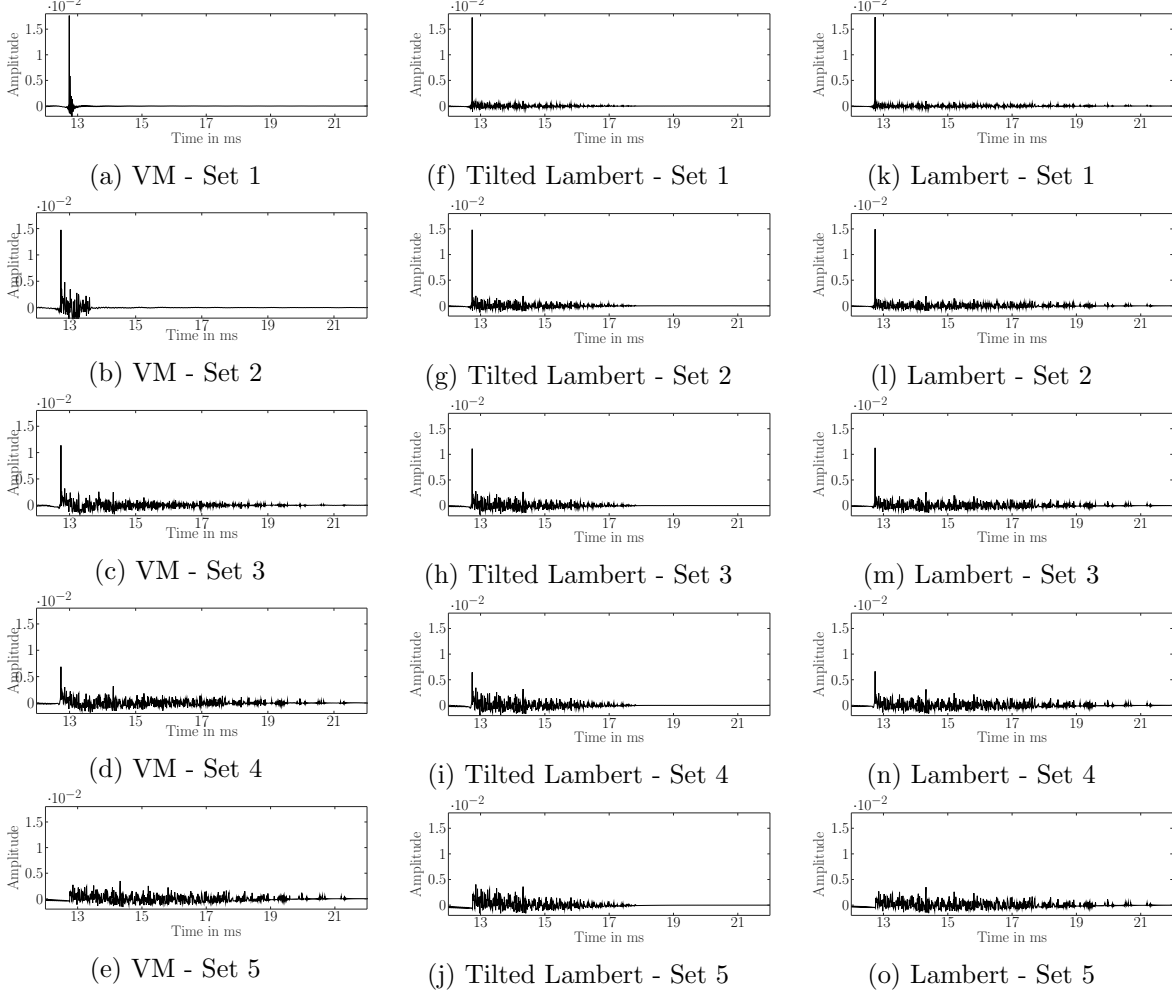


Figure 3.9: First-order diffuse reflection for different scattering coefficients and distributions.

occurs that no or only a few diffuse reflections around the specular reflection are received.

For the second Set, the higher scattering coefficient is influencing the directionality and more diffuse reflections occur (see Figure 3.9b). Therefore, as described in Section 3.11, VM loses the directionality for higher scattering coefficients. This loss of directionality is recognizable by the slower decay of the diffuse reflections.

Another difference of the VM method are the stronger diffuse reflections for smaller scattering coefficients in comparison to the Lambertian and the tilted Lambertian distribution. Due to the normalization, an obtained diffuse reflection at small scattering is weighted stronger when using the VM method. In contrast to VM, the Lambertian distribution and the tilted Lambertian distribution always receive the same amount of diffuse reflections independent of the scattering coefficient. The scattering coefficient is only scaling the strength of the diffuse reflections. Hence, the decaying tail stays the same for all scattering coefficients for the Lambertian and the tilted Lambertian distribution. The difference between the Lambertian and the tilted Lambertian distribution is the decaying time and the strength of the diffuse reflections.

In Section 3.11, the directionality of the tilted Lambertian distribution was described. This directionality leads to a faster decay of the diffuse reflections. Also, the diffuse reflections which arrive directly after the specular reflection, are stronger for the tilted Lambertian compared to the Lambertian distribution (e.g. compare Figure 3.9h and Figure 3.9m). In all methods, the attenuation of the specular component is the same. In the edge case of only diffuse reflections (Set 5), the specular component completely vanishes. Furthermore, in Figure 3.9e and Figure 3.9o it can be seen that the VM method and the Lambertian distribution yield the same result of the fifth Set.

In conclusion, the simulated first-order diffuse reflection follows the expected behavior described in Section 3.11. The Lambertian distribution leads to a decay of the diffuse reflection, which is applicable for a completely diffuse environment such as late diffuse reflections. The tilted Lambertian distribution leads to faster decay and stronger diffuse reflections after the specular reflection. The most flexible way to model the first-order diffuse reflections is the VM method, due to the incorporation of the scattering coefficient for the diffuse directions.

3.13 Summary

In this chapter, the implementation of a simulator for the first-order diffuse reflections was described. For the simulation of the diffuse reflections, a model was implemented which is similar to the models used, e.g. in the radiosity method. The difference to the radiosity method lies in the obtaining of the strength of the diffuse reflections. For this task, three different models were implemented. With the use of three different models, the implemented RIR generator yields flexibility in terms of the properties of the diffuse reflections. Now, a simulation with directional diffuse reflections is possible. One novelty of this implemented algorithm is the direct determination of the pressure impulse response. Also, the computational complexity introduced by the use of VM, was lowered with the use of pre-calculated factors.

Further, the difference between the used methods was examined. It was seen, that the simple

3. SIMULATION OF FIRST-ORDER DIFFUSE REFLECTIONS

use of the direction of the specular reflection yields a different behavior compared to the simple Lambertian distribution. With the incorporation of the scattering coefficient, the most flexible way to simulate directionality is given by VM. With the use of the tilted Lambertian distribution and the VM, two different methods for the simulation of directional diffuse reflections are available.

With the implemented RIR generator, it is now possible to simulate diffused first-order reflections, with three different methods. The implementation provides the basis for further research conducted with the impact of diffuse reflections on an RGI algorithm.

Chapter 4

Impact of Diffuse Reflections

In the following chapter, the impact on a state-of-the-art RGI is evaluated. The evaluated RGI algorithm is not based on the processing of the measured audio signal but utilizes the signals for image-based processing. The used algorithm is described in [BWH18]. First, a brief introduction of the used algorithm is given. The evaluation will provide a look at the errors, which can be introduced due to diffuse first-order reflections. The errors or the impact of diffuse reflection will be examined in a microscopic and a macroscopic perspective. Further, countermeasures are presented to cope with the impact of the diffuse reflection on the performance of the RGI algorithm. These countermeasures are then evaluated as well.

4.1 Overview

The use of RGI algorithms is concerned with localization of reflecting boundaries (the walls, the floor and the ceiling of a room). For this task different methods have been introduced to gain information about the location of the reflecting boundaries. One disadvantage many of these presented methods is their performance evaluation with only specular impulse responses. As described in section 2.1.2, not only specular but also diffuse reflections occur. For that reason, an RGI algorithm should be examined in terms of the performance in a diffuse reflecting environment.

4.1.1 RGI Algorithm

In this section, an introduction of the used algorithm is given. The algorithm relies on sets of times of arrivals (TOAs), which are obtained from the RIRs. The TOAs correspond to the reflections of the reflecting boundaries in a room. For the gathering of the RIRs, arrays with up

4. IMPACT OF DIFFUSE REFLECTIONS

to 64 loudspeakers and a microphone are used. The loudspeaker array is further divided into four sub-arrays. From the RIRs, the TOAs are gathered and lead to inference on the room geometry. In Figure 4.1a, the RIRs of two loudspeakers, placed at a different location, are exemplarily shown. The RIRs of one sub-array are then stacked to visualize the RIRs. The peaks of the RIRs correspond to the direct path of the sound and the reflections from the reflecting boundaries. To disambiguate the TOAs is done with the help of the linear radon transform (LRT) [BWH17]. With the visualization, the peaks of the RIRs can be represented by stack-lines (SLs).

In Figure 4.1b, for one sub-array such a representation of the RIRs as resized stacks is depicted. The rows of this stack correspond to the number of used loudspeakers. Hence, the RIRs of the individual speakers are used and then represented as an image. In the stack, the strength of the reflection is indicated by the color. Yellow represents a high amplitude and blue a low amplitude. It is seen that the stacked RIRs, lead to distinct patterns which are representing an incoming wavefront. The SLs then approximate these patterns. Next, these SLs are determined with the above-mentioned LRT.

The LRT can be seen as an image beamformer. At a timepoint t it is summing up the amplitudes for different angles ϕ . Therefore, the maxima of the LRT, correspond to the time-of-arrival and the angle of the arriving wavefronts in the stack. In Figure 4.1c, the LRT and the detected maxima of one stack are shown. The amplitudes again correspond to the colors, as in the stack representation. The obtained maxima correspond to the TOA and the tilt (angle) of the wavefront and therefore to the SLs. In Figure 4.1d, the obtained SLs calculated by the LRT are shown. This process for obtaining the SLs is done for every sub-array of the array separately. The found SLs then are associated with their corresponding SL calculated in the other sub-arrays via a graph-based approach.

The reflector locations (RLs) are then calculated with the associated SLs. The steps to determine the RLs will not be described here any further. For a detailed explanation of these steps see [BWH18].

4.1.2 Simulated and Real RIR Stacks

In the example above, the RIRs were simulated with an only specular RIR generator. For the evaluation of the described RGI algorithm, the implemented first-order diffuse RIR generator is used, as described in Chapter 3. As described in 3.11, the use of the implemented generator leads to specular reflections, with a diffuse tail. Thus, the use of the generator leads to wavefronts with a decaying tail. In Figure 4.2a and Figure 4.2b, a simulated Stack with diffusion as well as a real measured stack are depicted. These two stacks are not shown for a direct comparison, due to differences such as the room size, the sampling frequency, and a different time scale.

However, what can be seen in the stacks, is that diffuse reflections are present in the real stack.

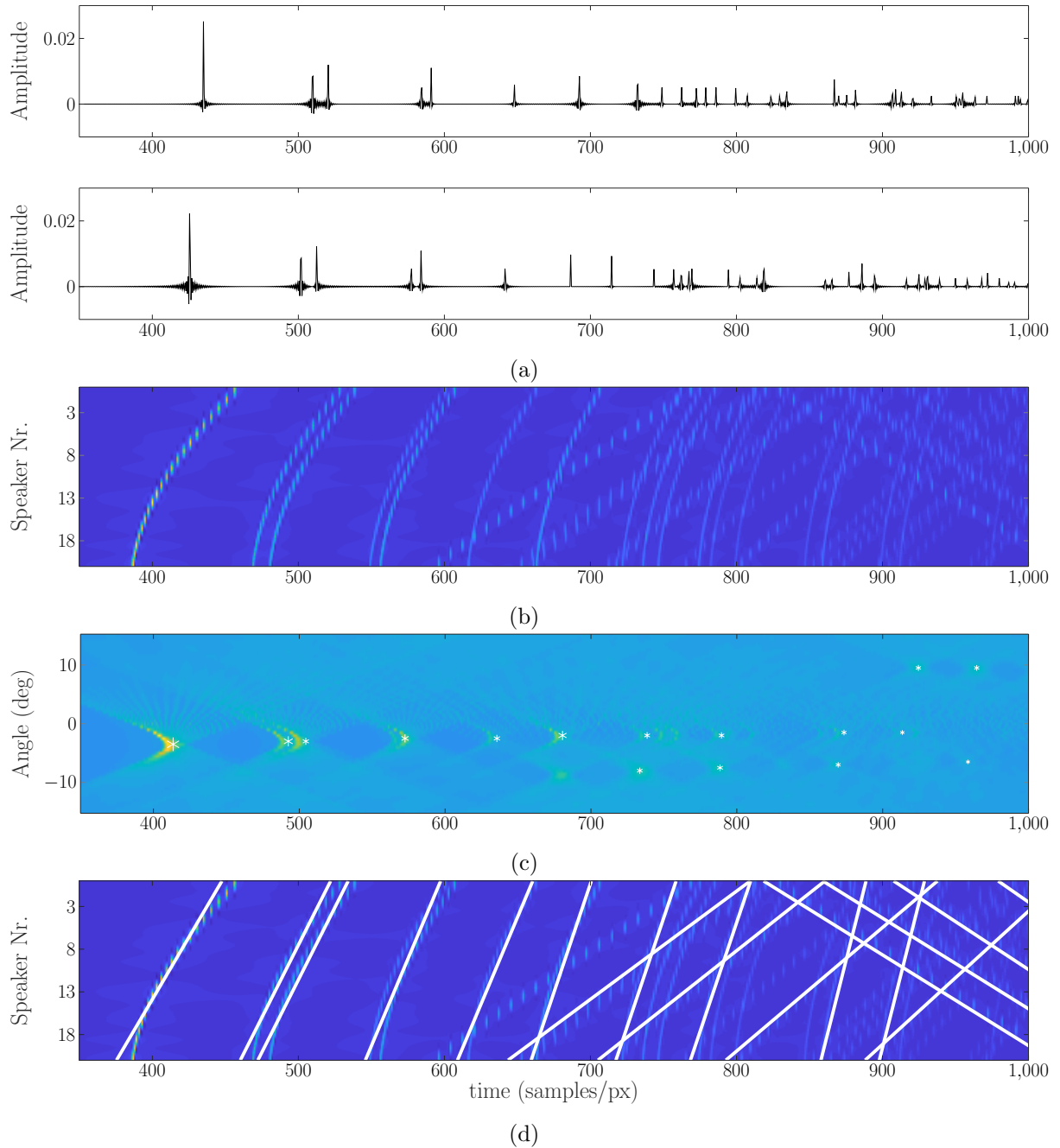


Figure 4.1: Example of the algorithm steps: Obtained RIRs for two different positions in (a) and (b), stack representation in (c), linear radon transform in (d) and detected stack-lines in (d).

4. IMPACT OF DIFFUSE REFLECTIONS

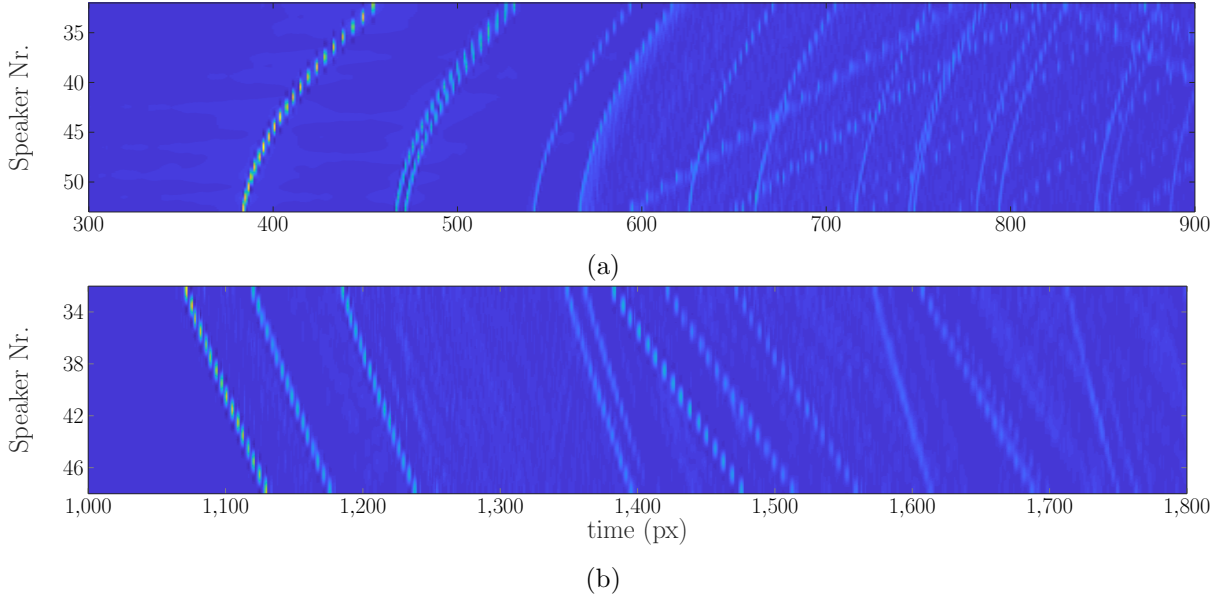


Figure 4.2: RIR stacks for a diffuse simulation in (a) and a real measurement in (b).

In the real stack the presence of the diffuse reflection is seen e.g. at the wavefront at around the 1200th time pixel. Therefore, the simulation of the diffuse reflection should provide more realistic results for a diffuse environment. Depending on the used method and the used scattering coefficient, this tail can differ in its appearance.

4.2 Evaluation Setup

For the examination of the impact of diffuse reflections, different setups in terms of diffuse conditions were used. The simulations of these different setups were done for six different rooms with thirteen different microphone positions per room and an array with 64 loudspeakers. The array is placed parallel to one wall, except in the sixth room. In terms of consistency, the same room dimensions as in [BWH18] are used as well as the same microphone positions. The loudspeakers are simulated as a uniform rectangular array with the dimensions of 1.5 x 0.9 m. The simulations were done for shoe-box rooms. In Table 4.1 the dimensions of the rooms are shown. The chosen sampling frequency used in every simulation was 96kHz. The distance of the phantom sources was chosen to $d_{ph}=0.2$. The evaluation parameters, used for the SL detection and the reflector localization (RL) were chosen as in the before mentioned publication.

For the simulation of diffuse conditions, different combinations of scattering coefficients, diffusely reflecting walls and the different methods were used. The scattering coefficients that are chosen in a setup are the same for every diffuse reflecting wall in a room. The individual setups for the diffuse conditions were then used for every one of the six rooms. The reflection factor was chosen

Room	Width (m)	Depth (m)	Heights (m)
1	4.5	5	2.5
2	6	4	2.9
3	6	8.5	3.5
4	9	7.5	3
5	6	12	3
6	4.5	5	3

Table 4.1: Room dimensions used for every simulation.

Set	s(f) (f in kHz)										Method	DW
	0.25	0.4	0.5	1	2	4	8	16	32	48		
1	0.05	0.10	0.20	0.20	0.30	0.40	0.50	0.50	0.60	0.60	All	4
2	0.05	0.10	0.70	0.80	0.80	0.80	0.80	0.80	0.80	0.80	All	4
3	0.05	0.05	0.05	0.20	0.30	0.40	0.60	0.90	0.90	0.90	VM	2
4	0	0	0	0.05	0.10	0.15	0.20	0.25	0.25	0.25	VM	6
5	0.05	0.05	0.05	0.10	0.20	0.30	0.40	0.50	0.50	0.50	VM	6
6	0.05	0.05	0.05	0.15	0.30	0.45	0.60	0.75	0.75	0.75	VM	6
7	0.05	0.05	0.05	0.20	0.40	0.60	0.80	1.00	1.00	1.00	VM	6

Table 4.2: Simulation sets with the used scattering coefficient, number of diffuse reflecting walls (DW) and the used method/distribution.

to $\beta = 0.6$ in all frequency bands and for all setups. In Table 4.2, the setup parameters for the simulation are shown. Set 1 and 2 were simulated with the Lambertian, the tilted Lambertian distribution and VM.

4.3 A Microscopic View on the Impact of Diffuse Reflections

In this section, a microscopic view on the errors induced by the diffuse reflections is given. This section is called microscopic view, as the impact of the diffuse reflections is not evaluated for the whole algorithm, but is evaluated for an important part of it. This part of the investigation is concentrating on the impact on the SL detection and therefore also on the LRT. Hence, this view is limited to the stacks of the sub-arrays. For this view, different errors in the SL detection are shown by examples of the effects.

The aim of this microscopic view is gaining a better understanding of how diffuse reflections change the behavior in terms of SLs detection. In the following, different types of errors are indicated. The section follows a certain organization. The errors evaluated first are the most prominent, whereas the error mentioned last was the rarest error observed in the evaluation. Also, a case is introduced, where diffuse reflection can provide better detection of SLs.

4. IMPACT OF DIFFUSE REFLECTIONS

4.3.1 Non-Existent Wave Front Detection

The most prominent error that occurs due to diffuse reflections in SLs detection is the detection of non-existent SLs. In this context, non-existent SLs are detected SLs which do not represent a wavefront due to reflection at a reflecting boundary. In Figure 4.3a and in Figure 4.3b the detected SL for the diffuse and the specular case are shown, respectively. This detection was taken from simulation of Room 1 and from the diffuse Set 2 with tilted Lambertian distribution (see Table 4.1 and 4.2). It is seen, that the diffuse and specular case yield a very different result. In the diffuse case, wrong SLs are detected compared to the specular case (shown as red SLs in Figure 4.3b).

This erroneous detection is induced by diffuse reflections. The reason for this false detection of SLs shall be explained by the LRT of the shown examples. The LRT is detecting these diffuse reflections as their amplitude is relatively high in the specular region due to the high scattering. The curvature of the specular wavefront is one factor in the false detection of the SLs. Due to the curvature, the obtained maxima by the LRT is lower compared to a non-curved wavefront. All these factors taken together, the LRT tends to a similar value for the diffuse reflections compared to the specular wavefront.

This effect is seen as smearing of the LRT. In Figure 4.3c, the LRT for the specular case and in Figure 4.3d, the LRT for the diffuse case is depicted. In the region of the falsely detected SLs, it is seen, that the peaks of the LRT are not as distinguishable as in the specular case. Hence, the smearing of the peaks, due to diffuse reflections leads to false detection of non-existent wavefronts. The shown example was chosen as this effect is very dominant due to the chosen distribution (tilted Lambertian distribution) and the high scattering coefficient. However, this effect also occurred for other sets and distributions (e.g., Set 1 with VM). Besides, wrong detected SLs are not only occurring in the region of a specular reflection but also appear in the decaying tail of a diffuse reflection.

4.3.2 Time-Shift of the Detected Stack Lines

The next prominent error that occurs due to diffuse reflections is the time-shift of the detected SLs. This effect can also be seen in the before shown example. In Figure 4.3b, the detected SLs for the specular wavefront are indicated as the green SLs. When comparing the SLs which are identified for the specular case, with the SLs of the diffuse case, the position of the SLs differs. Therefore, the diffuse reflections can lead to a time-shift of the SLs. Again, this can be explained by the smearing of the LRT. As the diffuse reflections lead to temporal smearing of the specular reflection, this temporal smearing also occurs in LRT. The maxima of the obtained LRT are also smeared and thus shifted in time. This effect was encountered in most of the simulations with diffuse reflections.

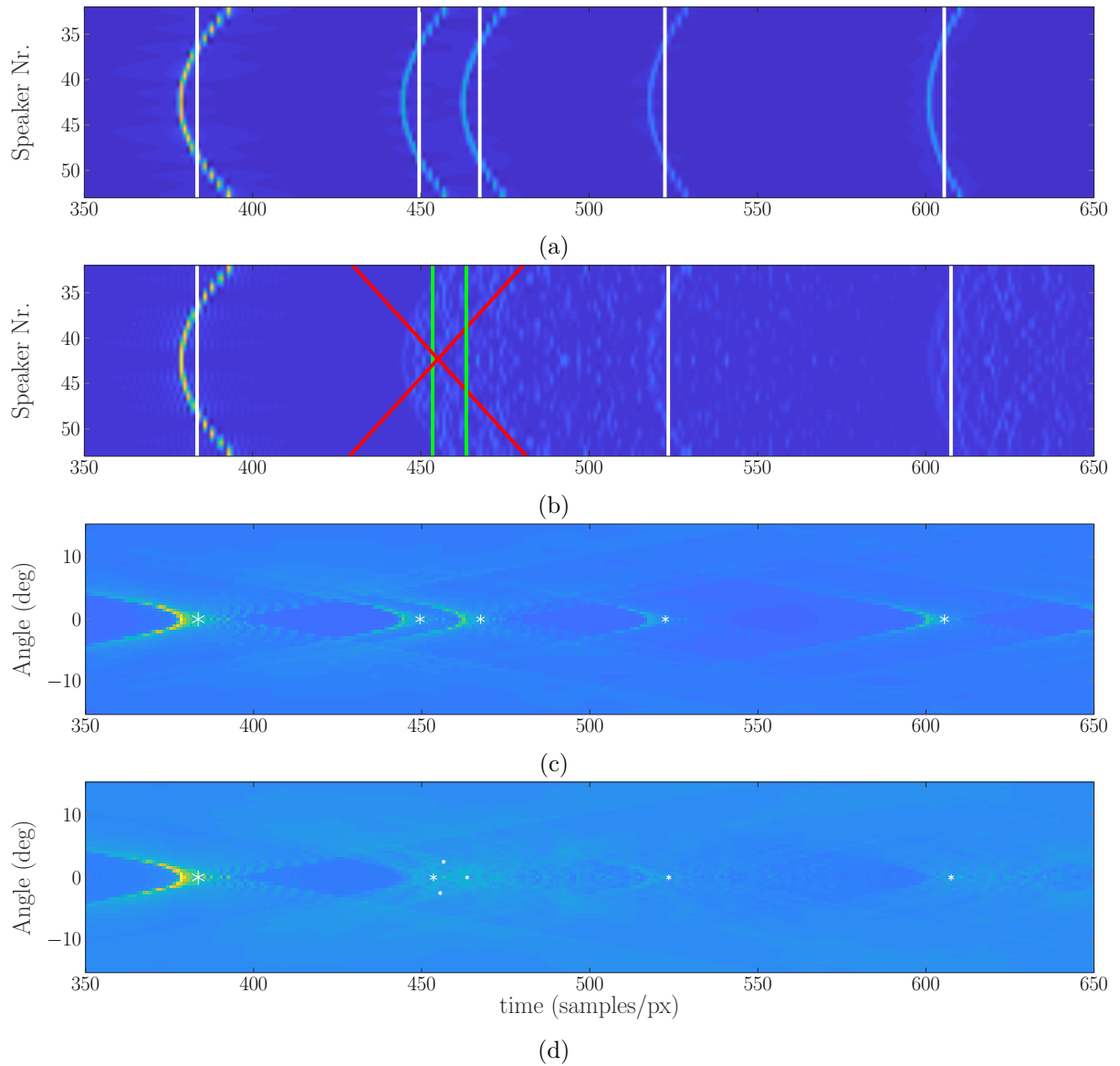


Figure 4.3: Detected SLs for a specular simulation in (a) and a diffuse simulation in (b). The corresponding linear radon transform for the specular simulation in (c) and for the diffuse simulation in (d)

4. IMPACT OF DIFFUSE REFLECTIONS

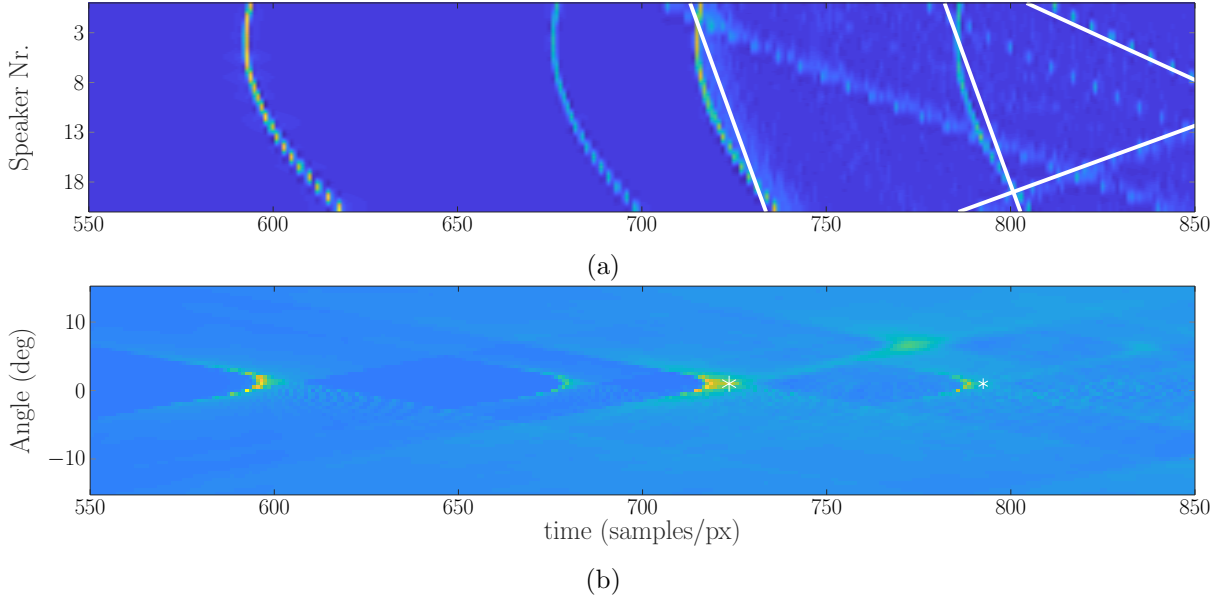


Figure 4.4: Example of the stack-lines in (a) and the corresponding linear radon transform in (b), for a false detection of the direct sound

4.3.3 Angular Tilt

A further error caused by diffuse reflections is an angular tilt of the SLs. The smearing due to the diffuse reflections is not only limited to the time domain but also in the angular domain of the LRT. Therefore, the detected peak of the LRT can also be shifted in the angular domain and will lead to a tilt of the SLs. This effect is mostly occurring at high scattering coefficients. Additionally, it has to be stated, that this error is often observed when two consecutive wavefronts are arriving closely and are reflected diffusely.

4.3.4 False Detection of the Direct Sound

Another impact on the detection of the SLs is the false detection of the direct sound. When the direct sound is not detected, a wall reflection is detected as the direct sound of the stack. Thus, a minimum of one wavefront is not detected correctly as a reflection. In Figure 4.4a and Figure 4.4b such an case is shown. The described example occurred for Room 2 with Set 1 simulated with VM.

Here, in the shown example the direct sound is detected as the third wavefront of the sound. The error is due to the assumption that the direct sound is the strongest part of the impulse response. This assumption is physically correct, as following wavefronts are reflected, therefore attenuated and also attenuated due to the reflections at a wall. However, in this particular case, different circumstances lead to the false detection of the direct peak. The falsely detected peak is not only

due to the diffuse reflections. Also, the occurrence of another wavefront is influencing the wrong estimation. The presence of the diffuse reflections and the overlapping of another wavefront lead to false detection. Furthermore, the linearity of the linear radon transform is also one reason for false detection. Due to the linearity of the LRT, not all peaks of the wavefront are contributing to the obtained maximum of the real direct sound. If all peaks of the wavefront contributed, this false detection would not occur. With the linearity of the LRT, all three components which were before described are contributing. Thus, the overall obtained value by the LRT is higher than for the direct wavefront or the second wavefront. A consequence of false detection is also a different detection for the following SLs. The relative threshold is set according to the estimated direct-sound [BWH18]. Hence, the threshold for the detection of the peaks is higher and therefore fewer SLs can be detected. Further, wavefronts arriving before the false detected direct-sound are omitted and will not be included in further processing. However, this false detection only occurs when the described circumstances are present, which is somewhat rare.

4.3.5 Boosting of the LRT Peak

In all the cases before, different cases were examined which lead to an false detection of SLs. However, the impact of the diffuse reflections is not only of a negative nature. In some scenarios, the diffuse reflections improved the detection of the SLs. This improvement in the detection is introduced for curved wavefronts. The diffuse reflections, which occur at a curved wavefront are also summed by the linear radon transform and can strengthen the resulting peak. Whereas in the specular case the maximum of the LRT is obtained by only two intersections of the SL with the wavefront (see Figure 4.3a). Due to this, the maximum can fall under the peak detection threshold and is therefore not detected. While in the non-specular case, the diffuse reflections in between the curved wavefront will increase the value of the LRT peak. In such cases, diffuse reflection can even sometimes improve the detection of the SLs. An improving effect mostly occurs, if the diffuse decay tail is short enough. For such a case, the boosting effect is more prominent than the deleterious effect of the smearing.

4.4 A Macroscopic View on the Impact of Diffuse Reflections

In the above microscopic view, an insight was given for the errors that are induced by the diffuse reflections on the detecting of single SL in one sub-array. Here, the performance in diffuse conditions of the whole algorithm is evaluated, as the algorithm uses all obtained SLs of every sub-array to estimate the TOAs. Additionally, the performance in terms of RL is carried out. For the following evaluation, it should be reminded that the results obtained in Set 1 for VM, cannot be directly compared to the results obtained in Set 4 to Set 7. In Set 1, four walls were

4. IMPACT OF DIFFUSE REFLECTIONS

Order Room	All FDR%	direct sound		TPR% RMSE μs	1		2	
		TPR%	RMSE μs		TPR% RMSE μs	TPR% RMSE μs	TPR% RMSE μs	
1	10.8	100.0	107.7	89.7 151.4	57.7 129.6	55.6 114.1	57.7 111.9	144.3 112.9
2	10.7	100.0	79.2	96.2 129.6	55.6 114.1	64.1 111.9	60.5 124.5	140.9 124.5
3	6.8	100.0	78.5	100.0 114.1	64.1 111.9	60.5 124.5	52.9 124.1	113.4 131.5
4	8.1	100.0	78.8	98.7 111.9	60.5 112.9	56.0 124.1	57.8 124.1	133.0 133.4
5	11.7	100.0	80.7	100.0 112.9	52.9 124.1	56.0 124.1	57.8 124.1	137.3 133.4
6	13.1	100.0	98.6	96.2 124.5	56.0 124.1	57.8 124.1	57.8 124.1	131.5 133.4
AVG	10.2	100.0	87.3	96.8 124.1	57.8 124.1	57.8 124.1	57.8 124.1	133.4 133.4

Table 4.3: TOA detection and disambiguation metrics for the specular simulation

simulated as diffusely reflecting. Whereas in Set 4 to Set 7, six walls were simulated as diffusely reflecting.

For comparison purpose, also results for a specular simulation are shown. It should be noted, that these results can not be directly compared with the results obtained in [BWH18]. Due to different simulation parameters, different results are obtained. Further, this algorithm is in constant development and differs in the version used for the evaluations. The complete metrics for all sets shown in Table 4.2, are listed in Appendix A and in Appendix B.

4.4.1 TOA Detection and Disambiguation Evaluation

For the evaluation of the performance in terms of TOA and disambiguation, three different metrics were used. The true positive rate (TPR) indicates the rate of correct estimated SLs. A TOA is estimated correctly when the root mean square error (RMSE) of the detected TOAs lies within a range of 0.5ms compared to the true TOAs. The TPR and the RMSE were evaluated for direct sound and up to the second-order reflections. Also, the failed detection rate (FDR) is evaluated. The FDR indicates the percentage of wrong detected TOAs for all orders. For every room, the results are averaged over the thirteen microphones. These obtained averaged results are again averaged over the six different rooms. The averaged result is indicated in the Tables by "AVG". For comparison purposes, the results of the specular simulation are shown in Table 4.3.

Different Scattering Distributions

In the following, the results in terms of the usage of different scattering methods are evaluated. In Table 4.4 the TOA detection and disambiguation metrics for the different methods are shown, respectively. The impact of the diffuse reflections for the averaged TOA detection and disambiguation metrics yield relatively similar results for the different used methods. The biggest discrepancy between the methods is seen for VM in Room 2.

In VM, the case occurs where the direct sound is estimated wrong for two different microphone positions (86.4% corresponds to eleven accurate detected direct sound SLs). Due to the wrong

detection of the direct sound, the TPR for Room 2 for the first-order reflections drops to 83.3%. However, in overall, the average TPR of the first-order reflections lies within a range of 94.7% - 96.6% which is a near perfect rate, even in the case of diffuse reflections.

In the case of the FDR, the algorithm performs slightly worse in the diffuse case compared to the specular case. Whereas in the specular case, the FDR lies in a range of 11% - 13%, in the diffuse case (for all used methods) the FDR lies within 10% - 20%, which is also reasonable, considering that later reflection orders are also included and should be even more impacted by the diffuse reflections.

Another interesting result is that the average RMSE is also in the same region as the estimated one. Only the TPR of the second-order reflection is considerably lower than in the specular case. However, which is again at a reasonable rate from around 42% - 57%, for the detection of second-order reflections. The average RMSE, for the second-order reflections, also shows similar results, when comparing the three different methods to the specular case.

Different Scattering Coefficients

In the evaluation before, we have seen that the algorithm provides a robust estimation for all methods and a scattering coefficient of up to 0.6, in terms of TOA detection and disambiguation. In the next evaluation, for the same distribution (VM), different scattering coefficients are used. For this evaluation the Sets 4 to 7 are examined (see Table 4.2).

When comparing the average performance, it is seen that the differences of the sets are relatively small (see Table 4.5). The direct-sound was detected in every case. For the average detection rate of the first-order reflections, the results are in a nearly perfect range (96.2% - 93.2%). Whereas, the set with the highest scattering coefficient yields the lowest average TPR (Set 7, see Table 4.5d). Set 5 (Table 4.5b), performs similar compared to Set 4 in terms of the first-order TPR, although Set 4 (Table 4.5a) was simulated with a lower scattering coefficient and lies in ranges, where the reflection directions for VM behave more specularly. For the first room setup, the performance increases for the sets with a higher scattering coefficient, except for Set 7. The worst performance for the detection of the first-order reflection is seen in the second room for Set 6 (Table 4.5c), where the TPR drops to 79.5%.

Another interesting result is the increase of the average TPR for the second-order diffuse reflections. The simulation with the highest scattering coefficient leads to the best results for the detection rate of the second-order reflections. Here, the reason for this difference is not seen from the tables but shall be explained. In case of a smaller scattering coefficient, the algorithms detected more SLs of the third reflection order compared to the case of a higher scattering coefficient. It can lead to smaller TPR for the second-order reflections. The same effect can be seen, when comparing the before evaluated results from Set 1 (Table 4.4c) to the results of Set 4 to 7. Here, the difference is even higher, due to the use of only four diffuse reflecting walls in Set 1.

4. IMPACT OF DIFFUSE REFLECTIONS

Order Room	All FDR%	direct sound		TPR% 1	RMSE μs	TPR% 2	RMSE μs
		TPR%	RMSE μs	TPR%	RMSE μs	TPR%	RMSE μs
1	17.3	100.0	107.7	87.2	151.0	54.3	158.5
2	17.9	100.0	79.1	91.0	123.1	50.9	149.9
3	12.4	100.0	78.5	100.0	109.2	50.0	123.4
4	16.7	100.0	78.8	98.7	105.2	52.4	139.1
5	13.0	100.0	80.7	100.0	125.2	47.1	143.6
6	19.3	100.0	98.6	97.4	120.7	46.2	131.4
AVG	16.1	100.0	87.2	95.7	122.4	50.1	141.0

(a) Lambertian distribution							
Order Room	All FDR%	direct sound		TPR% 1	RMSE μs	TPR% 2	RMSE μs
		TPR%	RMSE μs	TPR%	RMSE μs	TPR%	RMSE μs
1	15.2	100.0	107.7	88.5	145.6	53.8	161.0
2	19.4	100.0	79.1	93.6	118.3	46.6	140.4
3	13.7	100.0	78.5	98.7	103.4	51.3	121.9
4	12.6	100.0	78.8	100.0	105.1	57.3	143.9
5	11.6	100.0	80.7	100.0	125.2	50.0	149.4
6	19.7	100.0	98.6	98.7	122.5	47.0	133.9
AVG	15.4	100.0	87.2	96.6	120.0	51.0	141.7

(b) Tilted Lambertian distribution							
Order Room	All FDR%	direct sound		TPR% 1	RMSE μs	TPR% 2	RMSE μs
		TPR%	RMSE μs	TPR%	RMSE μs	TPR%	RMSE μs
1	17.1	100.0	107.7	88.5	151.2	52.6	161.3
2	17.6	84.6	80.1	83.3	121.7	48.7	146.1
3	16.9	100.0	78.5	100.0	110.6	45.3	129.9
4	11.8	100.0	78.9	100.0	117.3	46.5	131.7
5	10.0	100.0	80.8	100.0	145.7	41.8	141.2
6	16.8	100.0	98.6	96.2	117.2	47.0	129.3
AVG	15.0	97.4	87.4	94.7	127.3	47.0	139.9

(c) Vector mixing							
Order Room	All FDR%	direct sound		TPR% 1	RMSE μs	TPR% 2	RMSE μs
		TPR%	RMSE μs	TPR%	RMSE μs	TPR%	RMSE μs
1	17.1	100.0	107.7	88.5	151.2	52.6	161.3
2	17.6	84.6	80.1	83.3	121.7	48.7	146.1
3	16.9	100.0	78.5	100.0	110.6	45.3	129.9
4	11.8	100.0	78.9	100.0	117.3	46.5	131.7
5	10.0	100.0	80.8	100.0	145.7	41.8	141.2
6	16.8	100.0	98.6	96.2	117.2	47.0	129.3
AVG	15.0	97.4	87.4	94.7	127.3	47.0	139.9

Table 4.4: TOA detection and disambiguation metrics for Set 1 with different distributions.

The RMSE of the first-order reflection is on average in a range from $123\mu s$ - $133\mu s$. A decrease of performance is only observable from Set 4 to Set 5. However, the increase of the RMSE is of only $10\mu s$, which is just a minimal increase. The average RMSE stays constant for Set 5 to Set 7. Therefore, the higher scattering coefficient is only leading to a degradation of the RMSE up to a certain point. Above a specific scattering coefficient, the algorithm provides robustness in terms of the RMSE.

In overall, the algorithm is very robust in terms of the TOA disambiguation in case of diffuse reflections. An observable impairment of these metrics is only noticeable for a very high scattering coefficient (Set 7). Also, the RMSE is staying nearly constant, for different scattering coefficients.

4.4 A MACROSCOPIC VIEW ON THE IMPACT OF DIFFUSE REFLECTIONS

Order	All	direct sound			1	2	
Room	FDR%	TPR%	RMSE μs	TPR%	RMSE μs	TPR%	RMSE μs
1	10.3	100.0	107.7	92.3	152.9	59.0	156.3
2	10.8	100.0	79.1	87.2	112.3	56.4	133.3
3	12.7	100.0	78.5	100.0	111.2	46.6	125.1
4	8.2	100.0	78.8	100.0	109.9	54.6	134.8
5	10.8	100.0	80.7	100.0	130.8	43.8	131.1
6	12.1	100.0	98.6	97.4	118.5	54.7	120.1
AVG	10.8	100.0	87.2	96.2	122.6	52.5	133.5

(a) Set 4							
Order	All	direct sound			1	2	
Room	FDR%	TPR%	RMSE μs	TPR%	RMSE μs	TPR%	RMSE μs
1	10.3	100.0	107.7	96.2	143.3	60.3	152.7
2	9.8	100.0	78.7	87.2	123.3	57.3	134.6
3	11.8	100.0	78.3	98.7	128.2	53.0	129.8
4	16.0	100.0	78.6	98.7	130.7	45.6	140.2
5	14.6	100.0	80.5	98.7	146.4	48.1	136.5
6	15.1	100.0	98.6	98.7	125.1	55.1	133.9
AVG	12.9	100.0	87.1	96.4	132.8	53.2	137.9

(b) Set 5							
Order	All	direct sound			1	2	
Room	FDR%	TPR%	RMSE μs	TPR%	RMSE μs	TPR%	RMSE μs
1	13.7	100.0	107.7	98.7	150.1	60.3	155.8
2	11.4	100.0	79.4	79.5	128.8	59.0	149.8
3	11.7	100.0	78.5	93.6	128.1	60.3	132.3
4	11.5	100.0	78.8	93.6	121.1	61.7	126.6
5	13.3	100.0	80.7	94.9	145.6	52.4	136.3
6	15.4	100.0	98.6	98.7	122.6	56.8	122.7
AVG	12.8	100.0	87.3	93.2	132.7	58.4	137.3

(c) Set 6							
Order	All	direct sound			1	2	
Room	FDR%	TPR%	RMSE μs	TPR%	RMSE μs	TPR%	RMSE μs
1	14.6	100.0	107.7	89.7	157.9	59.0	141.9
2	10.6	100.0	79.0	85.9	129.2	59.4	145.4
3	12.4	100.0	78.5	93.6	125.7	59.4	121.8
4	8.9	100.0	78.8	93.6	120.0	64.9	130.7
5	16.8	100.0	80.7	92.3	142.0	54.8	141.7
6	15.3	100.0	98.6	97.4	122.5	59.4	123.2
AVG	13.1	100.0	87.2	92.1	132.9	59.5	134.1

(d) Set 7

Table 4.5: TOA detection and disambiguation metrics for different scattering coefficients.

4. IMPACT OF DIFFUSE REFLECTIONS

Room	E_{ML} (cm)	D_{RL} (cm)	O_{RL} (degrees)	% of full RGI	est. refl.
1	26.467 ± 31.320	10.402 ± 10.876	4.088 ± 4.177	61.5	5.62
2	24.261 ± 24.126	9.358 ± 9.896	3.625 ± 3.268	69.2	5.62
3	24.877 ± 28.467	7.265 ± 6.218	2.414 ± 1.954	92.3	5.92
4	24.950 ± 28.199	7.749 ± 6.722	2.507 ± 2.183	100.0	6
5	29.703 ± 39.453	10.863 ± 8.682	2.433 ± 1.924	69.2	5.54
6	25.434 ± 28.846	9.932 ± 9.399	3.978 ± 3.248	0.0	4.85

Table 4.6: Reflector localization performance metrics for the specular simulation.

4.4.2 Reflector Localization

The next evaluation is concerned with the accuracy of the estimated reflectors. For this task the Euclidean distance $E_{ML} = \|\mathbf{m} - \hat{\mathbf{m}}\|$ between the real microphone \mathbf{m} and the estimated microphone $\hat{\mathbf{m}}$ was calculated. Also, an orientation error was calculated. The orientation error $O_{RL} = |\arccos(\langle \mathbf{n}_r, \hat{\mathbf{n}}_r \rangle)|$ is calculated as the rotation of the estimated reflector normal $\hat{\mathbf{n}}_r$ and the real reflector normal \mathbf{n}_r . In addition, the offset $D_{RL} = ||\langle \mathbf{n}_r, (\mathbf{m} - \mathbf{x}) \rangle|| - ||\langle \hat{\mathbf{n}}_r, (\mathbf{m} - \hat{\mathbf{x}}) \rangle||$ is calculated as the difference of the distance from the real reflector \mathbf{x} to the real microphone and the distance from estimated reflector $\hat{\mathbf{x}}$ to the real microphone position.

The metrics are averaged over the thirteen different microphone positions for every room. Additionally, the standard deviation was calculated (shown in the tables after \pm). These metrics are the same as used in [BWH18], where also a visual representation can be found. For these three parameters, a lower value indicates better performance.

Furthermore, the average number of the estimated reflector was calculated for all microphone positions in one room. The percentage of full RGI indicates how much cases it was possible to determine all reflectors in the room. Here, a higher value indicates better performance. As for the evaluation of the TOA disambiguation, the results of the specular case are shown in Table 4.6.

The evaluation is done for the same sets used in the evaluation of the TOA disambiguation evaluation. Therefore, the first evaluation is done for Set 1 for all of the three different evaluation methods.

Different Scattering Distributions

In Table 4.7a to 4.7c, the performance metrics for the RL are shown for the different distributions. The differences of the diffuse cases, to the specular case, are worse only for certain cases. For some cases, they are even better for the diffuse case. This contrary result can be explained by the boosting of the LRT shown in Section 4.3. When comparing the number of estimated reflectors, diffuse reflections can even increase this number and the percentage of full RGI. It is seen, e.g.

for room 5 for all distributions.

However, the higher number of the estimated reflector is coupled with a higher estimation error. This is also present for the specular case, as more reflectors are estimated. These additionally estimated reflectors can yield to a higher error and therefore leading to worse RL performance metrics. The highest estimation error for the Euclidean distance E_{ML} is observed in the vector mixing for Room 5 with 41cm. The other two methods yield a reasonable difference of 4cm compared to the specular case.

Further, the orientation error O_{RL} for the diffuse sets is in the region of the specular case. The most significant degradation of the performance for the orientation error is seen for VM in Room 2. The orientation error rises from about 3.6 degrees to an error of 8 degrees. This higher error also results in a higher offset error D_{RL} . The reason for the error is the non-detection of the direct-sound. Therefore, this SLs detection failure can lead to a high error for the RL for O_{RL} and D_{RL} . Though, this error only occurs for individual microphone positions, when the conditions described in Section 4.3.4 are met. For this choice of scattering coefficients, the VM method tends to produce stronger diffuse reflection right after the specular reflection. However, it also shows the robustness of the algorithm for the different distributions, for the choice of a scattering coefficient in the range from 0.2 - 0.6. Only for VM, the E_{ML} is considerable higher in Room 5.

Different Scattering Coefficients

The next evaluation was done for Set 4 to 7. This part of the evaluation is concerned with different scattering coefficients. In Table 4.7, the performance metrics for RL are seen. Here, a trend is observed for the rate of full room reconstruction (% of full RGI), and thus the estimated reflector is seen. In the case of the smallest scattering coefficient, the algorithm can reconstruct a room full for all microphone positions (Room 4 - Set 4). Whereas for a higher scattering coefficient (Set 5), the highest rate achieved is at 85%. For the highest scattering coefficient (Set 7), at only every second microphone position a full room reconstruction is reached (maximum of 54%). Hence, the biggest degradation is observed for high scattering coefficients.

4.5 Countermeasures for Diffuse Reflections

As seen in the evaluation, there is an impact of the diffuse reflections on the performance of the algorithm. Although, the performance degradation was observed for a highly diffuse simulation, countermeasures should be taken into account, in order to encounter this impact. With countermeasures, the algorithm should be then able to produce good results even in bad conditions. As the evaluated algorithm is working with image processing techniques, the countermeasures will also be image based. The filters introduced in the following are applied on

4. IMPACT OF DIFFUSE REFLECTIONS

Room	E_{ML} (cm)	D_{RL} (cm)	O_{RL} (degrees)	% of full RGI	est. refl
1	25.696 ± 30.302	10.919 ± 11.459	3.937 ± 4.663	61.5	5.54
2	23.031 ± 21.914	9.174 ± 11.728	3.792 ± 4.326	69.2	5.62
3	25.454 ± 28.450	7.977 ± 6.602	2.506 ± 1.987	92.3	5.92
4	23.040 ± 26.086	7.674 ± 6.678	2.320 ± 2.015	84.6	5.85
5	33.737 ± 42.814	10.500 ± 8.211	2.669 ± 2.132	84.6	5.77
6	25.261 ± 30.018	10.580 ± 11.796	3.993 ± 3.677	0.0	4.85

(a) Lambertian distribution					
Room	E_{ML} (cm)	D_{RL} (cm)	O_{RL} (degrees)	% of full RGI	est. refl
1	23.959 ± 31.679	10.446 ± 11.390	3.599 ± 4.173	61.5	5.54
2	23.576 ± 24.558	9.235 ± 10.292	3.498 ± 3.787	69.2	5.62
3	25.891 ± 28.026	8.331 ± 6.546	2.534 ± 1.965	100.0	6
4	22.476 ± 24.342	7.803 ± 6.653	2.274 ± 1.913	92.3	5.92
5	33.904 ± 42.723	10.528 ± 8.269	2.678 ± 2.146	84.6	5.77
6	25.770 ± 30.090	10.380 ± 11.677	4.043 ± 3.655	0.0	4.92

(b) Tilted Lambertian distribution					
Room	E_{ML} (cm)	D_{RL} (cm)	O_{RL} (degrees)	% of full RGI	est. refl
1	22.022 ± 26.027	9.806 ± 10.664	3.388 ± 3.341	53.8	5.31
2	29.619 ± 26.668	18.741 ± 33.571	8.349 ± 13.759	61.5	5.23
3	28.171 ± 29.746	9.384 ± 9.543	2.702 ± 2.740	100.0	6
4	24.952 ± 24.336	8.883 ± 6.774	2.590 ± 2.221	84.6	5.77
5	40.629 ± 46.984	12.002 ± 8.639	3.343 ± 3.695	76.9	5.69
6	26.143 ± 31.104	11.433 ± 13.609	4.274 ± 4.114	0.0	4.85

(c) Vector mixing					
Room	E_{ML} (cm)	D_{RL} (cm)	O_{RL} (degrees)	% of full RGI	est. refl
1	22.022 ± 26.027	9.806 ± 10.664	3.388 ± 3.341	53.8	5.31
2	29.619 ± 26.668	18.741 ± 33.571	8.349 ± 13.759	61.5	5.23
3	28.171 ± 29.746	9.384 ± 9.543	2.702 ± 2.740	100.0	6
4	24.952 ± 24.336	8.883 ± 6.774	2.590 ± 2.221	84.6	5.77
5	40.629 ± 46.984	12.002 ± 8.639	3.343 ± 3.695	76.9	5.69
6	26.143 ± 31.104	11.433 ± 13.609	4.274 ± 4.114	0.0	4.85

Table 4.7: Reflector localization performance metrics for Set 1.

Room	E_{ML} (cm)	D_{RL} (cm)	O_{RL} (degrees)	% of full RGI	est. refl
1	30.506 ± 34.911	12.058 ± 13.825	5.177 ± 8.329	76.9	5.77
2	20.289 ± 21.287	7.886 ± 8.678	2.862 ± 2.453	61.5	5.31
3	28.122 ± 29.361	7.949 ± 6.438	2.629 ± 1.923	92.3	5.92
4	26.141 ± 26.190	8.430 ± 6.408	2.575 ± 1.992	100.0	6
5	34.967 ± 39.459	11.227 ± 8.048	2.744 ± 1.891	92.3	5.85
6	22.594 ± 25.003	8.570 ± 8.316	3.401 ± 2.336	0.0	4.85

(a) Set 4					
Room	E_{ML} (cm)	D_{RL} (cm)	O_{RL} (degrees)	% of full RGI	est. refl
1	26.452 ± 29.236	9.860 ± 10.361	3.858 ± 3.452	84.6	5.85
2	26.671 ± 28.418	10.428 ± 10.262	4.208 ± 5.518	53.8	5.38
3	28.258 ± 28.745	9.573 ± 7.185	2.708 ± 1.900	61.5	5.54
4	27.539 ± 30.188	9.340 ± 7.651	2.816 ± 2.454	61.5	5.62
5	38.440 ± 41.850	11.654 ± 10.312	3.262 ± 2.499	61.5	5.54
6	26.274 ± 31.174	10.790 ± 12.600	4.023 ± 3.811	0.0	4.92

(b) Set 5					
Room	E_{ML} (cm)	D_{RL} (cm)	O_{RL} (degrees)	% of full RGI	est. refl
1	25.882 ± 30.300	9.398 ± 9.518	3.792 ± 3.371	76.9	5.77
2	23.567 ± 24.559	10.729 ± 12.098	3.928 ± 6.936	53.8	4.85
3	30.879 ± 29.236	10.114 ± 8.774	2.936 ± 2.103	61.5	5.46
4	24.135 ± 27.239	8.484 ± 6.574	2.503 ± 2.197	46.2	5.15
5	40.771 ± 45.173	12.252 ± 8.553	3.279 ± 2.354	46.2	5.23
6	26.451 ± 31.271	11.666 ± 14.144	3.952 ± 3.895	0.0	5

(c) Set 6					
Room	E_{ML} (cm)	D_{RL} (cm)	O_{RL} (degrees)	% of full RGI	est. refl
1	21.978 ± 22.498	9.696 ± 9.680	3.236 ± 2.764	46.2	5.46
2	29.115 ± 27.561	12.659 ± 13.605	3.959 ± 3.240	53.8	5.38
3	33.511 ± 30.715	10.433 ± 9.202	3.587 ± 3.094	46.2	5.38
4	27.617 ± 28.702	8.426 ± 6.545	2.858 ± 2.372	53.8	5.46
5	43.557 ± 47.131	13.436 ± 13.236	3.560 ± 2.795	46.2	5.15
6	24.779 ± 30.439	10.273 ± 10.735	3.742 ± 3.468	0.0	4.77

(d) Set 7					
Room	E_{ML} (cm)	D_{RL} (cm)	O_{RL} (degrees)	% of full RGI	est. refl
1	21.978 ± 22.498	9.696 ± 9.680	3.236 ± 2.764	46.2	5.46
2	29.115 ± 27.561	12.659 ± 13.605	3.959 ± 3.240	53.8	5.38
3	33.511 ± 30.715	10.433 ± 9.202	3.587 ± 3.094	46.2	5.38
4	27.617 ± 28.702	8.426 ± 6.545	2.858 ± 2.372	53.8	5.46
5	43.557 ± 47.131	13.436 ± 13.236	3.560 ± 2.795	46.2	5.15
6	24.779 ± 30.439	10.273 ± 10.735	3.742 ± 3.468	0.0	4.77

Table 4.8: Reflector localization performance metrics for different scattering coefficients.

4. IMPACT OF DIFFUSE REFLECTIONS

the resized RIR stack.

4.5.1 Bilateral Filter

The goal of the processing is the filtering of the diffuse reflections, but at the same time, the specular wavefront should be preserved. In terms of image processing, the specular wavefront can be seen as an image edge and the diffuse reflection as noise. The assumption of an image edge is due to the higher amplitude of the specular wavefront compared to the amplitude of the diffuse reflections. A filter which both combines these properties is the bilateral filter. The bilateral filter was introduced by Tomasi and Manduchi in [TM98]. The bilateral filter is capable of preserving edges as well as filtering noise at the same time. The bilateral filter is defined as

$$I_f(x) = \frac{1}{W(x)} \sum_{x_i \in \Omega} G_{\sigma_s}(\|x_i - x\|) G_{\sigma_r}(\|\mathbf{I}(\mathbf{x}_i) - \mathbf{I}(\mathbf{x})\|), \quad (4.1)$$

where G_{σ_s} is the space kernel, G_{σ_r} the range kernel, x denotes the pixel Ω is the filtering window centered at x , I_f the filtered image, I the input image and $I(x)$ is the intensity at pixel s .

The kernels can be chosen Gaussian and the spatial kernel is then described as

$$G_{\sigma_s}(\|x_i - x\|) = \exp \left(\left(\frac{-(\|x_i - x\|)}{2\sigma_s} \right)^2 \right) \quad (4.2)$$

and the range kernel by

$$G_{\sigma_r}(\|x_i - x\|) = \exp \left(\left(\frac{-(\|\mathbf{I}(\mathbf{x}_i) - \mathbf{I}(\mathbf{x})\|)}{2\sigma_r} \right)^2 \right). \quad (4.3)$$

Therefore, the parameters which are adjusted and determine the behavior of the filter are the space parameter σ_s and the range parameter σ_r . The space parameter determines the spatial extent of the kernel, thus the amount of the considered pixels in the neighborhood of the recent pixel. The range parameter can be seen as the "minimum" amplitude of an edge. The used bilateral filter in the implementation was kindly provided by the Image and Visual Representation Lab (EPFL) of Prof. Sabine Süsstrunk¹. For the determination of the space parameter, the size of the image is used. The space parameter is obtained by

$$\sigma_s = \frac{\min(N, M)}{21}, \quad (4.4)$$

where N and M denote the size of the image in pixels.

¹<https://ivrl.epfl.ch/people/people-susstrunk/>

The determination of the range parameter should be chosen according to the range of the edges to detect. Therefore, the amplitude of the reflections is taken into account. The determination of this parameter is done by the obtained RIRs. In the RIRs, the first seven maxima are estimated and the first maximum is omitted, as it should correspond to the direct sound. These maxima are searched for all RIRs of the corresponding sub-arrays. Then, the determination of the range parameter reads as

$$\sigma_r = \frac{\sum_{i=1}^M p_i}{6Mc}, \quad (4.5)$$

where p_i denote the obtained maxima, M is the number of speakers and c is a scaling factor. The search of the maxima is done, as the strength of the reflection can differ profoundly for different setups. Thus, it should be scaled according to the edges which correspond to the specular reflections. The scaling is introduced, as the estimation of the peaks could include errors, as the used peak finding algorithm is expected not to work perfectly. Hence, it is used to avoid filtering of the specular reflections.

4.5.2 Extended Prewitt Filter

The next filter to encounter the impact of diffuse reflections is the here called extended Prewitt filter, due to similarity to the well-known Prewitt filter. The difference to the Prewitt filter is the extension of the dimensions in the time domain. This filter is described and used by the author of the evaluated algorithm in [BWH17]. The filter is defined as

$$\begin{pmatrix} -1 & \dots & -1 & 0 & 1 & \dots & 1 \\ -1 & \dots & -1 & 0 & 1 & \dots & 1 \\ -1 & \dots & -1 & 0 & 1 & \dots & 1 \end{pmatrix}, \quad (4.6)$$

where each row defined by L negative ones, one 0 and L positive ones. After the filtering an a non-linearity $g(\nu) = \max(0, \nu)$ is applied to the filtered image. The non-linearity is used to equalize the negative values introduced by the filtering. The negative values are equalized by setting them to 0. Besides, the filter should also provide equalization of the diffuse tail. Due to the use of L positive and negative values, they should add up destructively in the diffuse tail and thus lead to a filtering of the diffuse reflections.

The introduced filters can be applied independently or combined. In the combined usage of the filters, the bilateral filter is used first and afterward the extended Prewitt filter is applied.

4. IMPACT OF DIFFUSE REFLECTIONS

4.5.3 Filtered Stack-Lines

An example shows the effect of the before introduced filters on the RIR stack. In Figure 4.5a, the RIR stack with no filter applied is shown.

In Figure 4.5b, the RIR stack processed with the bilateral filter is depicted. It can be seen, that the diffuse reflections are filtered to a certain extent. Mainly, the later diffuse reflections of the decaying tail are filtered. Hence, it provides filtering of the diffuse reflections, whereas the wavefront from the specular reflection is preserved. Certainly, the amount of filtered diffuse reflections depends on the choice of the range parameter. The range parameter has to be chosen carefully. The choice of a small range parameter could lead to no filtering at all. The other way round, a high choice could lead to a filtering of the specular wavefronts.

In Figure 4.5c, the extended Prewitt filter is applied. The filter provides stronger filtering of the diffuse reflections. However, the stronger filtering is coupled to a drawback. Due to the size of the filter, the specular wavefronts will be smeared by a minimum amount of L samples, which has to be accounted for by a time-shift. This smearing of the SLs is also prominent in the LRT. The smearing leads to a broadening of the LRT peak for one wavefront, in the angular and in the time domain. The smearing could then introduce ambiguity in terms of the peak estimation.

The combination of both filters is shown in Figure 4.5d. By visual inspection, the difference of the combination and the extended Prewitt filter is small. However, as one example is not representative for all cases, the performance has to be evaluated in terms of the above-used performance metrics.

4.6 Evaluation of the Countermeasures

In this section, the impact on the performance of the filtering is evaluated. For this evaluation, the bilateral filter, the extended Prewitt filter and the combination of both filters is evaluated. For the evaluation, the same sets are used for comparison with the beforehand used sets. The organization of this part of the evaluation, differs from the evaluation above. The results of TOA detection and disambiguation are shown together with the results of the RL. The results are evaluated for only bilateral filtering, only the extended Prewitt filter, and both filters combined. For the evaluation, not all sets are used compared to Section 4.4, due to the high amount of data. The sets which are not evaluated can be found in the Annex A and B. The results are discussed with the focus on the difference to the non-filtered stacks. After the evaluation of the bilateral filter, the results will be compared with hindsight to the differences of the filters.

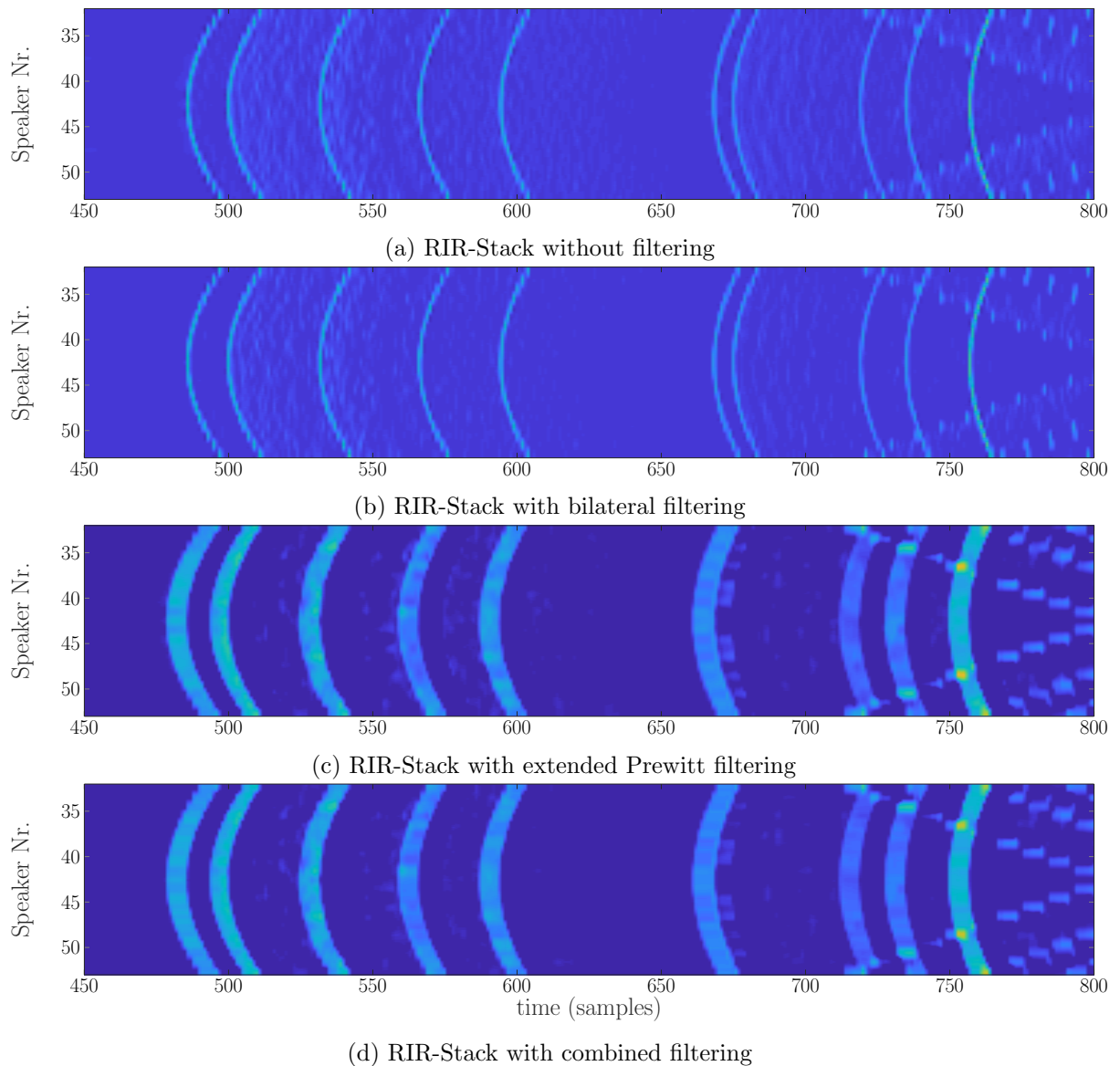


Figure 4.5: RIR stacks without filter in (a), with bilateral filter in (b), with extended Prewitt filter in (c) and with combination of both filters in (d).

4. IMPACT OF DIFFUSE REFLECTIONS

4.6.1 Bilateral Filter

In this part, the bilateral filter is applied and the impact on the performance is investigated. Here, the scaling factor of the range parameter is set to $c = 10$ in all evaluated sets.

In Table 4.9, the TOA detection and disambiguation metrics for Set 5 and Set 7 are seen. For Set 5, it can be seen that the bilateral filtering is not improving the average TPR for the first-order reflections compared to the non-filtered results. The overall performance is decreasing from 96% to 95%. This decrease of the average TPR is mainly introduced due to Room 5. Whereas the bilateral filtering is decreasing the TPR from about 99% to only 83%. For every other room in this set, the TPR for the first-order reflections is only slightly increasing or decreasing.

A more significant difference is seen for the RMSE for the first-order reflections. Here, the RMSE is decreasing from $132.8\mu\text{s}$ to $123.5\mu\text{s}$. For the TPR of the second-order reflections, no improvement is achieved. The average TPR is decreasing from 53% to only 32.1%. This decrease occurs as the second-order reflections are not strong enough and therefore not detected as edges. Further, the failed detection rate is increased compared to the non-filtered results. This increase is closely related to filtering of the second-order reflections. Due to the filtering, more second-order reflections are not detected. The algorithm is then associating more second-order SLs wrongly. However, this is a rather unimportant issue, as the first-order reflections are more important.

The most notable improvement in comparison to the different scattering coefficients are reached for the highest scattering coefficient (Set 7 - see Table 4.9b). Here, the behavior of VM has to be taken into account. For a higher scattering coefficient, VM is behaving more directionless. For this reason, the diffuse reflections around the specular reflection are not as strong as for smaller scattering coefficients and lead to a longer decay of the diffuse reflections. This decay is filtered more by the bilateral filter and therefore it results in a higher improvement.

We have seen, that the bilateral filter can lead to improvement in terms of TOA detection and disambiguation. However, there are also cases, where the filter fails. In Table 4.10, such a case is shown. The average TPR for the first-order reflection is dropping from 97% to 87%. Also, the FDR gets worse compared to the unfiltered case. The drop of the FDR can be explained by the wrong estimation of the range parameter. The two non-diffuse reflecting walls introduce this false estimation. The non-diffuse reflection leads to a higher amplitude of the first-order reflections compared to the diffuse reflected first-order reflections.

For this reason, the range parameter is overestimated. Hence, the diffuse reflected first-order reflections are filtered to a certain extent and will lead to a decrease of performance. Therefore, incorrect estimation of the range parameter will decrease the performance.

4.6 EVALUATION OF THE COUNTERMEASURES

Order Room	All FDR%	direct sound		TPR%	1 RMSE μs	2	
		TPR%	RMSE μs			TPR%	RMSE μs
1	28.3	100.0	121.8	98.7	163.1	32.9	143.5
2	17.0	100.0	79.5	89.7	110.2	47.0	140.5
3	22.8	100.0	77.9	97.4	103.6	28.2	119.0
4	23.5	100.0	77.7	100.0	101.0	25.3	102.8
5	20.1	100.0	81.4	83.3	127.7	31.7	130.5
6	23.5	100.0	106.8	98.7	135.5	27.4	151.2
AVG	22.5	100.0	90.8	94.7	123.5	32.1	131.3

(a) Set 5

Order Room	All FDR%	direct sound		TPR%	1 RMSE μs	2	
		TPR%	RMSE μs			TPR%	RMSE μs
1	21.6	100.0	121.8	98.7	156.3	51.3	143.7
2	17.8	100.0	78.6	93.6	108.2	50.4	127.2
3	19.5	100.0	77.9	98.7	101.0	47.9	95.9
4	19.9	100.0	77.7	98.7	103.0	53.7	107.6
5	26.0	100.0	81.4	94.9	120.7	46.2	121.5
6	25.5	100.0	106.1	98.7	133.6	44.9	97.9
AVG	21.7	100.0	90.6	97.2	120.5	49.0	115.6

(b) Set 7

Table 4.9: TOA detection and disambiguation metrics with bilateral filtering.

Order Room	All FDR%	direct sound		TPR%	1 RMSE μs	2	
		TPR%	RMSE μs			TPR%	RMSE μs
1	30.6	100.0	121.8	88.5	156.9	35.0	121.1
2	21.4	100.0	79.5	98.7	119.8	41.0	150.8
3	26.7	100.0	77.9	84.6	110.9	35.5	109.9
4	30.7	100.0	77.7	91.0	102.8	33.5	106.7
5	30.4	100.0	81.4	73.1	112.9	37.5	138.2
6	26.5	100.0	106.8	85.9	121.7	36.8	106.9
AVG	27.7	100.0	90.8	87.0	120.8	36.5	122.3

Table 4.10: TOA detection and disambiguation metrics with bilateral filtering for Set 1 and the tilted Lambertian distribution.

Next, the impact of the bilateral filter on the RL is examined. For this task, the results of Set 7 are used. In Table 4.11, the performance metrics for RL with the bilateral filter is shown. The bilateral filter improves the average number of the estimated reflectors and also the percentage of full RGI in every case. Furthermore, the Euclidean distance stays in the same region or is even improved. The maximum Euclidean distance is lowered from 44cm to 34cm. The maximum distance offset is also decreased from 13cm to 11cm. The maximum orientation error stays about the same as for the non-filtered case, but in overall, the orientation error also decreases.

4. IMPACT OF DIFFUSE REFLECTIONS

Room	E_{ML} (cm)	D_{RL} (cm)	O_{RL} (degrees)	% of full RGI	est. refl
1	24.029 ± 28.463	9.784 ± 11.012	3.383 ± 2.988	84.6	5.85
2	21.060 ± 22.750	8.804 ± 8.898	3.387 ± 3.799	76.9	5.77
3	26.656 ± 27.746	8.492 ± 7.080	2.523 ± 1.969	92.3	5.92
4	22.839 ± 26.557	7.334 ± 7.157	2.231 ± 2.034	100.0	6
5	34.105 ± 43.175	11.207 ± 9.563	2.562 ± 1.987	76.9	5.69
6	26.495 ± 29.876	11.123 ± 11.197	3.828 ± 3.254	0.0	4.92

Table 4.11: Reflector localization performance metrics with bilateral filtering for Set 7.

Therefore, the bilateral filter can also provide an improvement in terms of RL.

4.6.2 Extended Prewitt Filter

In the following, the performance parameters for the extended Prewitt filter introduced in Section 4.5.2. For this evaluation, the length of the Prewitt filter was chosen to $L = 4$. In terms of the evaluation, the same sets as for the bilateral filter are examined.

The use of the extended Prewitt filter also provides good results in terms of TOA disambiguation. In Table 4.12, the results for Set 5 and Set 7 are shown. For the first-order TPRs the filtering yields better results for Set 5, whereas for Set 7 the results are similar. The better results in Set 5 are mainly due to the better performance for Room 2 and Room 5. Here, the impact of the destructive effect of the smearing due to diffuse reflections is occurring. In this case, the extended Prewitt filter can eliminate these reflections in contrast to the bilateral filter. Hence, for such cases, the extended Prewitt filter provides better results.

As shown, the extended Prewitt filter leads to no improvement for the average RMSE. It is able to eliminate diffuse reflections, but also an estimation error due to the smearing of the wavefront can be introduced. Again it has to be mentioned, that the increase of the RMSE is in a minimal range of about $10\mu\text{s}$.

Here, Set 1 for the tilted Lambertian distribution is not further examined, as it should provide an example where the bilateral filter can fail.

The RL performance of the filtered signal with the extended Prewitt filter yields a near-perfect result in terms of the number of estimated reflectors (see Table 4.13). For the Set 1 to 5, a nearly perfect rate is achieved. The disadvantage compared to the bilateral filter, are the higher Euclidean distance, distance offset, and orientation error due to the broadening of the wavefronts.

Order Room	All FDR%	direct sound		TPR%	1 RMSE μs	2	
		TPR%	RMSE μs			TPR%	RMSE μs
1	16.8	100.0	107.9	93.6	155.6	49.1	154.8
2	12.7	100.0	77.3	93.6	121.1	50.9	143.6
3	19.0	100.0	76.9	100.0	131.8	41.0	124.2
4	26.5	100.0	76.6	100.0	123.9	31.6	140.6
5	22.0	100.0	79.6	98.7	135.7	45.2	126.0
6	23.1	100.0	95.1	97.4	129.0	40.6	134.8
AVG	20.0	100.0	85.6	97.2	132.8	43.1	137.3

(a) Set 5							
Order Room	All FDR%	direct sound		TPR%	1 RMSE μs	2	
		TPR%	RMSE μs			TPR%	RMSE μs
1	16.8	100.0	107.9	92.3	153.8	55.1	147.0
2	13.2	100.0	77.3	96.2	135.6	57.7	142.3
3	16.1	100.0	76.9	100.0	112.8	50.0	119.0
4	13.7	100.0	76.6	98.7	116.4	54.5	138.6
5	17.7	100.0	79.6	100.0	146.5	50.5	143.3
6	23.1	100.0	95.1	98.7	126.6	47.0	141.1
AVG	16.8	100.0	85.6	97.6	132.0	52.5	138.5

(b) Set 7							
Order Room	All FDR%	direct sound		TPR%	1 RMSE μs	2	
		TPR%	RMSE μs			TPR%	RMSE μs
1	16.8	100.0	107.9	92.3	153.8	55.1	147.0
2	13.2	100.0	77.3	96.2	135.6	57.7	142.3
3	16.1	100.0	76.9	100.0	112.8	50.0	119.0
4	13.7	100.0	76.6	98.7	116.4	54.5	138.6
5	17.7	100.0	79.6	100.0	146.5	50.5	143.3
6	23.1	100.0	95.1	98.7	126.6	47.0	141.1
AVG	16.8	100.0	85.6	97.6	132.0	52.5	138.5

Table 4.12: TOA detection and disambiguation metrics with extended Prewitt filtering.

Room	$E_{ML}(\text{cm})$	$D_{RL}(\text{cm})$	$O_{RL}(\text{degrees})$	% of full RGI	est. refl
1	32.012 ± 43.467	13.134 ± 18.063	4.864 ± 5.961	92.3	5.92
2	26.110 ± 28.330	10.816 ± 13.645	4.285 ± 6.140	92.3	5.92
3	25.950 ± 28.980	7.957 ± 6.792	2.504 ± 2.058	100.0	6
4	25.121 ± 28.961	7.529 ± 7.121	2.462 ± 2.300	100.0	6
5	39.499 ± 45.813	12.408 ± 10.422	2.913 ± 2.223	92.3	5.92
6	25.563 ± 28.104	11.636 ± 14.457	3.919 ± 3.533	0.0	4.92

Table 4.13: Reflector localization performance metrics with extended Prewitt filtering for Set 7.

4.6.3 Filter Combination

The last evaluation is concerned with the performance of the combination of the two filters. The same filter parameters as above were used.

In Table 4.14, the TOA detection and disambiguation metrics for the combination of the filters are shown for Set 5 and Set 7. The combination of the bilateral filter and the extended Prewitt filter yields similar results for most of the evaluated parameters compared to the use of only the extended Prewitt filter. The only difference is the lower RMSE for the first-order diffuse reflections.

4. IMPACT OF DIFFUSE REFLECTIONS

Order Room	All FDR%	direct TPR%	sound RMSE μs	TPR%	1 RMSE μs	TPR%	2 RMSE μs
1	19.4	100.0	108.0	92.3	151.7	42.7	143.6
2	15.7	100.0	77.4	94.9	119.2	44.9	138.1
3	20.8	100.0	77.0	100.0	112.1	34.2	125.6
4	25.2	100.0	77.3	100.0	110.0	28.5	150.4
5	19.4	100.0	79.7	96.2	127.7	40.4	129.8
6	25.6	100.0	95.4	98.7	125.2	35.9	130.3
AVG	21.0	100.0	85.8	97.0	124.3	37.8	136.3

(a) Set 5

Order Room	All FDR%	direct TPR%	sound RMSE μs	TPR%	1 RMSE μs	TPR%	2 RMSE μs
1	15.4	100.0	108.6	93.6	144.3	56.8	136.2
2	11.9	100.0	77.4	96.2	131.8	58.5	151.5
3	13.3	100.0	76.7	100.0	113.6	50.9	120.9
4	14.8	100.0	77.0	100.0	112.6	53.1	137.8
5	18.0	100.0	79.4	98.7	148.1	49.0	136.8
6	21.5	100.0	95.1	100.0	132.6	48.3	126.0
AVG	15.8	100.0	85.7	98.1	130.5	52.8	134.9

(b) Set 7

Table 4.14: TOA disambiguation and performance metrics with bilateral and extended Prewitt filtering.

Room	$E_{ML}(\text{cm})$	$D_{RL}(\text{cm})$	$O_{RL}(\text{degrees})$	% of full RGI	est. refl
1	27.357 ± 33.915	11.149 ± 12.216	3.926 ± 3.873	100.0	6
2	25.898 ± 28.097	10.883 ± 12.634	4.267 ± 5.553	92.3	5.92
3	26.087 ± 29.431	8.408 ± 7.539	2.342 ± 1.897	100.0	6
4	23.380 ± 26.788	7.584 ± 6.776	2.301 ± 2.045	100.0	6
5	38.409 ± 47.119	12.939 ± 11.135	2.996 ± 3.275	76.9	5.77
6	27.891 ± 30.453	12.884 ± 15.228	4.267 ± 3.744	0.0	5

Table 4.15: Reflector localization performance metrics with bilateral and extended Prewitt filtering for Set 7.

The higher differences are observed when comparing to the results of the bilateral filter. The difference, to the bilateral filter, is mainly observed for the TPR of the second-order reflections. With the use of the combined filter, an increase of the second-order TPR is achieved compared to the use of only a bilateral filter. However, also a decrease compared to the use of only the extended Prewitt filter for Set 5. The dominant filter in the combination is the extended Prewitt filter in terms of TOA disambiguation performance.

In Table 4.15, the dominance of the extended Prewitt filter is also observable for the RL performance. The obtained metrics only differ to a small extent. Whereas for the first room a better result is obtained for the number of average estimated reflectors, the combined filter application yields a worse performance for Room 5. Therefore, improvement with the use of the combination is not observable.

4.7 Summary

In this chapter, we have seen how the diffuse reflections can affect the RGI algorithm. The impact of the diffuse reflections was evaluated by different simulated sets. It was shown, that the impact on the detection of SLs is not neglectable in terms of the individual estimation of wavefronts for one sub-array. Several different possibilities of errors were shown. In contrast to the impairment of the detection, a case was shown where diffuse reflections can improve SL detection.

Away from the impact on the detection of individual SLs in the sub-arrays, the algorithm provides a very robust TOA disambiguation in the case of diffuse reflections. The robustness is gained due to the use of all sub-arrays. Degradation of the performance was only observed for high scattering coefficients and six diffusely reflecting walls. However, also in these cases, the algorithm provided good results.

A more noticeable degradation of the performance was observed for the RL. At high scattering coefficients, the number of average estimated reflectors was decreasing with an increasing scattering coefficient. For the worst case (Set 7), the algorithm was able to detect all reflectors for only about every second microphone position.

Two different filter methods were introduced to encounter the impact of diffuse reflections - the bilateral filter as well as an extended version of the Prewitt filter. The filtering showed an improvement in most of the evaluated cases. The improvement resulted in nearly perfect rates for the first-order TPRs and the percentage of full room reconstruction. Whereas, for the combination of both filters, no improvement compared to the single use was achieved. In some cases, the bilateral filter failed due to wrongly estimated input parameters. In overall, the implemented filters resulted in an improvement in terms of the evaluated metrics.

Chapter 5

Conclusions

In this thesis, we studied the impact of diffuse and disturbed reflection on a state-of-the-art room geometry inference algorithm. For this study, a RIR generator was extended, to handle first order diffuse reflections. The RIR generator is capable of simulating diffuse reflections with more sophisticated and flexible models compared to other RIR generators. On the basis of this simulator, investigations were carried out to understand the impact of diffuse reflections on the evaluated algorithm.

In the first part, an approach was presented which obtains the pressure RIR directly for first-order diffuse reflections. Further, the scattering distributions were not used in terms of probability, but they were used to obtain the strength of a diffuse reflection directly. We have seen, that different model for diffuse reflection yield different simulation results. The use of the vector mixing model profoundly differs from the behavior of the classic Lambertian model or the tilted Lambert. However, in this thesis, no research was conducted in terms of the realism of the used models. Nevertheless, with the use of three different models, different scenarios can now be simulated.

The second part was concerned with the impact of diffuse reflections. The investigation led to a better understanding of the impact of diffuse reflection. Further, it was shown that the evaluated algorithm is mostly able to work robustly in diffuse conditions. The investigation included extensive evaluation of different scenarios. Only in some situations, the algorithm was impaired in terms of performance.

With the investigation of the impact, filtering approaches were introduced. These filtering approaches, namely the bilateral filter and the extended Prewitt filter, were applied to cope with diffuse reflections. It was shown, that the proposed filtering techniques lead to an equalization of the impact of diffuse reflection. We were able to achieve nearly perfect results with the use of these filtering techniques for diffuse simulations.

5. CONCLUSIONS

In future research, the proposed RIR generator can be extended to higher-order diffuse reflections. Additionally, research can be conducted in terms of the realism of the method. The analysis, in terms of the impact on the RGI algorithm, can be extended by investigating more set-ups for diffuse conditions. Moreover, the improvement due to the proposed filtering techniques has to be conducted for real-world scenarios. Lastly, other filtering techniques can be included in the algorithm and investigating the impact on the performance.

Appendix A

TOA Detection and Disambiguation Metrics

In this chapter, all TOA disambiguation and performance Metrics for the evaluated sets are listed. For every set, the evaluation results are grouped as:

- (a) No filtering
- (b) Bilateral filtering
- (c) Extended Prewitt filtering
- (d) Combination of the filtering

The tables are then listed according their set number. For the first and the second set, the results are ordered as:

1. Lambert
2. Tilted Lambert
3. Vector Mixing

For the sake of completeness, the sets and the rooms are listed again in Table A.2 and Table A.1, respectively.

A. TOA DETECTION AND DISAMBIGUATION METRICS

Room	Width (m)	Depth (m)	Heights (m)
1	4.5	5	2.5
2	6	4	2.9
3	6	8.5	3.5
4	9	7.5	3
5	6	12	3
6	4.5	5	3

Table A.1: Room dimensions

Set	s(f) (f in kHz)										Method	DW
	0.25	0.4	0.5	1	2	4	8	16	32	48		
1	0.05	0.10	0.20	0.20	0.30	0.40	0.50	0.50	0.60	0.60	All	4
2	0.05	0.10	0.70	0.80	0.80	0.80	0.80	0.80	0.80	0.80	All	4
3	0.05	0.05	0.05	0.20	0.30	0.40	0.60	0.90	0.90	0.90	VM	2
4	0	0	0	0.05	0.10	0.15	0.20	0.25	0.25	0.25	VM	6
5	0.05	0.05	0.05	0.10	0.20	0.30	0.40	0.50	0.50	0.50	VM	6
6	0.05	0.05	0.05	0.15	0.30	0.45	0.60	0.75	0.75	0.75	VM	6
7	0.05	0.05	0.05	0.20	0.40	0.60	0.80	1.00	1.00	1.00	VM	6

Table A.2: Diffuse simulation sets (DW: Nr. of diffuse walls, TL: Tilted Lambert

A. TOA DETECTION AND DISAMBIGUATION METRICS

Order	All	direct sound			1		2
Room	FDR%	TPR%	RMSE μs	TPR%	RMSE μs	TPR%	RMSE μs
1	17.3	100.0	107.7	87.2	151.0	54.3	158.5
2	17.9	100.0	79.1	91.0	123.1	50.9	149.9
3	12.4	100.0	78.5	100.0	109.2	50.0	123.4
4	16.7	100.0	78.8	98.7	105.2	52.4	139.1
5	13.0	100.0	80.7	100.0	125.2	47.1	143.6
6	19.3	100.0	98.6	97.4	120.7	46.2	131.4
AVG	16.1	100.0	87.2	95.7	122.4	50.1	141.0

(a)							
Order	All	direct sound			1		2
Room	FDR%	TPR%	RMSE μs	TPR%	RMSE μs	TPR%	RMSE μs
1	30.1	100.0	121.8	85.9	150.7	35.9	130.3
2	23.5	100.0	79.5	93.6	120.3	41.9	139.2
3	26.2	100.0	77.9	75.6	118.1	36.8	107.9
4	30.1	100.0	77.7	79.5	104.5	36.6	108.2
5	26.3	100.0	81.4	74.4	114.6	39.4	133.7
6	26.7	100.0	106.8	84.6	122.7	37.2	101.2
AVG	27.2	100.0	90.8	82.3	121.8	38.0	120.1

(b)							
Order	All	direct sound			1		2
Room	FDR%	TPR%	RMSE μs	TPR%	RMSE μs	TPR%	RMSE μs
1	19.8	100.0	107.7	91.0	152.6	48.3	155.6
2	17.4	100.0	77.3	93.6	115.0	47.4	153.3
3	18.2	100.0	76.9	96.2	111.4	38.5	126.2
4	23.7	100.0	76.6	100.0	111.2	39.3	129.5
5	19.4	100.0	79.6	97.4	130.6	40.4	146.9
6	25.1	100.0	95.1	94.9	121.5	35.9	133.6
AVG	20.6	100.0	85.5	95.5	123.7	41.6	140.8

(c)							
Order	All	direct sound			1		2
Room	FDR%	TPR%	RMSE μs	TPR%	RMSE μs	TPR%	RMSE μs
1	21.3	100.0	108.4	84.6	149.4	41.0	158.5
2	17.6	100.0	77.7	91.0	116.4	46.2	141.8
3	19.9	100.0	77.0	92.3	111.1	37.6	126.2
4	23.9	100.0	77.3	94.9	109.9	36.6	147.4
5	24.7	100.0	79.7	73.1	113.8	38.5	148.9
6	24.6	100.0	95.4	87.2	116.0	36.3	132.1
AVG	22.0	100.0	85.9	87.2	119.4	39.4	142.5

(d)

Table A.3: Set 1 - Lambert

A. TOA DETECTION AND DISAMBIGUATION METRICS

Order Room	All FDR%	direct sound		1		2	
		TPR%	RMSE μs	TPR%	RMSE μs	TPR%	RMSE μs
1	15.2	100.0	107.7	88.5	145.6	53.8	161.0
2	19.4	100.0	79.1	93.6	118.3	46.6	140.4
3	13.7	100.0	78.5	98.7	103.4	51.3	121.9
4	12.6	100.0	78.8	100.0	105.1	57.3	143.9
5	11.6	100.0	80.7	100.0	125.2	50.0	149.4
6	19.7	100.0	98.6	98.7	122.5	47.0	133.9
AVG	15.4	100.0	87.2	96.6	120.0	51.0	141.7

(a)

Order Room	All FDR%	direct sound		1		2	
		TPR%	RMSE μs	TPR%	RMSE μs	TPR%	RMSE μs
1	30.6	100.0	121.8	88.5	156.9	35.0	121.1
2	21.4	100.0	79.5	98.7	119.8	41.0	150.8
3	26.7	100.0	77.9	84.6	110.9	35.5	109.9
4	30.7	100.0	77.7	91.0	102.8	33.5	106.7
5	30.4	100.0	81.4	73.1	112.9	37.5	138.2
6	26.5	100.0	106.8	85.9	121.7	36.8	106.9
AVG	27.7	100.0	90.8	87.0	120.8	36.5	122.3

(b)

Order Room	All FDR%	direct sound		1		2	
		TPR%	RMSE μs	TPR%	RMSE μs	TPR%	RMSE μs
1	19.4	100.0	107.7	92.3	158.7	47.9	150.5
2	15.9	100.0	77.5	88.5	116.4	46.6	160.7
3	21.8	100.0	76.9	96.2	110.9	38.5	113.1
4	21.9	100.0	76.6	100.0	108.2	42.0	132.8
5	21.4	100.0	79.6	94.9	123.2	43.3	143.4
6	24.0	100.0	95.1	96.2	123.9	37.6	122.5
AVG	20.7	100.0	85.6	94.7	123.5	42.6	137.2

(c)

Order Room	All FDR%	direct sound		1		2	
		TPR%	RMSE μs	TPR%	RMSE μs	TPR%	RMSE μs
1	21.3	100.0	108.4	89.7	147.9	40.2	150.0
2	17.1	100.0	77.7	92.3	112.9	46.2	154.2
3	22.3	100.0	77.0	93.6	110.6	36.3	119.3
4	20.7	100.0	77.3	93.6	110.0	41.1	138.7
5	27.9	100.0	79.7	74.4	126.7	40.4	155.3
6	24.4	100.0	95.3	85.9	110.8	37.2	130.0
AVG	22.3	100.0	85.9	88.2	119.8	40.2	141.2

(d)

Table A.4: Set 1 - Tilted Lambert

A. TOA DETECTION AND DISAMBIGUATION METRICS

Order	All	direct sound			1		2
Room	FDR%	TPR%	RMSE μs	TPR%	RMSE μs	TPR%	RMSE μs
1	17.1	100.0	107.7	88.5	151.2	52.6	161.3
2	17.6	84.6	80.1	83.3	121.7	48.7	146.1
3	16.9	100.0	78.5	100.0	110.6	45.3	129.9
4	11.8	100.0	78.9	100.0	117.3	46.5	131.7
5	10.0	100.0	80.8	100.0	145.7	41.8	141.2
6	16.8	100.0	98.6	96.2	117.2	47.0	129.3
AVG	15.0	97.4	87.4	94.7	127.3	47.0	139.9

(a)							
Order	All	direct sound			1		2
Room	FDR%	TPR%	RMSE μs	TPR%	RMSE μs	TPR%	RMSE μs
1	28.9	100.0	121.8	98.7	152.3	35.9	131.1
2	22.3	100.0	79.0	94.9	109.9	41.5	141.2
3	21.5	100.0	77.9	100.0	100.0	34.6	128.6
4	22.6	100.0	77.7	100.0	93.3	33.9	105.3
5	16.8	100.0	81.4	97.4	111.0	36.1	138.1
6	26.7	100.0	106.8	96.2	129.4	34.2	113.2
AVG	23.1	100.0	90.8	97.9	116.0	36.0	126.3

(b)							
Order	All	direct sound			1		2
Room	FDR%	TPR%	RMSE μs	TPR%	RMSE μs	TPR%	RMSE μs
1	21.2	100.0	108.2	91.0	178.4	44.4	142.3
2	21.5	100.0	78.2	91.0	121.2	44.0	151.5
3	17.9	100.0	76.9	100.0	119.7	41.0	129.1
4	21.6	100.0	76.6	98.7	108.8	38.4	129.9
5	16.7	100.0	79.6	100.0	135.5	37.5	139.7
6	20.4	100.0	95.1	98.7	118.5	40.6	139.1
AVG	19.9	100.0	85.8	96.6	130.4	41.0	138.6

(c)							
Order	All	direct sound			1		2
Room	FDR%	TPR%	RMSE μs	TPR%	RMSE μs	TPR%	RMSE μs
1	20.2	92.3	110.4	92.3	167.1	38.5	140.6
2	19.0	100.0	77.9	88.5	125.0	42.7	151.9
3	21.7	100.0	77.0	100.0	109.0	33.8	136.1
4	17.5	100.0	77.3	98.7	108.4	35.2	132.5
5	16.5	100.0	79.7	98.7	136.9	34.1	146.3
6	21.2	100.0	95.7	98.7	120.6	37.2	147.5
AVG	19.4	98.7	86.3	96.2	127.8	36.9	142.5

Table A.5: Set 1 - Vector Mixing

A. TOA DETECTION AND DISAMBIGUATION METRICS

Order Room	All FDR%	direct sound		TPR%	1 RMSE μs	TPR%	2 RMSE μs
		TPR%	RMSE μs				
1	16.9	100.0	107.7	87.2	130.2	40.6	162.0
2	15.6	100.0	79.2	93.6	125.8	40.2	143.4
3	10.3	100.0	78.5	100.0	119.6	38.5	135.8
4	15.1	100.0	78.8	97.4	117.3	37.5	147.9
5	13.4	100.0	80.7	98.7	147.1	40.9	160.9
6	14.6	100.0	98.6	93.6	126.5	38.0	122.4
AVG	14.3	100.0	87.3	95.1	127.7	39.3	145.4

(a)

Order Room	All FDR%	direct sound		TPR%	1 RMSE μs	TPR%	2 RMSE μs
		TPR%	RMSE μs				
1	28.9	100.0	121.8	98.7	152.3	35.9	131.1
2	22.3	100.0	79.0	94.9	109.9	41.5	141.2
3	21.5	100.0	77.9	100.0	100.0	34.6	128.6
4	22.6	100.0	77.7	100.0	93.3	33.9	105.3
5	16.8	100.0	81.4	97.4	111.0	36.1	138.1
6	26.7	100.0	106.8	96.2	129.4	34.2	113.2
AVG	23.1	100.0	90.8	97.9	116.0	36.0	126.3

(b)

Order Room	All FDR%	direct sound		TPR%	1 RMSE μs	TPR%	2 RMSE μs
		TPR%	RMSE μs				
1	14.9	100.0	107.7	88.5	137.9	37.2	146.3
2	16.9	100.0	77.3	88.5	123.9	40.6	159.9
3	16.3	100.0	76.9	100.0	115.5	30.3	126.9
4	19.9	100.0	76.6	100.0	113.3	31.2	142.1
5	19.7	100.0	79.6	98.7	144.2	34.1	145.3
6	21.3	100.0	95.1	89.7	112.7	30.8	130.7
AVG	18.2	100.0	85.5	94.2	124.6	34.0	141.9

(c)

Order Room	All FDR%	direct sound		TPR%	1 RMSE μs	TPR%	2 RMSE μs
		TPR%	RMSE μs				
1	15.4	100.0	108.4	75.6	132.4	36.3	150.8
2	12.3	100.0	77.7	91.0	131.0	41.0	153.2
3	17.2	100.0	77.0	96.2	119.4	28.2	128.4
4	22.3	100.0	77.3	96.2	117.1	31.2	144.2
5	19.0	100.0	79.7	96.2	144.8	32.7	134.9
6	22.5	100.0	95.4	75.6	107.1	29.1	103.4
AVG	18.1	100.0	85.9	88.5	125.3	33.1	135.8

(d)

Table A.6: Set 2 - Lambert

A. TOA DETECTION AND DISAMBIGUATION METRICS

Order	All	direct sound			1		2
Room	FDR%	TPR%	RMSE μs	TPR%	RMSE μs	TPR%	RMSE μs
1	18.0	100.0	107.7	88.5	127.0	40.2	170.3
2	13.7	100.0	79.2	89.7	123.0	42.3	147.7
3	10.5	100.0	78.5	100.0	117.8	38.9	153.7
4	14.9	100.0	78.8	100.0	117.1	40.1	149.8
5	12.3	100.0	80.7	98.7	150.3	39.4	150.2
6	17.7	100.0	98.6	93.6	123.6	37.6	115.5
AVG	14.5	100.0	87.3	95.1	126.5	39.8	147.9

(a)

Order	All	direct sound			1		2
Room	FDR%	TPR%	RMSE μs	TPR%	RMSE μs	TPR%	RMSE μs
1	26.4	100.0	121.8	78.2	151.8	32.1	116.5
2	22.8	100.0	78.6	89.7	111.4	30.8	125.0
3	19.1	100.0	77.9	96.2	104.8	28.6	112.4
4	27.3	100.0	77.7	93.6	95.0	26.2	124.9
5	23.4	100.0	81.4	93.6	137.1	33.2	121.0
6	24.0	100.0	106.3	75.6	119.8	29.5	108.5
AVG	23.8	100.0	90.6	87.8	120.0	30.1	118.0

(b)

Order	All	direct sound			1		2
Room	FDR%	TPR%	RMSE μs	TPR%	RMSE μs	TPR%	RMSE μs
1	14.9	100.0	107.8	91.0	132.6	38.5	152.8
2	14.3	100.0	77.3	88.5	118.6	39.7	163.2
3	17.8	100.0	76.9	100.0	120.3	29.5	131.0
4	19.2	100.0	76.6	100.0	113.4	36.1	135.8
5	17.6	100.0	79.6	100.0	139.6	36.1	153.9
6	22.3	100.0	95.1	93.6	123.3	30.3	124.9
AVG	17.7	100.0	85.6	95.5	124.6	35.0	143.6

(c)

Order	All	direct sound			1		2
Room	FDR%	TPR%	RMSE μs	TPR%	RMSE μs	TPR%	RMSE μs
1	14.4	100.0	107.7	91.0	125.6	39.7	172.9
2	14.4	100.0	79.2	93.6	119.0	41.0	156.1
3	15.7	100.0	78.5	100.0	123.6	37.6	136.1
4	16.4	100.0	78.8	98.7	114.5	36.1	146.3
5	15.0	100.0	80.7	98.7	147.7	38.5	146.5
6	16.7	100.0	98.6	93.6	122.7	37.2	121.4
AVG	15.4	100.0	87.3	95.9	125.5	38.4	146.5

(d)

Table A.7: Set 2 - Tilted Lambert

A. TOA DETECTION AND DISAMBIGUATION METRICS

Order Room	All FDR%	direct sound		TPR%	1 RMSE μs	TPR%	2 RMSE μs
		TPR%	RMSE μs				
1	14.4	100.0	107.7	91.0	125.6	39.7	172.9
2	14.4	100.0	79.2	93.6	119.0	41.0	156.1
3	15.7	100.0	78.5	100.0	123.6	37.6	136.1
4	16.4	100.0	78.8	98.7	114.5	36.1	146.3
5	15.0	100.0	80.7	98.7	147.7	38.5	146.5
6	16.7	100.0	98.6	93.6	122.7	37.2	121.4
AVG	15.4	100.0	87.3	95.9	125.5	38.4	146.5

(a)

Order Room	All FDR%	direct sound		TPR%	1 RMSE μs	TPR%	2 RMSE μs
		TPR%	RMSE μs				
1	25.6	100.0	121.8	82.1	150.1	31.2	115.4
2	19.4	100.0	78.6	94.9	120.4	31.2	126.9
3	18.1	100.0	77.9	97.4	105.3	26.9	118.4
4	27.4	100.0	77.7	91.0	96.2	25.3	120.7
5	20.5	100.0	81.4	97.4	131.0	31.3	120.1
6	22.5	100.0	106.3	80.8	116.8	29.9	109.8
AVG	22.3	100.0	90.6	90.6	120.0	29.3	118.5

(b)

Order Room	All FDR%	direct sound		TPR%	1 RMSE μs	TPR%	2 RMSE μs
		TPR%	RMSE μs				
1	13.9	100.0	107.8	93.6	134.3	35.9	134.4
2	17.4	100.0	77.3	88.5	126.3	38.5	152.9
3	18.5	100.0	76.9	100.0	121.1	29.9	127.6
4	21.2	100.0	76.6	100.0	116.9	29.4	139.2
5	18.1	100.0	79.6	98.7	143.9	33.7	144.3
6	18.9	100.0	95.1	96.2	118.9	31.6	122.6
AVG	18.0	100.0	85.6	96.2	126.9	33.2	136.8

(c)

Order Room	All FDR%	direct sound		TPR%	1 RMSE μs	TPR%	2 RMSE μs
		TPR%	RMSE μs				
1	18.1	100.0	108.4	79.5	137.5	32.9	136.1
2	17.3	100.0	77.4	87.2	126.9	38.0	153.6
3	17.1	100.0	77.0	98.7	118.5	28.2	132.0
4	22.4	100.0	77.3	98.7	116.2	29.4	142.1
5	17.7	100.0	79.7	96.2	142.5	32.2	145.5
6	21.0	100.0	95.4	80.8	111.5	27.4	106.3
AVG	18.9	100.0	85.9	90.2	125.5	31.3	135.9

(d)

Table A.8: Set 2 - Vector Mixing

A. TOA DETECTION AND DISAMBIGUATION METRICS

Order	All	direct sound			1		2
Room	FDR%	TPR%	RMSE μs	TPR%	RMSE μs	TPR%	RMSE μs
1	10.6	100.0	107.7	92.3	136.9	54.3	142.3
2	14.1	100.0	79.2	93.6	117.5	49.1	133.5
3	9.9	100.0	78.5	100.0	101.2	51.7	126.1
4	6.2	100.0	78.6	100.0	98.2	56.5	123.2
5	5.7	100.0	80.5	98.7	119.0	44.7	130.7
6	17.6	100.0	98.6	98.7	118.6	45.7	123.9
AVG	10.7	100.0	87.2	97.2	115.2	50.3	130.0

(a)							
Order	All	direct sound			1		2
Room	FDR%	TPR%	RMSE μs	TPR%	RMSE μs	TPR%	RMSE μs
1	22.7	100.0	121.8	93.6	150.9	31.6	147.0
2	15.9	100.0	79.5	93.6	114.9	43.2	138.2
3	18.1	100.0	77.9	93.6	101.0	26.1	127.7
4	21.7	100.0	77.7	96.2	97.3	24.9	106.4
5	18.4	100.0	81.4	74.4	106.0	30.8	131.4
6	24.2	100.0	106.8	98.7	137.6	26.1	141.1
AVG	20.2	100.0	90.8	91.7	118.0	30.4	132.0

(b)							
Order	All	direct sound			1		2
Room	FDR%	TPR%	RMSE μs	TPR%	RMSE μs	TPR%	RMSE μs
1	17.6	100.0	107.7	96.2	154.7	38.9	147.7
2	14.2	100.0	77.3	94.9	116.7	45.7	135.2
3	12.8	100.0	76.9	100.0	112.7	41.0	122.5
4	17.0	100.0	76.6	100.0	107.5	38.4	124.8
5	14.9	100.0	79.6	96.2	128.1	38.5	131.9
6	24.1	100.0	95.1	98.7	120.3	36.8	131.1
AVG	16.8	100.0	85.5	97.6	123.4	39.9	132.2

(c)							
Order	All	direct sound			1		2
Room	FDR%	TPR%	RMSE μs	TPR%	RMSE μs	TPR%	RMSE μs
1	23.1	100.0	108.4	97.4	137.6	28.6	151.1
2	14.8	100.0	77.4	94.9	117.3	43.6	143.0
3	15.7	100.0	77.0	97.4	106.9	32.5	135.2
4	16.0	100.0	77.3	97.4	102.5	30.7	132.3
5	13.2	100.0	79.7	92.3	125.9	33.2	140.2
6	25.0	100.0	95.4	96.2	122.0	25.2	124.1
AVG	18.0	100.0	85.9	95.9	118.7	32.3	137.6

Table A.9: Set 3

A. TOA DETECTION AND DISAMBIGUATION METRICS

Order Room	All FDR%	direct sound		TPR%	1 RMSE μs	TPR%	2 RMSE μs
		TPR%	RMSE μs				
1	10.3	100.0	107.7	92.3	152.9	59.0	156.3
2	10.8	100.0	79.1	87.2	112.3	56.4	133.3
3	12.7	100.0	78.5	100.0	111.2	46.6	125.1
4	8.2	100.0	78.8	100.0	109.9	54.6	134.8
5	10.8	100.0	80.7	100.0	130.8	43.8	131.1
6	12.1	100.0	98.6	97.4	118.5	54.7	120.1
AVG	10.8	100.0	87.2	96.2	122.6	52.5	133.5

(a)

Order Room	All FDR%	direct sound		TPR%	1 RMSE μs	TPR%	2 RMSE μs
		TPR%	RMSE μs				
1	28.3	100.0	121.8	98.7	163.1	32.9	143.5
2	17.0	100.0	79.5	89.7	110.2	47.0	140.5
3	22.8	100.0	77.9	97.4	103.6	28.2	119.0
4	23.5	100.0	77.7	100.0	101.0	25.3	102.8
5	20.1	100.0	81.4	83.3	127.7	31.7	130.5
6	23.5	100.0	106.8	98.7	135.5	27.4	151.2
AVG	22.5	100.0	90.8	94.7	123.5	32.1	131.3

(b)

Order Room	All FDR%	direct sound		TPR%	1 RMSE μs	TPR%	2 RMSE μs
		TPR%	RMSE μs				
1	21.0	100.0	107.8	96.2	159.2	45.7	145.4
2	12.8	100.0	77.3	92.3	122.2	48.3	143.7
3	17.8	100.0	76.9	100.0	118.6	39.3	131.6
4	20.7	100.0	76.6	100.0	107.0	39.3	132.1
5	17.2	100.0	79.4	100.0	122.6	38.9	124.9
6	21.3	100.0	95.1	98.7	128.3	42.3	124.2
AVG	18.5	100.0	85.5	97.9	126.3	42.3	133.6

(c)

Order Room	All FDR%	direct sound		TPR%	1 RMSE μs	TPR%	2 RMSE μs
		TPR%	RMSE μs				
1	26.0	100.0	108.4	93.6	159.1	31.6	153.0
2	14.2	100.0	77.3	94.9	128.8	42.7	144.9
3	18.7	100.0	77.0	100.0	112.1	34.2	130.7
4	19.9	100.0	77.3	100.0	104.7	30.3	142.7
5	12.8	100.0	79.7	97.4	129.5	35.6	134.6
6	24.8	100.0	95.5	97.4	125.2	30.3	146.6
AVG	19.4	100.0	85.9	97.2	126.6	34.1	142.1

(d)

Table A.10: Set 4

A. TOA DETECTION AND DISAMBIGUATION METRICS

Order	All	direct sound			1		2
Room	FDR%	TPR%	RMSE μs	TPR%	RMSE μs	TPR%	RMSE μs
1	10.3	100.0	107.7	96.2	143.3	60.3	152.7
2	9.8	100.0	78.7	87.2	123.3	57.3	134.6
3	11.8	100.0	78.3	98.7	128.2	53.0	129.8
4	16.0	100.0	78.6	98.7	130.7	45.6	140.2
5	14.6	100.0	80.5	98.7	146.4	48.1	136.5
6	15.1	100.0	98.6	98.7	125.1	55.1	133.9
AVG	12.9	100.0	87.1	96.4	132.8	53.2	137.9

(a)							
Order	All	direct sound			1		2
Room	FDR%	TPR%	RMSE μs	TPR%	RMSE μs	TPR%	RMSE μs
1	26.0	100.0	121.8	94.9	158.8	41.0	149.7
2	17.9	100.0	79.5	92.3	111.1	46.6	134.0
3	19.5	100.0	77.9	98.7	105.1	32.5	127.5
4	24.0	100.0	77.7	100.0	98.6	30.7	118.4
5	24.4	100.0	81.4	83.3	122.5	43.3	123.8
6	23.7	100.0	106.3	98.7	135.3	36.3	115.5
AVG	22.6	100.0	90.8	94.7	121.9	38.4	128.2

(b)							
Order	All	direct sound			1		2
Room	FDR%	TPR%	RMSE μs	TPR%	RMSE μs	TPR%	RMSE μs
1	16.8	100.0	107.9	93.6	155.6	49.1	154.8
2	12.7	100.0	77.3	93.6	121.1	50.9	143.6
3	19.0	100.0	76.9	100.0	131.8	41.0	124.2
4	26.5	100.0	76.6	100.0	123.9	31.6	140.6
5	22.0	100.0	79.6	98.7	135.7	45.2	126.0
6	23.1	100.0	95.1	97.4	129.0	40.6	134.8
AVG	20.0	100.0	85.6	97.2	132.8	43.1	137.3

(c)							
Order	All	direct sound			1		2
Room	FDR%	TPR%	RMSE μs	TPR%	RMSE μs	TPR%	RMSE μs
1	19.4	100.0	108.0	92.3	151.7	42.7	143.6
2	15.7	100.0	77.4	94.9	119.2	44.9	138.1
3	20.8	100.0	77.0	100.0	112.1	34.2	125.6
4	25.2	100.0	77.3	100.0	110.0	28.5	150.4
5	19.4	100.0	79.7	96.2	127.7	40.4	129.8
6	25.6	100.0	95.4	98.7	125.2	35.9	130.3
AVG	21.0	100.0	85.8	97.0	124.3	37.8	136.3

(d)							
Table A.11: Set 5							

A. TOA DETECTION AND DISAMBIGUATION METRICS

Order Room	All FDR%	direct sound		TPR%	1 RMSE μs	TPR%	2 RMSE μs
		TPR%	RMSE μs				
1	13.7	100.0	107.7	98.7	150.1	60.3	155.8
2	11.4	100.0	79.4	79.5	128.8	59.0	149.8
3	11.7	100.0	78.5	93.6	128.1	60.3	132.3
4	11.5	100.0	78.8	93.6	121.1	61.7	126.6
5	13.3	100.0	80.7	94.9	145.6	52.4	136.3
6	15.4	100.0	98.6	98.7	122.6	56.8	122.7
AVG	12.8	100.0	87.3	93.2	132.7	58.4	137.3

(a)

Order Room	All FDR%	direct sound		TPR%	1 RMSE μs	TPR%	2 RMSE μs
		TPR%	RMSE μs				
1	22.6	100.0	121.8	98.7	159.0	49.1	147.4
2	15.8	100.0	78.6	94.9	119.2	50.4	134.5
3	18.7	100.0	77.9	100.0	103.8	44.9	116.6
4	22.0	100.0	77.7	100.0	97.2	45.6	106.3
5	23.0	100.0	81.4	93.6	123.6	45.2	115.4
6	25.9	100.0	106.1	97.4	130.0	43.6	99.1
AVG	21.3	100.0	90.6	97.4	122.1	46.5	119.9

(b)

Order Room	All FDR%	direct sound		TPR%	1 RMSE μs	TPR%	2 RMSE μs
		TPR%	RMSE μs				
1	16.9	100.0	107.7	93.6	180.4	53.0	140.7
2	15.3	100.0	77.3	91.0	123.7	54.3	142.2
3	14.3	100.0	76.9	98.7	116.7	45.7	117.9
4	22.8	100.0	77.2	100.0	115.3	40.2	138.9
5	15.1	100.0	79.6	100.0	130.7	47.6	131.1
6	21.5	100.0	95.1	98.7	126.5	44.4	125.2
AVG	17.6	100.0	85.6	97.0	132.2	47.5	132.7

(c)

Order Room	All FDR%	direct sound		TPR%	1 RMSE μs	TPR%	2 RMSE μs
		TPR%	RMSE μs				
1	13.5	100.0	108.4	96.2	165.5	55.1	133.7
2	15.9	100.0	77.4	94.9	127.7	51.7	149.1
3	15.2	100.0	76.7	100.0	108.9	46.2	114.7
4	22.5	100.0	77.0	98.7	115.8	38.4	137.5
5	14.4	100.0	79.4	97.4	132.1	46.6	135.9
6	20.4	100.0	95.1	97.4	123.2	48.7	132.7
AVG	17.0	100.0	85.7	97.4	128.9	47.8	133.9

(d)

Table A.12: Set 6

A. TOA DETECTION AND DISAMBIGUATION METRICS

Order	All	direct sound			1		2
Room	FDR%	TPR%	RMSE μs	TPR%	RMSE μs	TPR%	RMSE μs
1	14.6	100.0	107.7	89.7	157.9	59.0	141.9
2	10.6	100.0	79.0	85.9	129.2	59.4	145.4
3	12.4	100.0	78.5	93.6	125.7	59.4	121.8
4	8.9	100.0	78.8	93.6	120.0	64.9	130.7
5	16.8	100.0	80.7	92.3	142.0	54.8	141.7
6	15.3	100.0	98.6	97.4	122.5	59.4	123.2
AVG	13.1	100.0	87.2	92.1	132.9	59.5	134.1

(a)							
Order	All	direct sound			1		2
Room	FDR%	TPR%	RMSE μs	TPR%	RMSE μs	TPR%	RMSE μs
1	21.6	100.0	121.8	98.7	156.3	51.3	143.7
2	17.8	100.0	78.6	93.6	108.2	50.4	127.2
3	19.5	100.0	77.9	98.7	101.0	47.9	95.9
4	19.9	100.0	77.7	98.7	103.0	53.7	107.6
5	26.0	100.0	81.4	94.9	120.7	46.2	121.5
6	25.5	100.0	106.1	98.7	133.6	44.9	97.9
AVG	21.7	100.0	90.6	97.2	120.5	49.0	115.6

(b)							
Order	All	direct sound			1		2
Room	FDR%	TPR%	RMSE μs	TPR%	RMSE μs	TPR%	RMSE μs
1	16.8	100.0	107.9	92.3	153.8	55.1	147.0
2	13.2	100.0	77.3	96.2	135.6	57.7	142.3
3	16.1	100.0	76.9	100.0	112.8	50.0	119.0
4	13.7	100.0	76.6	98.7	116.4	54.5	138.6
5	17.7	100.0	79.6	100.0	146.5	50.5	143.3
6	23.1	100.0	95.1	98.7	126.6	47.0	141.1
AVG	16.8	100.0	85.6	97.6	132.0	52.5	138.5

(c)							
Order	All	direct sound			1		2
Room	FDR%	TPR%	RMSE μs	TPR%	RMSE μs	TPR%	RMSE μs
1	15.4	100.0	108.6	93.6	144.3	56.8	136.2
2	11.9	100.0	77.4	96.2	131.8	58.5	151.5
3	13.3	100.0	76.7	100.0	113.6	50.9	120.9
4	14.8	100.0	77.0	100.0	112.6	53.1	137.8
5	18.0	100.0	79.4	98.7	148.1	49.0	136.8
6	21.5	100.0	95.1	100.0	132.6	48.3	126.0
AVG	15.8	100.0	85.7	98.1	130.5	52.8	134.9

(d)

Table A.13: Set 7

Appendix B

Reflector Localization Performance Metrics

The organization of the RL evalution tables follow the same order as above.

B. REFLECTOR LOCALIZATION PERFORMANCE METRICS

Room	E_{ML} (cm)	D_{RL} (cm)	O_{RL} (degrees)	% of full RGI	est. refl
1	25.696 ± 30.302	10.919 ± 11.459	3.937 ± 4.663	61.5	5.54
2	23.031 ± 21.914	9.174 ± 11.728	3.792 ± 4.326	69.2	5.62
3	25.454 ± 28.450	7.977 ± 6.602	2.506 ± 1.987	92.3	5.92
4	23.040 ± 26.086	7.674 ± 6.678	2.320 ± 2.015	84.6	5.85
5	33.737 ± 42.814	10.500 ± 8.211	2.669 ± 2.132	84.6	5.77
6	25.261 ± 30.018	10.580 ± 11.796	3.993 ± 3.677	0.0	4.85

(a)					
Room	E_{ML} (cm)	D_{RL} (cm)	O_{RL} (degrees)	% of full RGI	est. refl
1	22.516 ± 26.975	8.558 ± 10.093	3.444 ± 4.199	53.8	5.46
2	23.294 ± 26.053	10.708 ± 12.410	3.911 ± 4.461	76.9	5.69
3	13.882 ± 19.823	6.033 ± 7.010	1.692 ± 1.853	15.4	4.62
4	16.825 ± 23.788	6.180 ± 6.441	1.919 ± 1.995	38.5	4.92
5	12.306 ± 17.697	9.527 ± 10.358	1.855 ± 2.564	0.0	4.08
6	19.306 ± 24.917	9.017 ± 10.437	3.091 ± 2.867	0.0	4

(b)					
Room	E_{ML} (cm)	D_{RL} (cm)	O_{RL} (degrees)	% of full RGI	est. refl
1	26.826 ± 33.395	9.978 ± 10.056	3.792 ± 3.887	76.9	5.77
2	23.531 ± 24.965	10.163 ± 12.831	3.833 ± 5.023	84.6	5.85
3	27.880 ± 29.731	9.170 ± 8.373	2.634 ± 2.297	76.9	5.77
4	25.741 ± 28.883	7.550 ± 6.637	2.749 ± 2.815	92.3	5.92
5	29.877 ± 35.104	10.893 ± 11.812	2.566 ± 2.279	61.5	5.54
6	25.827 ± 31.860	10.971 ± 10.872	3.772 ± 3.155	0.0	4.69

(c)					
Room	E_{ML} (cm)	D_{RL} (cm)	O_{RL} (degrees)	% of full RGI	est. refl
1	24.076 ± 28.184	10.512 ± 10.109	3.417 ± 4.180	61.5	5.62
2	22.367 ± 21.521	9.924 ± 9.246	3.821 ± 4.009	76.9	5.77
3	23.500 ± 25.985	8.346 ± 8.263	2.238 ± 1.788	61.5	5.46
4	22.599 ± 24.485	7.893 ± 6.566	2.446 ± 2.308	76.9	5.62
5	14.994 ± 22.082	10.694 ± 9.754	1.743 ± 1.697	0.0	4.23
6	18.215 ± 19.342	7.467 ± 7.626	2.956 ± 1.929	0.0	4.08

Table B.1: Set 1 - Lambert

B. REFLECTOR LOCALIZATION PERFORMANCE METRICS

Room	E_{ML} (cm)	D_{RL} (cm)	O_{RL} (degrees)	% of full RGI	est. refl
1	23.959 ± 31.679	10.446 ± 11.390	3.599 ± 4.173	61.5	5.54
2	23.576 ± 24.558	9.235 ± 10.292	3.498 ± 3.787	69.2	5.62
3	25.891 ± 28.026	8.331 ± 6.546	2.534 ± 1.965	100.0	6
4	22.476 ± 24.342	7.803 ± 6.653	2.274 ± 1.913	92.3	5.92
5	33.904 ± 42.723	10.528 ± 8.269	2.678 ± 2.146	84.6	5.77
6	25.770 ± 30.090	10.380 ± 11.677	4.043 ± 3.655	0.0	4.92

(a)					
Room	E_{ML} (cm)	D_{RL} (cm)	O_{RL} (degrees)	% of full RGI	est. refl
1	22.242 ± 23.541	8.367 ± 7.925	3.256 ± 2.893	61.5	5.54
2	22.809 ± 24.588	11.576 ± 14.199	4.003 ± 4.560	84.6	5.85
3	17.740 ± 22.933	7.343 ± 7.579	1.950 ± 1.905	38.5	5
4	19.921 ± 24.080	6.572 ± 6.131	2.153 ± 1.936	76.9	5.46
5	12.248 ± 17.823	9.411 ± 10.334	1.852 ± 2.618	0.0	4.08
6	18.619 ± 22.692	8.685 ± 9.647	2.974 ± 2.516	0.0	4.08

(b)					
Room	E_{ML} (cm)	D_{RL} (cm)	O_{RL} (degrees)	% of full RGI	est. refl
1	25.577 ± 30.530	10.818 ± 10.828	4.043 ± 4.237	69.2	5.62
2	22.400 ± 22.498	10.349 ± 13.583	3.657 ± 3.721	69.2	5.69
3	28.333 ± 31.823	8.823 ± 8.096	2.713 ± 2.437	84.6	5.85
4	24.832 ± 26.292	8.595 ± 7.257	2.593 ± 2.361	92.3	5.92
5	30.040 ± 36.627	10.272 ± 9.064	2.470 ± 2.082	76.9	5.54
6	25.453 ± 29.036	10.173 ± 9.847	3.699 ± 2.813	0.0	4.77

(c)					
Room	E_{ML} (cm)	D_{RL} (cm)	O_{RL} (degrees)	% of full RGI	est. refl
1	24.704 ± 28.983	10.631 ± 9.673	3.644 ± 4.230	69.2	5.69
2	24.000 ± 24.579	10.892 ± 13.698	4.170 ± 5.200	92.3	5.92
3	24.331 ± 26.454	8.786 ± 8.148	2.298 ± 1.809	69.2	5.54
4	21.265 ± 23.280	7.658 ± 6.402	2.246 ± 1.804	76.9	5.54
5	15.861 ± 25.607	9.734 ± 8.714	1.913 ± 2.011	7.7	4.23
6	18.512 ± 19.748	8.089 ± 7.611	3.016 ± 1.957	0.0	4.15

(d)					
-----	--	--	--	--	--

Table B.2: Set 1 - Tilted Lambert

B. REFLECTOR LOCALIZATION PERFORMANCE METRICS

Room	E_{ML} (cm)	D_{RL} (cm)	O_{RL} (degrees)	% of full RGI	est. refl
1	22.022 ± 26.027	9.806 ± 10.664	3.388 ± 3.341	53.8	5.31
2	29.619 ± 26.668	18.741 ± 33.571	8.349 ± 13.759	61.5	5.23
3	28.171 ± 29.746	9.384 ± 9.543	2.702 ± 2.740	100.0	6
4	24.952 ± 24.336	8.883 ± 6.774	2.590 ± 2.221	84.6	5.77
5	40.629 ± 46.984	12.002 ± 8.639	3.343 ± 3.695	76.9	5.69
6	26.143 ± 31.104	11.433 ± 13.609	4.274 ± 4.114	0.0	4.85

(a)					
Room	E_{ML} (cm)	D_{RL} (cm)	O_{RL} (degrees)	% of full RGI	est. refl
1	25.207 ± 24.375	10.071 ± 8.720	3.779 ± 3.014	84.6	5.85
2	21.471 ± 21.514	8.341 ± 10.293	3.209 ± 2.629	92.3	5.85
3	28.061 ± 29.812	8.187 ± 6.984	2.578 ± 2.090	100.0	6
4	25.139 ± 31.061	7.586 ± 7.474	2.454 ± 2.342	100.0	6
5	35.681 ± 45.368	10.066 ± 7.799	2.846 ± 2.817	84.6	5.77
6	23.219 ± 28.482	9.410 ± 9.123	3.434 ± 2.886	0.0	4.77

(b)					
Room	E_{ML} (cm)	D_{RL} (cm)	O_{RL} (degrees)	% of full RGI	est. refl
1	30.553 ± 38.075	14.010 ± 15.641	5.138 ± 8.496	61.5	5.54
2	22.694 ± 24.050	10.985 ± 15.565	3.644 ± 4.441	76.9	5.69
3	30.938 ± 31.926	11.556 ± 16.048	3.222 ± 4.455	92.3	5.92
4	23.755 ± 25.654	7.917 ± 6.857	2.492 ± 2.358	92.3	5.92
5	32.369 ± 36.891	10.343 ± 8.847	2.657 ± 2.214	76.9	5.69
6	25.531 ± 31.656	10.058 ± 9.561	3.739 ± 3.043	0.0	4.92

(c)					
Room	E_{ML} (cm)	D_{RL} (cm)	O_{RL} (degrees)	% of full RGI	est. refl
1	26.341 ± 30.265	15.206 ± 18.452	4.909 ± 6.351	61.5	5.38
2	26.406 ± 28.009	12.552 ± 16.801	4.812 ± 7.150	76.9	5.77
3	29.395 ± 31.030	10.216 ± 8.640	2.581 ± 1.979	92.3	5.92
4	24.234 ± 26.016	8.032 ± 6.966	2.498 ± 2.359	92.3	5.92
5	35.177 ± 39.963	11.974 ± 13.360	2.885 ± 3.008	84.6	5.77
6	26.262 ± 31.613	11.017 ± 11.247	3.999 ± 3.943	0.0	4.92

(d)					
-----	--	--	--	--	--

Table B.3: Set 1 - Vector Mixing

B. REFLECTOR LOCALIZATION PERFORMANCE METRICS

Room	E_{ML} (cm)	D_{RL} (cm)	O_{RL} (degrees)	% of full RGI	est. refl
1	25.490 ± 26.377	10.181 ± 8.992	3.889 ± 4.441	76.9	5.69
2	23.840 ± 21.997	9.638 ± 9.536	3.318 ± 2.776	76.9	5.69
3	27.727 ± 27.347	9.785 ± 7.372	2.745 ± 2.192	100.0	6
4	22.362 ± 24.800	7.581 ± 5.916	2.280 ± 1.897	76.9	5.77
5	35.681 ± 46.252	11.008 ± 9.732	2.840 ± 2.195	69.2	5.62
6	32.286 ± 34.918	13.584 ± 18.311	6.071 ± 7.021	0.0	4.92

(a)					
Room	E_{ML} (cm)	D_{RL} (cm)	O_{RL} (degrees)	% of full RGI	est. refl
21	6.346 ± 36.730	10.517 ± 12.010	3.682 ± 4.700	46.2	5.15
2	27.300 ± 31.578	14.550 ± 19.813	4.749 ± 7.245	76.9	5.69
3	28.702 ± 28.222	9.955 ± 8.282	2.743 ± 2.208	84.6	5.54
4	22.828 ± 32.653	9.223 ± 12.663	2.116 ± 2.277	61.5	5.23
5	38.776 ± 50.436	12.504 ± 13.574	2.798 ± 2.535	53.8	5.31
6	28.613 ± 38.787	14.356 ± 19.018	5.546 ± 7.507	0.0	3.31

(b)					
Room	E_{ML} (cm)	D_{RL} (cm)	O_{RL} (degrees)	% of full RGI	est. refl
1	25.777 ± 27.638	10.962 ± 10.049	4.357 ± 4.462	76.9	5.69
2	29.381 ± 35.223	15.161 ± 23.594	5.334 ± 7.249	92.3	5.92
3	26.757 ± 28.782	9.262 ± 7.147	2.623 ± 1.990	100.0	6
4	26.086 ± 29.950	8.401 ± 7.572	2.607 ± 2.589	100.0	6
5	39.115 ± 47.543	10.940 ± 8.941	2.884 ± 2.432	100.0	6
6	24.478 ± 34.347	9.901 ± 14.639	4.776 ± 11.021	0.0	4.46

(c)					
Room	E_{ML} (cm)	D_{RL} (cm)	O_{RL} (degrees)	% of full RGI	est. refl
1	28.285 ± 35.734	13.768 ± 14.657	4.092 ± 4.943	69.2	5.46
2	29.137 ± 37.936	14.819 ± 22.937	5.028 ± 7.341	84.6	5.85
3	27.000 ± 28.403	10.175 ± 8.804	2.482 ± 1.835	76.9	5.69
4	21.935 ± 23.732	8.249 ± 6.684	2.298 ± 2.226	76.9	5.69
5	38.384 ± 44.661	11.151 ± 8.984	2.986 ± 2.618	84.6	5.77
6	23.722 ± 33.362	13.096 ± 24.232	5.008 ± 7.918	0.0	3.77

(d)					
-----	--	--	--	--	--

Table B.4: Set 2 - Lambert

B. REFLECTOR LOCALIZATION PERFORMANCE METRICS

Room	E_{ML} (cm)	D_{RL} (cm)	O_{RL} (degrees)	% of full RGI	est. refl
1	29.618 ± 31.372	11.071 ± 9.627	4.625 ± 5.322	92.3	5.92
2	26.025 ± 28.103	10.651 ± 12.567	4.356 ± 9.976	76.9	5.69
3	26.934 ± 27.328	9.321 ± 7.452	2.637 ± 2.164	100.0	6
4	23.018 ± 24.906	8.062 ± 6.555	2.334 ± 1.919	92.3	5.92
5	41.720 ± 52.181	11.821 ± 9.178	3.062 ± 2.427	92.3	5.92
6	31.896 ± 35.495	14.956 ± 19.360	5.293 ± 5.612	0.0	4.92

(a)					
Room	E_{ML} (cm)	D_{RL} (cm)	O_{RL} (degrees)	% of full RGI	est. refl
1	26.550 ± 33.445	11.299 ± 13.686	3.458 ± 4.447	46.2	5.23
2	24.604 ± 28.300	12.711 ± 17.859	4.134 ± 6.603	76.9	5.77
3	27.412 ± 26.841	9.344 ± 7.260	2.556 ± 2.026	84.6	5.69
4	19.773 ± 23.125	6.579 ± 6.256	2.061 ± 1.848	76.9	5.62
5	36.954 ± 47.274	10.728 ± 8.851	2.704 ± 2.381	69.2	5.54
6	28.292 ± 45.080	15.153 ± 27.702	4.876 ± 6.839	0.0	3.85

(b)					
Room	E_{ML} (cm)	D_{RL} (cm)	O_{RL} (degrees)	% of full RGI	est. refl
1	26.331	10.246 ± 10.102	3.876 ± 3.444	84.6	5.77
2	24.901 ± 30.736	11.685 ± 17.366	4.401 ± 6.375	69.2	5.62
3	30.251 ± 31.908	11.754 ± 15.823	3.210 ± 4.473	100.0	6
4	25.803 ± 29.438	7.870 ± 7.109	2.630 ± 2.551	92.3	5.92
5	38.711 ± 47.244	11.027 ± 8.642	3.005 ± 2.411	100.0	6
6	27.138 ± 32.178	13.328 ± 19.718	4.722 ± 5.302	0.0	4.69

(c)					
Room	E_{ML} (cm)	D_{RL} (cm)	O_{RL} (degrees)	% of full RGI	est. refl
1	26.441 ± 29.868	13.619 ± 13.892	3.824 ± 3.837	69.2	5.54
2	27.255 ± 31.731	13.018 ± 18.225	4.342 ± 5.696	76.9	5.77
3	27.926 ± 30.732	11.366 ± 14.195	2.863 ± 2.994	84.6	5.77
4	22.218 ± 24.300	7.612 ± 6.590	2.342 ± 2.266	76.9	5.69
5	37.885 ± 45.668	12.348 ± 15.885	3.226 ± 3.696	76.9	5.62
6	30.274 ± 41.222	14.160 ± 20.004	6.884 ± 13.178	0.0	4.15

Table B.5: Set 2 - Tilted Lambert

B. REFLECTOR LOCALIZATION PERFORMANCE METRICS

Room	E_{ML} (cm)	D_{RL} (cm)	O_{RL} (degrees)	% of full RGI	est. refl
1	25.979 ± 30.081	9.749 ± 9.798	4.046 ± 4.405	92.3	5.92
2	29.034 ± 35.189	12.869 ± 16.239	4.616 ± 6.269	92.3	5.92
3	28.239 ± 28.214	10.341 ± 13.447	3.193 ± 4.261	100.0	6
4	23.633 ± 25.917	8.028 ± 6.387	2.368 ± 1.995	92.3	5.92
5	42.568 ± 53.585	11.888 ± 9.309	3.097 ± 2.425	92.3	5.92
6	29.519 ± 33.886	14.327 ± 20.615	5.213 ± 5.833	0.0	4.85

(a)					
Room	E_{ML} (cm)	D_{RL} (cm)	O_{RL} (degrees)	% of full RGI	est. refl
1	28.356 ± 37.581	12.073 ± 14.215	3.457 ± 4.362	69.2	5.54
2	25.342 ± 28.069	13.754 ± 18.438	4.279 ± 6.421	92.3	5.92
3	27.079 ± 27.280	8.882 ± 6.825	2.610 ± 1.977	92.3	5.77
4	19.296 ± 23.357	6.742 ± 6.506	2.042 ± 1.879	76.9	5.54
5	39.630 ± 49.026	10.860 ± 8.904	2.951 ± 2.313	84.6	5.77
6	24.464 ± 34.135	14.040 ± 24.644	4.325 ± 5.806	0.0	3.92

(b)					
Room	E_{ML} (cm)	D_{RL} (cm)	O_{RL} (degrees)	% of full RGI	est. refl
1	24.938 ± 26.027	11.882 ± 9.793	4.249 ± 4.368	76.9	5.77
2	31.451 ± 36.950	17.009 ± 27.972	6.036 ± 9.161	84.6	5.85
3	30.656 ± 32.281	11.692 ± 15.816	3.176 ± 4.427	100.0	6
4	27.286 ± 31.180	8.603 ± 7.384	2.793 ± 2.909	100.0	6
5	37.559 ± 45.342	11.183 ± 9.056	2.855 ± 2.413	92.3	5.92
6	26.215 ± 29.787	10.639 ± 13.907	4.144 ± 3.869	0.0	4.85

(c)					
Room	E_{ML} (cm)	D_{RL} (cm)	O_{RL} (degrees)	% of full RGI	est. refl
1	27.259 ± 30.923	14.807 ± 18.511	5.377 ± 9.332	61.5	5.38
2	33.843 ± 43.567	16.785 ± 24.214	6.535 ± 10.648	84.6	5.85
3	28.225 ± 29.331	10.328 ± 8.367	2.520 ± 1.901	84.6	5.85
4	23.555 ± 26.148	8.475 ± 7.340	2.338 ± 1.988	84.6	5.85
5	35.377 ± 42.225	11.588 ± 9.276	2.633 ± 1.885	76.9	5.69
6	25.782 ± 35.154	12.525 ± 22.220	4.764 ± 7.204	0.0	4.08

(d)					
Room	E_{ML} (cm)	D_{RL} (cm)	O_{RL} (degrees)	% of full RGI	est. refl
1	27.259 ± 30.923	14.807 ± 18.511	5.377 ± 9.332	61.5	5.38
2	33.843 ± 43.567	16.785 ± 24.214	6.535 ± 10.648	84.6	5.85
3	28.225 ± 29.331	10.328 ± 8.367	2.520 ± 1.901	84.6	5.85
4	23.555 ± 26.148	8.475 ± 7.340	2.338 ± 1.988	84.6	5.85
5	35.377 ± 42.225	11.588 ± 9.276	2.633 ± 1.885	76.9	5.69
6	25.782 ± 35.154	12.525 ± 22.220	4.764 ± 7.204	0.0	4.08

Table B.6: Set 2 - Vector Mixing

B. REFLECTOR LOCALIZATION PERFORMANCE METRICS

Room	E_{ML} (cm)	D_{RL} (cm)	O_{RL} (degrees)	% of full RGI	est. refl
1	26.887 ± 34.698	10.149 ± 11.422	4.099 ± 4.716	92.3	5.92
2	23.701 ± 25.264	10.617 ± 12.057	3.534 ± 3.479	69.2	5.62
3	25.467 ± 28.692	8.432 ± 7.050	2.438 ± 2.000	100.0	6
4	23.336 ± 25.672	7.786 ± 6.679	2.337 ± 1.974	100.0	6
5	35.808 ± 44.892	10.452 ± 8.372	2.663 ± 2.105	92.3	5.92
6	28.150 ± 34.682	9.593 ± 9.496	4.214 ± 3.873	0.0	5

(a)					
Room	E_{ML} (cm)	D_{RL} (cm)	O_{RL} (degrees)	% of full RGI	est. refl
1	24.478 ± 27.532	9.258 ± 8.594	3.823 ± 4.300	76.9	5.77
2	21.903 ± 23.366	9.689 ± 10.989	3.850 ± 4.220	92.3	5.92
3	22.349 ± 26.931	6.633 ± 6.270	2.206 ± 2.000	76.9	5.62
4	19.835 ± 21.808	6.457 ± 5.579	2.094 ± 1.813	84.6	5.77
5	13.230 ± 19.403	9.453 ± 10.322	1.801 ± 2.408	0.0	4.23
6	28.884 ± 35.082	10.565 ± 11.201	4.155 ± 3.727	0.0	4.92

(b)					
Room	E_{ML} (cm)	D_{RL} (cm)	O_{RL} (degrees)	% of full RGI	est. refl
1	27.605 ± 35.298	10.994 ± 11.177	4.137 ± 4.686	84.6	5.85
2	23.375 ± 28.349	12.057 ± 16.652	3.790 ± 4.214	92.3	5.85
3	32.560 ± 34.820	10.388 ± 10.680	2.874 ± 2.478	92.3	5.92
4	23.597 ± 25.391	7.724 ± 6.159	2.525 ± 2.393	84.6	5.85
5	32.092 ± 39.708	11.640 ± 14.965	2.767 ± 2.909	69.2	5.62
6	25.389 ± 31.670	10.009 ± 9.917	3.628 ± 3.103	0.0	4.92

(c)					
Room	E_{ML} (cm)	D_{RL} (cm)	O_{RL} (degrees)	% of full RGI	est. refl
1	25.072 ± 30.320	9.807 ± 9.497	3.656 ± 3.512	92.3	5.92
2	22.123 ± 28.763	11.119 ± 13.846	3.396 ± 3.980	84.6	5.85
3	27.166 ± 31.912	8.513 ± 7.482	2.535 ± 2.201	76.9	5.77
4	22.405 ± 24.439	7.744 ± 6.447	2.308 ± 1.935	76.9	5.77
5	26.540 ± 35.732	11.294 ± 13.065	2.319 ± 1.910	38.5	5.15
6	26.413 ± 32.062	10.589 ± 11.339	3.750 ± 3.248	0.0	4.77

(d)					
-----	--	--	--	--	--

Table B.7: Set 3

B. REFLECTOR LOCALIZATION PERFORMANCE METRICS

Room	E_{ML} (cm)	D_{RL} (cm)	O_{RL} (degrees)	% of full RGI	est. refl
1	30.506 ± 34.911	12.058 ± 13.825	5.177 ± 8.329	76.9	5.77
2	20.289 ± 21.287	7.886 ± 8.678	2.862 ± 2.453	61.5	5.31
3	28.122 ± 29.361	7.949 ± 6.438	2.629 ± 1.923	92.3	5.92
4	26.141 ± 26.190	8.430 ± 6.408	2.575 ± 1.992	100.0	6
5	34.967 ± 39.459	11.227 ± 8.048	2.744 ± 1.891	92.3	5.85
6	22.594 ± 25.003	8.570 ± 8.316	3.401 ± 2.336	0.0	4.85

(a)					
Room	E_{ML} (cm)	D_{RL} (cm)	O_{RL} (degrees)	% of full RGI	est. refl
1	25.661 ± 28.101	10.512 ± 9.557	3.902 ± 3.736	84.6	5.85
2	22.059 ± 23.117	10.081 ± 13.622	3.878 ± 4.458	92.3	5.85
3	26.396 ± 31.405	7.536 ± 6.734	2.509 ± 2.200	92.3	5.85
4	22.902 ± 24.867	7.093 ± 6.019	2.277 ± 1.959	100.0	6
5	17.390 ± 25.706	8.991 ± 10.150	1.845 ± 2.491	15.4	4.69
6	26.824 ± 34.881	10.649 ± 10.839	3.735 ± 3.457	0.0	4.92

(b)					
Room	E_{ML} (cm)	D_{RL} (cm)	O_{RL} (degrees)	% of full RGI	est. refl
1	25.755 ± 31.506	9.840 ± 9.120	4.104 ± 4.653	69.2	5.69
2	23.930 ± 25.596	11.213 ± 13.930	3.944 ± 4.185	84.6	5.85
3	30.141 ± 34.075	9.229 ± 10.386	2.754 ± 2.455	92.3	5.92
4	24.404 ± 27.005	7.923 ± 7.098	2.430 ± 2.089	92.3	5.92
5	32.386 ± 36.710	11.937 ± 13.271	2.682 ± 2.696	84.6	5.77
6	26.494 ± 32.141	11.133 ± 10.606	3.848 ± 3.354	0.0	4.92

(c)					
Room	E_{ML} (cm)	D_{RL} (cm)	O_{RL} (degrees)	% of full RGI	est. refl
1	25.772 ± 31.308	11.046 ± 11.135	4.322 ± 4.732	61.5	5.62
2	21.693 ± 23.118	9.763 ± 11.956	3.448 ± 3.543	84.6	5.85
3	30.394 ± 33.103	9.416 ± 10.203	2.733 ± 2.394	100.0	6
4	23.650 ± 26.009	7.957 ± 6.250	2.370 ± 2.037	92.3	5.92
5	31.282 ± 37.191	11.129 ± 12.939	2.554 ± 2.799	76.9	5.69
6	23.424 ± 24.636	10.353 ± 9.459	3.440 ± 2.526	0.0	4.85

(d)					
-----	--	--	--	--	--

Table B.8: Set 4

B. REFLECTOR LOCALIZATION PERFORMANCE METRICS

Room	E_{ML} (cm)	D_{RL} (cm)	O_{RL} (degrees)	% of full RGI	est. refl
1	26.452 ± 29.236	9.860 ± 10.361	3.858 ± 3.452	84.6	5.85
2	26.671 ± 28.418	10.428 ± 10.262	4.208 ± 5.518	53.8	5.38
3	28.258 ± 28.745	9.573 ± 7.185	2.708 ± 1.900	61.5	5.54
4	27.539 ± 30.188	9.340 ± 7.651	2.816 ± 2.454	61.5	5.62
5	38.440 ± 41.850	11.654 ± 10.312	3.262 ± 2.499	61.5	5.54
6	26.274 ± 31.174	10.790 ± 12.600	4.023 ± 3.811	0.0	4.92

(a)					
Room	E_{ML} (cm)	D_{RL} (cm)	O_{RL} (degrees)	% of full RGI	est. refl
1	30.559 ± 39.617	9.945 ± 9.773	4.513 ± 5.169	92.3	5.92
2	21.425 ± 23.364	9.375 ± 8.986	3.592 ± 3.697	76.9	5.77
3	26.295 ± 28.777	8.725 ± 12.385	2.838 ± 3.827	92.3	5.92
4	23.531 ± 25.115	7.820 ± 6.900	2.345 ± 1.947	100.0	6
5	21.212 ± 33.174	10.171 ± 13.730	1.965 ± 2.499	23.1	4.85
6	26.456 ± 35.141	10.954 ± 11.350	3.809 ± 3.627	0.0	4.92

(b)					
Room	E_{ML} (cm)	D_{RL} (cm)	O_{RL} (degrees)	% of full RGI	est. refl
1	30.406 ± 39.342	10.812 ± 9.889	4.999 ± 5.818	76.9	5.77
2	22.899 ± 25.782	11.094 ± 16.097	3.777 ± 4.861	84.6	5.85
3	28.773 ± 31.082	10.585 ± 18.074	3.248 ± 6.999	69.2	5.69
4	26.723 ± 33.749	8.180 ± 9.036	2.729 ± 2.746	84.6	5.85
5	37.444 ± 43.143	11.369 ± 13.321	2.857 ± 2.826	92.3	5.92
6	27.959 ± 34.258	12.111 ± 11.721	4.128 ± 3.680	0.0	4.85

(c)					
Room	E_{ML} (cm)	D_{RL} (cm)	O_{RL} (degrees)	% of full RGI	est. refl
1	32.304 ± 45.077	10.486 ± 10.478	4.963 ± 5.953	92.3	5.92
2	23.622 ± 29.638	9.842 ± 9.588	3.971 ± 6.941	84.6	5.85
3	27.096 ± 28.639	8.594 ± 7.564	2.411 ± 1.866	92.3	5.92
4	23.788 ± 26.003	7.604 ± 5.982	2.445 ± 2.204	100.0	6
5	31.775 ± 37.524	11.868 ± 16.406	2.652 ± 2.837	84.6	5.77
6	29.432 ± 37.386	11.706 ± 11.861	4.377 ± 4.799	0.0	5

Table B.9: Set 5

B. REFLECTOR LOCALIZATION PERFORMANCE METRICS

Room	E_{ML} (cm)	D_{RL} (cm)	O_{RL} (degrees)	% of full RGI	est. refl
1	25.882 ± 30.300	9.398 ± 9.518	3.792 ± 3.371	76.9	5.77
2	23.567 ± 24.559	10.729 ± 12.098	3.928 ± 6.936	53.8	4.85
3	30.879 ± 29.236	10.114 ± 8.774	2.936 ± 2.103	61.5	5.46
4	24.135 ± 27.239	8.484 ± 6.574	2.503 ± 2.197	46.2	5.15
5	40.771 ± 45.173	12.252 ± 8.553	3.279 ± 2.354	46.2	5.23
6	26.451 ± 31.271	11.666 ± 14.144	3.952 ± 3.895	0.0	5

(a)					
Room	E_{ML} (cm)	D_{RL} (cm)	O_{RL} (degrees)	% of full RGI	est. refl
1	26.328 ± 34.782	10.261 ± 10.807	3.583 ± 3.462	92.3	5.92
2	21.613 ± 24.846	8.837 ± 8.693	3.364 ± 3.502	84.6	5.85
3	25.574 ± 27.704	7.707 ± 6.774	2.566 ± 2.166	92.3	5.92
4	21.707 ± 24.179	7.261 ± 6.677	2.193 ± 1.910	100.0	6
5	28.534 ± 37.558	9.713 ± 7.981	2.483 ± 1.928	61.5	5.38
6	24.882 ± 32.264	10.653 ± 10.152	3.537 ± 3.105	0.0	4.85

(b)					
Room	E_{ML} (cm)	D_{RL} (cm)	O_{RL} (degrees)	% of full RGI	est. refl
1	37.699 ± 49.802	13.043 ± 12.988	5.381 ± 5.892	100.0	6
2	22.873 ± 28.288	8.067 ± 7.810	3.674 ± 4.042	92.3	5.85
3	27.144 ± 30.037	7.063 ± 6.313	2.598 ± 2.132	92.3	5.92
4	26.412 ± 34.471	8.444 ± 8.102	2.605 ± 2.695	100.0	6
5	35.398 ± 43.798	10.547 ± 8.723	2.652 ± 2.484	100.0	6
6	25.006 ± 28.228	10.514 ± 9.541	3.885 ± 3.796	0.0	4.92

(c)					
Room	E_{ML} (cm)	D_{RL} (cm)	O_{RL} (degrees)	% of full RGI	est. refl
1	35.473 ± 47.042	13.686 ± 14.299	5.208 ± 5.913	100.0	6
2	23.679 ± 32.760	10.933 ± 18.395	3.732 ± 4.630	92.3	5.85
3	25.783 ± 29.159	7.545 ± 6.215	2.444 ± 1.971	92.3	5.92
4	27.889 ± 35.032	9.816 ± 10.954	2.993 ± 3.068	92.3	5.85
5	31.270 ± 37.576	9.083 ± 7.760	2.564 ± 2.429	84.6	5.77
6	26.145 ± 31.135	12.674 ± 19.167	4.078 ± 4.963	0.0	4.92

Table B.10: Set 6

B. REFLECTOR LOCALIZATION PERFORMANCE METRICS

Room	E_{ML} (cm)	D_{RL} (cm)	O_{RL} (degrees)	% of full RGI	est. refl
1	21.978 ± 22.498	9.696 ± 9.680	3.236 ± 2.764	46.2	5.46
2	29.115 ± 27.561	12.659 ± 13.605	3.959 ± 3.240	53.8	5.38
3	33.511 ± 30.715	10.433 ± 9.202	3.587 ± 3.094	46.2	5.38
4	27.617 ± 28.702	8.426 ± 6.545	2.858 ± 2.372	53.8	5.46
5	43.557 ± 47.131	13.436 ± 13.236	3.560 ± 2.795	46.2	5.15
6	24.779 ± 30.439	10.273 ± 10.735	3.742 ± 3.468	0.0	4.77

(a)

Room	E_{ML} (cm)	D_{RL} (cm)	O_{RL} (degrees)	% of full RGI	est. refl
1	24.029 ± 28.463	9.784 ± 11.012	3.383 ± 2.988	84.6	5.85
2	21.060 ± 22.750	8.804 ± 8.898	3.387 ± 3.799	76.9	5.77
3	26.656 ± 27.746	8.492 ± 7.080	2.523 ± 1.969	92.3	5.92
4	22.839 ± 26.557	7.334 ± 7.157	2.231 ± 2.034	100.0	6
5	34.105 ± 43.175	11.207 ± 9.563	2.562 ± 1.987	76.9	5.69
6	26.495 ± 29.876	11.123 ± 11.197	3.828 ± 3.254	0.0	4.92

(b)

Room	E_{ML} (cm)	D_{RL} (cm)	O_{RL} (degrees)	% of full RGI	est. refl
1	32.012 ± 43.467	13.134 ± 18.063	4.864 ± 5.961	92.3	5.92
2	26.110 ± 28.330	10.816 ± 13.645	4.285 ± 6.140	92.3	5.92
3	25.950 ± 28.980	7.957 ± 6.792	2.504 ± 2.058	100.0	6
4	25.121 ± 28.961	7.529 ± 7.121	2.462 ± 2.300	100.0	6
5	39.499 ± 45.813	12.408 ± 10.422	2.913 ± 2.223	92.3	5.92
6	25.563 ± 28.104	11.636 ± 14.457	3.919 ± 3.533	0.0	4.92

(c)

Room	E_{ML} (cm)	D_{RL} (cm)	O_{RL} (degrees)	% of full RGI	est. refl
1	27.357 ± 33.915	11.149 ± 12.216	3.926 ± 3.873	100.0	6
2	25.898 ± 28.097	10.883 ± 12.634	4.267 ± 5.553	92.3	5.92
3	26.087 ± 29.431	8.408 ± 7.539	2.342 ± 1.897	100.0	6
4	23.380 ± 26.788	7.584 ± 6.776	2.301 ± 2.045	100.0	6
5	38.409 ± 47.119	12.939 ± 11.135	2.996 ± 3.275	76.9	5.77
6	27.891 ± 30.453	12.884 ± 15.228	4.267 ± 3.744	0.0	5

(d)

Table B.11: Set 7

Bibliography

- [AB79] Jont B. Allen and David A. Berkley. Image method for efficiently simulating small-room acoustics. *The Journal of the Acoustical Society of America*, 65(4):943–950, April 1979.
- [ACTM12] L. Antani, A. Chandak, M. Taylor, and D. Manocha. Direct-to-Indirect Acoustic Radiance Transfer. *IEEE Transactions on Visualization and Computer Graphics*, 18(2):261–269, February 2012.
- [ADV14] Marc Aretz, Pascal Dietrich, and Michael Vorländer. Application of the Mirror Source Method for Low Frequency Sound Prediction in Rectangular Rooms. *Acta Acustica united with Acustica*, 100(2):306–319, March 2014.
- [Bio68] M. A. Biot. Generalized Boundary Condition for Multiple Scatter in Acoustic Reflection. *The Journal of the Acoustical Society of America*, 44(6):1616–1622, December 1968.
- [Bor84a] Jeffrey Borish. *Electronic Simulation of Auditorium Acoustics*. PhD thesis, Elec. Eng. Dept., Stanford University, Stanford, California, 1984.
- [Bor84b] Jeffrey Borish. Extension of the image model to arbitrary polyhedra. *The Journal of the Acoustical Society of America*, 75(6):1827–1836, June 1984.
- [BRD13] H. Bai, G. Richard, and L. Daudet. Modeling early reflections of room impulse responses using a radiance transfer method. In *2013 IEEE Workshop on Applications of Signal Processing to Audio and Acoustics*, pages 1–4, October 2013.
- [BWH17] Y. El Baba, A. Walther, and E. A. P. Habets. Time of arrival disambiguation using the linear Radon transform. In *2017 IEEE International Conference on Acoustics, Speech and Signal Processing (ICASSP)*, pages 106–110, March 2017.
- [BWH18] Youssef El Baba, Andreas Walther, and Emanuel A. P. Habets. 3d Room Geometry Inference Based on Room Impulse Response Stacks. *IEEE/ACM Transactions on Audio, Speech, and Language Processing*, 26(5):857–872, May 2018.
- [CD09] Trevor J. Cox and Peter D’Antonio. *Acoustic absorbers and diffusers: theory, design and application*. Taylor & Francis, London ; New York, 2nd ed edition, 2009. OCLC: ocn227922698.
- [Chr05] Claus Lynge Christensen. A new scattering method that combines roughness and diffraction effects. *The Journal of the Acoustical Society of America*, 117(4):2499–2499, April 2005.
- [CLT⁺08] A. Chandak, C. Lauterbach, M. Taylor, Z. Ren, and D. Manocha. AD-Frustum: Adaptive Frustum Tracing for Interactive Sound Propagation. *IEEE Transactions on Visualization and Computer Graphics*, 14(6):1707–1722, November 2008.

BIBLIOGRAPHY

- [Cox06] T J Cox. A Tutorial on Scattering and Diffusion Coefficients for Room Acoustic Surfaces. *ACTA ACUSTICA UNITED WITH ACUSTICA*, 92:16, 2006.
- [CRT00] Nicola Campo, Paolo Rissone, and Marco Toderi. Adaptive pyramid tracing: a new technique for room acoustics. *Applied Acoustics*, 61(2):199–221, October 2000.
- [Dal96] Bengt-Inge L. Dalenbäck. Room acoustic prediction based on a unified treatment of diffuse and specular reflection. *The Journal of the Acoustical Society of America*, 100(2):899–909, August 1996.
- [DKS94] Bengt-Inge Dalenbäck, Mendel Kleiner, and Peter Svensson. A Macroscopic View of Diffuse Reflection. *J. Audio Eng. Soc*, 42(10):793–807, 1994.
- [DL00] I. A. Drumm and Y. W. Lam. The adaptive beam-tracing algorithm. *The Journal of the Acoustical Society of America*, 107(3):1405–1412, February 2000.
- [Emb82] Jean-Jacques Embrechts. Sound Field Distribution using Randomly Traced Sound Ray Techniques. *Acustica*, 51 (6), 1982.
- [Emb00] J. J. Embrechts. Broad spectrum diffusion model for room acoustics ray-tracing algorithms. *The Journal of the Acoustical Society of America*, 107(4):2068–2081, April 2000.
- [GJ72] Barry M Gibbs and DK Jones. A simple image method for calculating the distribution of sound pressure levels within an enclosure. *Acta Acustica united with Acustica*, 26(1):24–32, 1972.
- [Hab06] Emanuel AP Habets. Room impulse response generator. *Technische Universiteit Eindhoven, Tech. Rep*, 2(2.4):1, 2006.
- [Hei93] Renate Heinz. Binaural room simulation based on an image source model with addition of statistical methods to include the diffuse sound scattering of walls and to predict the reverberant tail. *Applied Acoustics*, 38(2-4):145–159, 1993.
- [HN06] Murray Hodgson and Eva-Marie Nosal. Experimental evaluation of radiosity for room sound-field prediction. *The Journal of the Acoustical Society of America*, 120(2):808–819, August 2006.
- [Hod91] Murray Hodgson. Evidence of diffuse surface reflections in rooms. *The Journal of the Acoustical Society of America*, 89(2):765–771, February 1991.
- [Hod96] Murray Hodgson. When is diffuse-field theory applicable? *Applied Acoustics*, 49(3):197–207, November 1996.
- [HSP80] T. Houtgast, H. J. M. Steeneken, and R. Plomp. Predicting Speech Intelligibility in Rooms from the Modulation Transfer Function. I. General Room Acoustics, September 1980.
- [HT73] John Kenneth Haviland and Balakrishna D. Thanedar. Monte Carlo applications to acoustical field solutions. *The Journal of the Acoustical Society of America*, 54(6):1442–1448, December 1973.
- [JIR08] Cheol-Ho Jeong, Jeong-Guon Ih, and Jens H. Rindel. An approximate treatment of reflection coefficient in the phased beam tracing method for the simulation of enclosed sound fields at medium frequencies. *Applied Acoustics*, 69(7):601–613, July 2008.

- [KBA01] N Korany, J Blauert, and O Abdel Alim. Acoustic simulation of rooms with boundaries of partially specular reflectivity. *Applied Acoustics*, page 13, 2001.
- [KBJJ13] Georgios I. Koutsouris, Jonas Brunskog, Cheol-Ho Jeong, and Finn Jacobsen. Combination of acoustical radiosity and the image source method. *The Journal of the Acoustical Society of America*, 133(6):3963–3974, June 2013.
- [Kel62] Joseph B. Keller. Geometrical Theory of Diffraction. *JOSA*, 52(2):116–130, February 1962.
- [KJM05] Bill Kapralos, Michael R Jenkin, and Evangelos Milios. Acoustical Modeling Using a Russian Roulette Strategy. page 8, 2005.
- [KKF93] U. R. Kristiansen, A. Kroksstad, and T. Follestad. Extending the image method to higher-order reflections. *Applied Acoustics*, 38(2):195–206, January 1993.
- [KP74] R. G. Kouyoumjian and P. H. Pathak. A uniform geometrical theory of diffraction for an edge in a perfectly conducting surface. *Proceedings of the IEEE*, 62(11):1448–1461, November 1974.
- [KSS68] A. Kroksstad, S. Strom, and S. Sørsdal. Calculating the acoustical room response by the use of a ray tracing technique. *Journal of Sound and Vibration*, 8(1):118–125, July 1968.
- [Kut17] Heinrich Kuttruff. *Room acoustics*. CRC Press/Taylor & Francis Group, Boca Raton, sixth edition edition, 2017.
- [Lam96] Y. W. Lam. A comparison of three diffuse reflection modeling methods used in room acoustics computer models. *The Journal of the Acoustical Society of America*, 100(4):2181–2192, October 1996.
- [LB92] Hilmar Lehnert and Jens Blauert. Principles of binaural room simulation. *Applied Acoustics*, 36(3-4):259–291, 1992.
- [LBB00] A. Le Bot and A. Bocquillet. Comparison of an integral equation on energy and the ray-tracing technique in room acoustics. *The Journal of the Acoustical Society of America*, 108(4):1732–1740, October 2000.
- [LCM07] C. Lauterbach, A. Chandak, and D. Manocha. Interactive sound rendering in complex and dynamic scenes using frustum tracing. *IEEE Transactions on Visualization and Computer Graphics*, 13(6):1672–1679, November 2007.
- [Leh93] Hilmar Lehnert. Systematic errors of the ray-tracing algorithm. *Applied Acoustics*, 38(2):207–221, January 1993.
- [Lew93] T. Lewers. A combined beam tracing and radiant exchange computer model of room acoustics. *Applied Acoustics*, 38(2-4):161–178, 1993.
- [LJ10] E A Lehmann and A M Johansson. Diffuse Reverberation Model for Efficient Image-Source Simulation of Room Impulse Responses. *IEEE Transactions on Audio, Speech, and Language Processing*, 18(6):1429–1439, August 2010.
- [LL88] Heewon Lee and Byung-Ho Lee. An efficient algorithm for the image model technique. *Applied Acoustics*, 24(2):87–115, January 1988.

BIBLIOGRAPHY

- [LSVA07] Tobias Lentz, Dirk Schröder, Michael Vorländer, and Ingo Assenmacher. Virtual Reality System with Integrated Sound Field Simulation and Reproduction. *EURASIP Journal on Advances in Signal Processing*, 2007(1), December 2007.
- [MBJN15] Gerd Marbjerg, Jonas Brunskog, Cheol-Ho Jeong, and Erling Nilsson. Development and validation of a combined phased acoustical radiosity and image source model for predicting sound fields in rooms. *The Journal of the Acoustical Society of America*, 138(3):1457–1468, September 2015.
- [MDW⁺01] Geoff Martin, Philippe Depalle, Wieslaw Woszczyk, Jason Corey, and René Quesnel. *A hybrid model for simulating diffused first reflections in two-dimensional synthetic acoustic environments*. PhD thesis, 2001.
- [MM76] M. L. Mehta and K. A. Mulholland. Effect of non-uniform distribution of absorption on reverberation time. *Journal of Sound and Vibration*, 46(2):209–224, May 1976.
- [Nay92] Graham Naylor. Treatment of early and late reflections in a hybrid computer model for room acoustics. *The Journal of the Acoustical Society of America*, 92(4):2345–2345, October 1992.
- [NMT93] Kiyoshi Nakagawa, Toru Miyajima, and Yasuhiko Tahara. An improved geometrical sound field analysis in rooms using scattered sound and an audible room acoustic simulator. *Applied Acoustics*, 38(2):115–129, January 1993.
- [PSV11] Sönke Pelzer, Dirk Schröder, and Michael Vorländer. The number of necessary rays in geometrically based simulations using the diffuse rain technique. In *Proceedings of DAGA*, 2011.
- [RC03] Jens Holger Rindel and Claus Lynge Christensen. Room acoustic simulation and auralization—how close can we get to the real room. In *Proc. 8th Western Pacific Acoustics Conference, Melbourne*, 2003.
- [RF03] Yong Rui and Dinei Florencio. New direct approaches to robust sound source localization. 1:I–737, 2003.
- [SAWG91] François X Sillion, James Arvo, Stephen Westin, and Donald P Greenberg. A Global Illumination Solution for General Reflectance Distributions. *Computer Graphics*, 25(4):11, 1991.
- [Sch] Dirk Schröder. Physically Based Real-Time Auralization of Interactive Virtual Environments. page 231.
- [SDV07] Dirk Schröder, Philipp Dross, and Michael Vorländer. A Fast Reverberation Estimator for Virtual Environments. page 10, 2007.
- [SLKS07] Samuel Siltanen, Tapio Lokki, Sami Kiminki, and Lauri Savioja. The room acoustic rendering equation. *The Journal of the Acoustical Society of America*, 122(3):1624–1635, September 2007.
- [SLTS12] Samu Siltanen, Tapio Lokki, Sakari Tervo, and Lauri Savioja. Modeling incoherent reflections from rough room surfaces with image sources. *The Journal of the Acoustical Society of America*, 131(6):4606–4614, June 2012.

- [SMD09] Steven M. Schimmel, Martin F. Muller, and Norbert Dillier. A fast and accurate "shoebox" room acoustics simulator. In *2009 IEEE International Conference on Acoustics, Speech and Signal Processing*, pages 241–244, Taipei, Taiwan, April 2009. IEEE.
- [SP09] Dirk Schröder and Alexander Pohl. Real-Time Hybrid Simulation Method Including Edge Diffraction. page 7, 2009.
- [SP13] Dirk Schröder and Alexander Pohl. Modeling (Non-)uniform scattering distributions in geometrical acoustics. pages 015112–015112, Montreal, Canada, 2013.
- [SS07] Uwe M Stephenson and U Peter Svensson. An improved energetic approach to diffraction based on the uncertainty principle. *19th Int. Cong. on Acoustics (ICA)*, 2007.
- [Ste10] Uwe M. Stephenson. An Energetic Approach for the Simulation of Diffraction within Ray Tracing Based on the Uncertainty Relation, June 2010.
- [SV99] Lauri Savioja and Riitta V'. Creating Interactive Virtual Acoustic Environments. page 31, 1999.
- [Sve02] U. Peter Svensson. Modelling Acoustic Spaces for Audio Virtual Reality. In *Proceedings of the 1st IEEE Benelux Workshop on Model based Processing and Coding of Audio (MPCA)*, 2002.
- [Ten07] Roberto A. Tenenbaum. Hybrid Method for Numerical Simulation of Room Acoustics with Auralization : Part 1 – Theoretical and Numerical Aspects. 2007.
- [TG97] Nicolas Tsingos and Jean-Dominique Gascuel. A general model for the simulation of room acoustics based on hierarchical radiosity. In *SIGGRAPH'97 technical sketch*, Los angeles, United States, 1997.
- [TM98] Carlo Tomasi and Roberto Manduchi. Bilateral filtering for gray and color images. 98(1):2, 1998.
- [TSK01] Rendell R. Torres, U. Peter Svensson, and Mendel Kleiner. Computation of edge diffraction for more accurate room acoustics auralization. *The Journal of the Acoustical Society of America*, 109(2):600–610, February 2001.
- [Twe57] Victor Twersky. On Scattering and Reflection of Sound by Rough Surfaces. *The Journal of the Acoustical Society of America*, 29(2):209–225, February 1957.
- [VB01] Jaco Vermaak and Andrew Blake. Nonlinear filtering for speaker tracking in noisy and reverberant environments. 5:3021–3024, 2001.
- [VM00] Michael Vorländer and Eckard Mommertz. Definition and measurement of random-incidence scattering coefficients. *Applied Acoustics*, 60(2):187–199, June 2000.
- [Vor89] Michael Vorländer. Simulation of the transient and steady-state sound propagation in rooms using a new combined ray-tracing/image-source algorithm. *The Journal of the Acoustical Society of America*, 86(1):172–178, July 1989.
- [WD81] John P. Walsh and Norman Dadoun. The design and development of Godot: A system for computer-aided room acoustics modeling and simulation. *The Journal of the Acoustical Society of America*, 69(S1):S36–S36, May 1981.

BIBLIOGRAPHY

- [WEJvS10] Andrew Wabnitz, Nicolas Epain, Craig Jin, and André van Schaik. Room acoustics simulation for multichannel microphone arrays. page 6, 2010.
- [Yam26] Ziro Yamauti. The Light Flux Distribution of a System of Interreflecting Surfaces. *Journal of the Optical Society of America*, 13(5):561, November 1926.